Universidade de São Paulo

Instituto de Química de São Carlos

Programa de Pós-graduação em Química

Mian Abdul Ali

Ethanol bioelectrocatalysis using alcohol dehydrogenase on quinone-functionalized carbon-based electrodes: from molecular electrochemistry to *operando*-electron paramagnetic resonance approach

São Carlos

2019

Mian Abdul Ali

Ethanol bioelectrocatalysis using alcohol dehydrogenase on quinone-functionalized carbon-based electrodes: from molecular electrochemistry to *operando*-electron paramagnetic resonance approach

Thesis submitted to the Institute of Chemistry of São Carlos (IQSC), University of São Paulo as part of the requirement for the award of degree of doctorate in chemistry.

Area of concentration: Bio-organic Chemistry

Supervisor: Prof. Dr. Frank Nelson Crespilho

São Carlos

2019

DEDICATION

This thesis is dedicated to my parents, Mian Abdul Bari and Shah Jehan Bibi, to my brother Mian Tufail Bari, to my daughter (Syyeda Hania Ali) and especially to my wife Asma Rahman whose prayers, love, guidance and cooperation inspired me to the intension.

ACKNOWLEDGEMENTS

- First of all thanks to Al-Mighty God, the most Merciful, the Compassionate and the Omniscient, whose clemency resulted into my success and all respect to his holy prophet (PBUH), who enables us to recognize our creator. He, who does not thank to people, is not thankful to God and Holy Prophet (PBUH).
- I am greatly thankful to my father Mian Abdul Bari and to my mother Shah Jehan Bibi for her love, support, co-operation and prayers, who always encouraged me during stress and hard times. His encouraging attitude always raised my moral at every single moment of my life.
- I am also very thankful to my brother and sisters for the encouragement, support and also their prayers for my success.
- I wish to express my deepest love and gratitude to my wife Asma Rahman for her love, support and appreciation at every single moment during these four and a half years of my research.
- I wish to express my heartiest and profound gratitude to my dearest, highly respectable, kind hearted, ideal and the most cooperative supervisor Prof. Dr. Frank Nelson Crespilho, without the kind guidance and keen interest of whom, the completion of this dissertation was not possible. His valuable gaudiness has brought success to my efforts. He has provided me constant input, advice and enthusiasm at every level of my research and his impulsive, cheerful, endless, and harmonious encouragements lift my spirit, and raised my personality to meet the challenges. Whatever I was able to achieve, as presented here, is only due to his keen interest and support.
- I wish to particularly thank to the funding agencies Third World Academy of Sciences (TWAS) and CNPq (Process No. 190172/2013-4) for financial support to complete my PhD research project and also for participation in international conferences.
- I would like to express my sincere appreciation and thanks to my friends in the Group of Bioelectrochemistry and Interfaces, who ended up becoming a family here in Sao Carlos: Antonio Francisco, Vitor Carvalho, Rodrigo Iost, Andressa Pereira, Kamila Pagnoncelli, Fernanda Sales, Graziela Sedenho, Andressa Dancini, Lucyano Macedo, Roberto Luz, Ayaz Hassan, Thiago Bertaglia. Thanks for the support, encouragement,

stimulating and fruitful discussion on science and all the fun we have in the last four years.

- Thanks to all my Pakistani friends Ayaz Hassan, Sajjad Ali, Sabir Khan, Sardar Hussain and especially Dr. Sajjad Ullah for the support, encouragement and best wishes throughout my research.
- I would also like to thank Prof. Daniel Rodrigues Cardoso (IQSC/USP) for making the use of the equipment Electron Paramagnetic Resonance (EPR) Spectroscopy and his valuable gaudiness and co-operation during performing In-situ EPR electrochemistry experiments.
- I would like to thank Prof. Dr. Renato Vitalino Gonçalves and Laboratory of Nanomaterials and Advanced Ceramics (IFSC/USP) for making the use of the equipment X-rays photoelectron spectroscopy and discussions about XPS.
- Prof. Dr. Germano Tremiliosi Filho and Prof. Dr. Fabio Henrique Barros de Lima (IQSC/USP) by participating in the bench of my qualification examination and for their insightful comments and encouragement.
- I wish to thank CAQI and its technicians, especially to Dr. Marcio de Paula for co-operation in some experiments for the characterization of Scanning Electron Microscopy.
- The Professors of the Institute of Chemistry of Sao Carlos (IQSC-USP) for my professional training.

“Nothing in life is to be feared, it is only to be understood. Now is the time to understand more, so that we may fear less.”

(Marie Curie)

“Never play with the feelings of others, because you may win the game but the risk is that you will surely lose the person for a life time.”

(William Shakespeare)

RESUMO

Diferentes estratégias têm sido propostas a fim de melhorar o desempenho dos bioeletrodos utilizados nas biocélulas a combustíveis e nos biossensores. Por exemplo, a funcionalização de eletrodos de carbono tem sido feita para esse fim. Neste estudo, propomos o desenvolvimento de fibras flexíveis de carbono (FFCs) funcionalizadas com grupos quinona e modificados com álcool desidrogenase (ADH) nicotinamida adenina dinucleotídeo (NAD) dependente para obter bioeletrodos para uma bio-eletrocatálise eficiente de etanol. Grupos quinona na superfície das FFCs foram obtidas utilizando o tratamento oxidativo com permanganato e também pelo ancoramento eletroquímico de antraquinona: ambas metodologias resultaram em bioeletrodos para a eletro-oxidação de reduzido nicotinamida adenina dinucleotídeo (NADH) que pode aumentar a bio-eletrocatálise do etanol. De acordo dados espectroscópicos, microscópicos, e eletroquímicos, defeitos contendo grupos C=O nos eletrodos de FFCs são atribuídos à melhora na oxidação do NADH, aumentando a bio-eletrocatálise do etanol. Para se investigar o papel dos grupos quinona na eletro-oxidação do NADH, propomos uma configuração experimental baseado na espectroscopia de ressonância paramagnética de elétrons em modo operando (operando-EPR). Com essa técnica, fomos capazes de mostrar a correlação entre o número de elétrons livres desemparelhados, a concentração superficial de quinonas e a oxidação do NADH com controle eletroquímico. A correlação para a concentração de spins revela um aumento no número de elétrons desemparelhados livres com o aumento do sobrepotencial aplicado e a oxidação do NADH, o que corrabora com a hipótese de que grupos quinona podem afetar a eletrocatálise rumo à oxidação do NADH a oxidado nicotinamida adenina dinucleotídeo (NAD^+). É vislumbrado que operando-EPR pode fornecer infromação útil para provar a dinâmica da transferência de elétrons em superfície de carbono podendo ser extendida a outros sistemas bioeletroquímicos.

Palavras-chave: fibras flexíveis de carbono, álcool desidrogenase, bioeletrocatálise, nicotinamida adenina dinucleotídeo, Ressonância paramagnética eletrônica.

ABSTRACT

There are several strategies to improve the performance of bioelectrodes applied in biosensors and biofuel cells. For instance, surface functionalization of the carbon-based electrodes has been used to this intend. Herein, we propose the development of flexible carbon fibers (FCFs) functionalized with quinone groups and modified with nicotinamide adenine dinucleotide (NAD) dependent alcohol dehydrogenase (ADH) to obtain bioelectrodes for efficient ethanol bioelectrocatalysis. Quinones groups on FCFs surfaces were obtained by using oxidative treatment with permanganate, and also by electrochemical grafting of anthraquinone: both these methodologies result in bioelectrodes for the electro-oxidation of reduced nicotinamide adenine dinucleotide (NADH) that can improve the ethanol bioelectrocatalysis. Based on spectroscopic, microscopic and electrochemical data, defects containing C=O groups on FCFs electrodes are attributed to improve the NADH oxidation, enhancing the ethanol bio-electrocatalysis. In order to investigate the role of quinone groups on the NADH electro-oxidation, we propose an experimental setup based on *operando* electron paramagnetic resonance spectroscopy (*operando* EPR). With this technique, we are able to show a correlation among the number of free unpaired electrons, surface concentration of quinones and NADH oxidation under electrochemical control. Correlation for the spin concentration reveals an increasing number of free unpaired electrons with increasing applied overpotential and NADH oxidation, which corroborates the hypothesis that quinone groups can act as electrocatalysts towards the oxidation of NADH to oxidized nicotinamide adenine dinucleotide (NAD^+). It is glimpsed that *operando* EPR can provide useful information in probing the electron transfer dynamics on a carbon surface and may be extended to others bioelectrochemical systems.

Keywords: flexible carbon fibers, alcohol dehydrogenase, bioelectrocatalysis, nicotinamide adenine dinucleotide, Electron paramagnetic resonance.

LIST OF FIGURES

Figure 32 – (a) Chronoamperometric response obtained in 0.1 mol L^{-1} sodium phosphate buffer solution (pH 7.5) containing NAD^+ (0.6 mmol L^{-1}) and different concentrations of ethanol (200 µL) at 0.6 V applied potential for pristine FCF-ADH (●), FCF1-ADH (●), and FCF-AQ-ADH (●). (b) Plot of the ethanol concentration versus current for pristine FCF-ADH (●), FCF1-ADH (●), and FCF-AQ-ADH (●) under the same condition in N_2-saturated environment at a scan rate: 50 mV s^{-1} at T= 25 °C…….....…….....76

LIST OF TABLES

LIST OF ABBREVIATIONS AND ACRONYMS

FCF – Flexible carbon fiber

PAN – Polyacrylonitrile

FCF1 – Flexible carbon fiber treated with $KMnO_4/H_2SO_4$ solution pH 0.34

FCF2 – Flexible carbon fiber treated with $KMnO_4$/phosphate buffer solution pH 7.0

FCF3 – Flexible carbon fiber treated with $KMnO_4$/NaOH solution pH 13.96

FCF-AQ – Flexible carbon fiber modified with anthraquinone in HCl + 1-AAQ/$NaNO_2$

AAQ – Aminoanthraquinone

AQ – Anthraquinone

CH_3CH_2OH – Ethanol

CH_3CHO – Acetaldehyde

$KMnO_4$ – Potassium permangante

$Ag/AgCl_{sat}$ – Reference electrode of silver chloride in saturated potassium chloride solution

ADH - Alcohol dehydrogenase

PDB – Protein data bank

NAD^+ - Nicotinamide adenine dinucleotide (oxidized)

NADH - Nicotinamide adenine dinucleotide (reduced)

SEM - Scanning electron microscopy

EDS - Dispersive energy spectroscopy

XPS - X-rays photoelectron spectroscopy

EPR - Electron paramagnetic resonance

LIST OF SYMBOLS

$\boldsymbol{E}$ – Potential

$\boldsymbol{E_{pa}}$ – Anodic peak potential

$\boldsymbol{E_{pc}}$ – Cathodic peak potential

$\boldsymbol{E-E^0}$ – Overpotential

$\boldsymbol{\Delta E}$ – Separation of peak potential

$\boldsymbol{E_{1/2}}$ – Half wave potential

$\boldsymbol{\Gamma}$ – Surface concentration

Q – Amount of charge

A – Ampere

mA – Miliampere

mA cm^{-2} – Miliampere per centimeter square

V – Volt

mV – Milivolt

eV – Electron volt

$\boldsymbol{j}$ – Current density

$\boldsymbol{j_{pa}}$ – Anodic peak current density

$\boldsymbol{j_{pc}}$ – Cathodic peak current density

$\boldsymbol{R}$ – Universal gas constant

$\boldsymbol{F}$ – Faraday constant

$\boldsymbol{T}$ – Temperature

n – Number of transferred electrons

α – Electrons transfer coefficient

ν – Scanning speed

k^0 – Standard rate constant at zero overpotential

$k_{oxi/red}$ – Rate constant of heterogeneous electron transfer of oxidation and reduction

CPS – Centipoises

G – Gauss

g – g-factor

GHz – Gigahertz

kHz – Kilohertz

SUMMARY

1 INTRODUCTION

1.1 Alcohol dehydrogenase and bioelectrocatalysis

The alcohol dehydrogenases (ADH) belongs to a subclass of oxidoreductase enzymes, the dehydrogenases that facilitates the oxidation of a variety of alcohols to carbonyl compounds with the concomitant interconversion of NAD^+/NADH redox couple,[1–3] these latter being the oxidized and reduced forms of the co-enzymes, the nicotinamide adenine dinucleotide (NAD). ADH is considered more stable and has greater specificity than the other sub-class of oxidoreductase enzymes such as alcohol oxidases, though both these enzymes catalyze the same reactions with the formation of the similar products, they follow a different reaction mechanisms. In the case of ADH, the alcohol oxidation reaction is stereospecific, and the enzyme can attack either side of NAD^+ ring resulting in different conformations, such as the syn- and anti-conformations and thus having different reactivity. For example, during the oxidation of ethanol by ADH in the presence of NAD^+, the ethanol is converted to acetaldehyde as shown in Figure 1, mechanistically; the coenzyme binds to the enzyme by oxidizing the alcoholic moieties in the enzyme. The dissociation of the enzyme-NADH complex is the rate determining step according to the recently reported mechanism,[4,5] and this enzymatic reaction can be utilized for the determination of ethanol in alcoholic beverages, medicine and has many applications in forensic science and toxicology. ADH has a high specificity for ethanol and is very stable when in isolated form. It is found in many microorganisms such as in the liver of animals, in yeast (*Saccharomyces cerevisiae*), which was first purified and crystallized by Negelein and Wulff in 1937. ADH has a molecular weight of 150 kDa and has a tetrameric structure with one NAD^+ as a coenzyme and Zn^{2+} as a cofactor in each subunit of the enzyme and each of these components is very important for the mechanism of bioelectrocatalysis.[5] Both coenzymes and cofactors are small, non-protein substances that play a vital role in the metabolic function of the cell by helping the enzymes to catalyze the biochemical reaction. The main difference is that coenzyme is a type of cofactor that loosely binds to the enzyme. The active site characteristics of ADH are: each subunit of one monomer contains one binding site for NAD^+ and two binding sites for Zn. Each Zn ion is ligated directly to the side chain of Cys-46, His-67, Cys-147 and a water molecule which is hydrogen bonded to Ser-48. Among the two binding sites where the Zn is located, there are two clefts: one which binds the NAD^+ and the other binds the substrate (ethanol). All these

features described above make the ADH as a suitable enzyme for use in biosensors and as a bioelectrodes in biofuel cells.

Figure 1 - Representation of the ADH structure from *Saccharomyces cerevisiae* (PDB: 4w6z). (b) Scheme of ethanol oxidation to acetaldehyde by the ADH in the presence of co-enzyme NAD^+

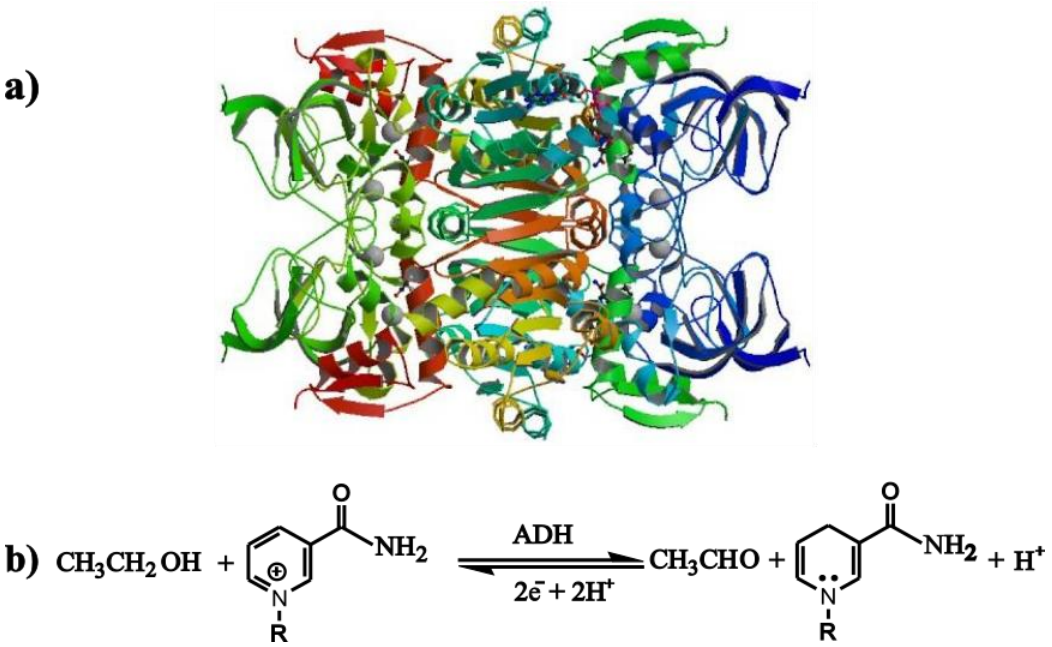

Source: Own authorship. The image of ADH was obtained by Protein Data Bank (PDB – 4w6z).

In a bioelectrocatalytic process, the electrode does not have simply the function of transferring electrons; it can effectively participate in the reaction, generating adsorption and electron transfer sites. When the electrode surface has sites that have the capacity of adsorbing the reactants, the probability of reaching an energetic state, favoring the transfer of electrons increases significantly, and the materials possessing this property are called electrocatalysts. Therefore, the performance as an electrocatalyst will depend on the electronic structure of the surface atoms presented in the electrode, as well as the chemical nature of the surface, morphology and crystalline structure. The electrocatalysts used in bioelectrocatalysis are basically biomolecules, especially oxidoreductase enzymes, which are further divided into the following subclasses; oxidases, dehydrogenases, hydroxylases, oxygenases, reductases and peroxidases.[1,6–8] Of these oxidoreductase enzymes, the dehydrogenase has been frequently exploited in bioelectrochemical reactions occurring in biosensors and biofuel cells with improved electrochemical performance. The additional advantage of using the dehydrogenase in bioelectrocatalysis is its ability to directly transfer the electron towards the electrode, if the surface of latter is properly modified, thus avoiding the possibility of using the redox

mediators. In this context using electrodes modified with quinone moieties have a potential to increase the efficiency of the electro-oxidation of NADH, thus making possible the requirements for the bioelectrocatalysis of the alcohol using NAD-dependent dehydrogenase enzyme, such as ADH.

1.1.1 Nicotinamide adenine dinucleotide: structure and properties

During the bioelectrocatalysis of ethanol by the ADH, the presence of the coenzyme NAD^+ is necessary for the processing of the reaction. During this reaction, one molecule of NAD^+ is used to convert ethanol to acetaldehyde through a proton transfer. During hydrogen transfer, two hydrogens are withdrawn up the ethanol by zinc. The coenzymes work catalytically and are recycled repeatedly without a change in the concentration of both NAD^+ and NADH. Both NAD^+ and NADH are the coenzymes for more than 200 dehydrogenses and act as bioelectrocatalyts for biosensors,[9–11] biofuel cells technology,[12–14] and food science[9,15]and are components of biomarker systems.[16] However, the bioavailability of either the one or the other coenzyme and their facile and efficient regeneration is still a major problem in the manufacturing of dehydrogenase based biosensors and biofuel cells. A number of methods have been proposed for the regeneration of NAD^+/NADH, required for biological redox reactions.[17] Enzymatic and chemical regeneration of NAD^+ from NADH require additional chemical reactions under controlled pH conditions. On the other hand, electro-oxidation of NADH to produce an enzymatically active NAD^+ by using redox mediator is an example of electrochemical system for the efficient regeneration of these coenzymes. Several authors have reported that quinones act as a redox mediators.[18–24] Even though the quinone–electrolyte interface plays an important role as an electron donor/acceptor, there is no consensus about the mechanism of electron transfer. As far as the experimental approach is concerned, there is an intrinsic problem in solving the reaction mechanism: both the mediated electron transfer mechanism and electrocatalysis can result in similar responses in steady-state electrochemistry because both increase the faradaic current at a low overpotential. However, if there is a catalytic effect on a reaction taking place at the surface of a quinone-modified electrode due to the electrode itself, an increase in the electrochemical reaction rate is expected, and the electronic properties of the electrode surface should change. However, to the best of our knowledge, there are no studies in the literature regarding this. One of the most widely used redox mediators for the electro-oxidation of NADH is the quinones, typically *ortho*-quinones and anthraquinones as shown in Figure 2. The electro-oxidation of NADH has been reported for the mediator modified electrode by using quinones between the surface of

the composite electrode and the immobilized enzyme.[25] Similarly, various other works have been reported,[26–28] where napthoquinones and anthraquinones have been used together with FAD and NAD-dependent enzyme towards the oxidation of NADH.

Figure 2 - (a) The structure of the ADH with the highlighted regions showing the binding of coenzyme NADH with the enzyme and the electro-oxidation of NADH to NAD^+ catalyzed by *ortho*-quinones and anthraquinones on the surface of the electrode. (b) Chemical structure of coenzyme NAD^+.

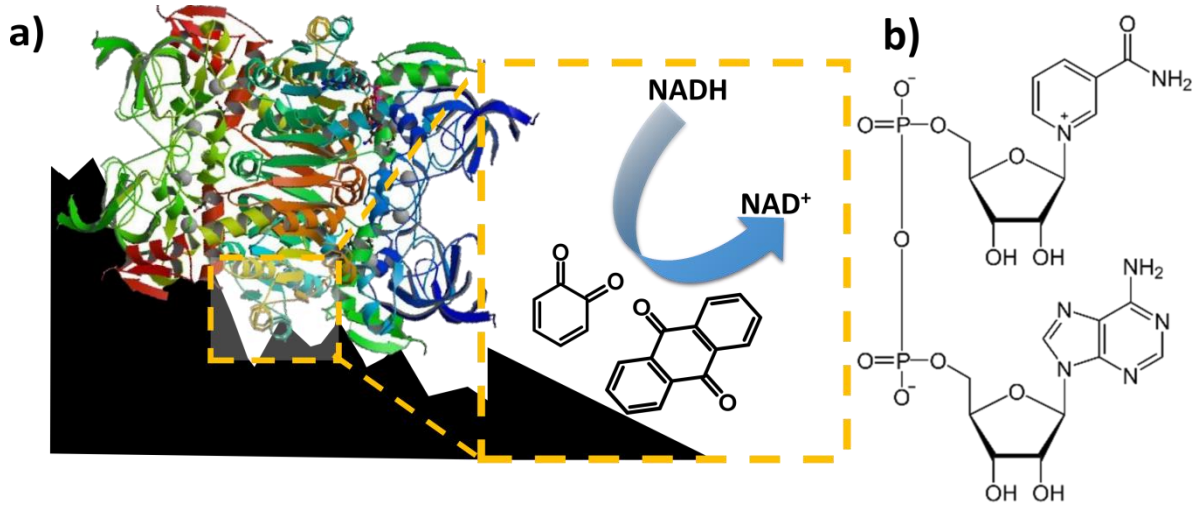

Source: Own authorship (PDB – 4w6z)

1.1.2 Immobilization of ADH on electrode surface

Different strategies can be used to immobilize the ADH on the surface of electrodes.[29] The manner through which the enzyme is immobilized on the electrode surface may influence its interaction with the substrate and the electron transfer from the redox site to the surface of the electrode and hence can affect the performance of the bioelectrode. When biomolecules are immobilized, they must maintain their structure, electrochemical activity, and should be strongly adsorbed to the surface of electrode. In the literature, the most commonly used methods of enzymes immobilization are: physical adsorption, entrapment, cross-linking, encapsulation and covalent bonding as shown in Figure 3.[29,30] The physical adsorption is the oldest and simplest method of enzyme immobilization. In this method enzyme is adsorbed to external surface of the support or carrier such as mineral support, organic support and ion exchange resin etc and there is no permanent bond formation between the carrier and enzyme. In the entrapment method enzymes are physically entrapped inside a porous matrix and the bonds involved in stabilizing the enzyme to the matrix may be covalent or non-covalent.

Cross linking is also called as co-polymerization and enzymes are directly linked by covalent bonds between various groups of enzymes via polyfunctional reagents. Unlike other methods, there is no matrix or support involved in this method. The encapsulation method of enzyme immobilization is done by enclosing the enzymes in a membrane capsule and the capsule will be made up of semi permeable membrane like nitro cellulose or nylone. The final method of enzyme immobilization is covalent bonding which involves the formation of covalent bond between the chemical groups in enzyme and to the chemical group on the support or carrier. Though, each of these immobilization methods has its own merits and demerits, it is necessary to perform a pre-treatment of the electrode surface, in order to have an efficient and strong physical adsorption or covalent attachment of the enzymes. For the functionalization of carbon-based electrodes, oxidative methods are generally employed, leading to the formation of oxygenated groups.[3–5] However, these groups are hydrophilic, so that the adsorption of enzymes is not favored, since for this purpose type of immobilization is required to have hydrophobic enzyme-electrode interactions.

Figure 3 - Enzymes immobilization on the surface of electrodes through various methods.

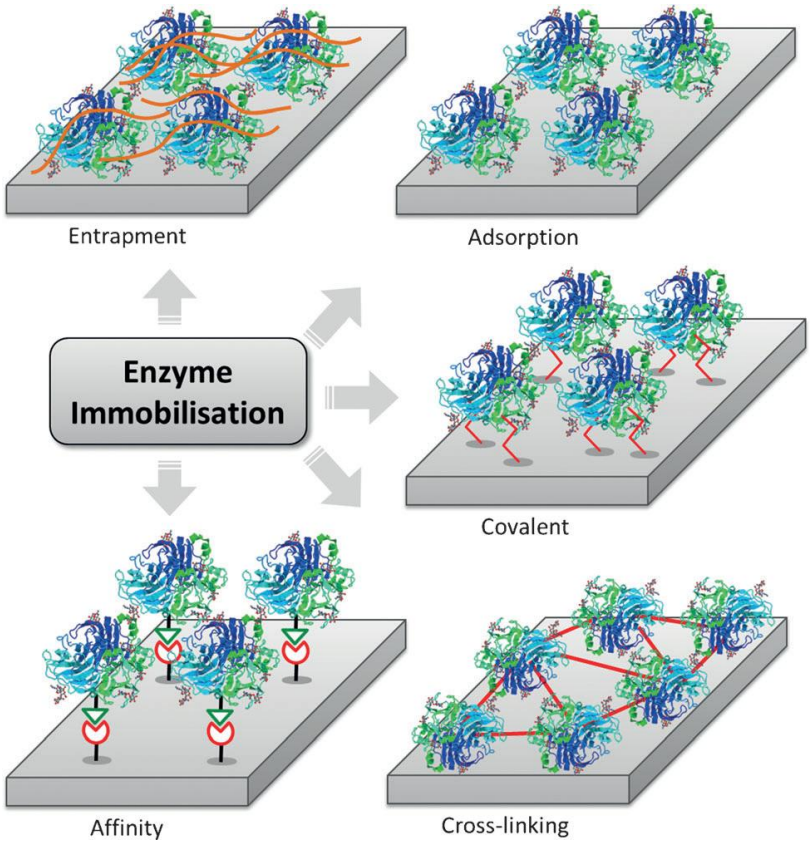

Source: Adapted from Luz, R. A. S., Pereira, R. A., Souza, J. C. P., Sales, F. C. P. F., Crespilho, F. N., 2014, p. 1758.

1.2 Electrode and functionalization

1.2.1 Flexible carbon fiber electrodes: synthesis and surface properties

Carbon is a versatile material since it is found in several allotropic forms, several microtextures, and different grades of graphitization and dimensionalities (from 0 to 3D). Carbon-based materials have widely been used in electrochemical studies due to their physicochemical properties, including high electrical and thermal conductivities, corrosion resistance, low density, and elasticity. Among the carbon- based materials, the flexible carbon fiber (FCF) deserve special attention and is widely used as electrode materials in electrochemical studies mainly because of its unique set of properties, such as light weight, high conductivity, electrochemical stability and can be obtained with a high degree of purity.[31–35] Though FCF can be produced from various precursors, the polyacrylonitrile (PAN), an attic and linear polymer, which contains highly polar nitrile groups, is the most popular acrylic precursor, widely used to produce the FCF.[36–41] Due to the strong dipole-dipole interactions between the nitrile groups, the PAN assumes a conformation of the irregular helical type.[36] The manufacturing process of the FCF from PAN consists of the thermal treatment of the PAN wires, this process is critical to obtaining high-quality carbon fibers and could take up to several hours, depending on the temperature, precursor diameter, and precursor fiber characteristics. The thermal treatment is divided into three stages of a complex heat treatment process and the complete mechanism of the manufacturing process can be found elsewhere.[34,36,40,41] The first step is the stabilization through oxidation under air at controlled low-temperature heating in the range of 200–300 °C in order to convert the precursor to such a form, which could be further heat treated without the melting or fusion of the fibers. During this process, the linear molecules of PAN-based polymer precursor are first converted into cyclic structures. The second step is the carbonization and the temperature of carbonization is usually determined by the application for which the resulting carbon fibers are used. For high-strength applications, the carbonization temperature in the range of 1500–1600 °C is preferred because at temperatures above 1600 °C, a decrease in the tensile strength occurs.[38] The third step consists of graphitization and occurs at a temperature > 2000 °C which generates the sp^2 hybridization, thus making it a conductive material. This step also improves the orientation of the basal planes and the stiffness of the FCFs.[39–41] During this step, the sp^2 hybridizations are stacked on top of one another until the formation of graphite crystallites, which are considered the basic structural units of the FCFs derived from PAN. However, the formation of these crystallites is imperfect, leading to the formation of a

turbostratic structure and graphitization that is never complete, so in the structure there are also carbons with the sp^3 hybridization.[32] The FCF obtained from PAN precursor usually contains nitrogen and silicon contaminants, because of the nature of precursor used. Therefore, some further cleaning and activation procedures are performed, if the utilization of the FCF as electrode materials with improved electrochemical properties is desired. In particular for the fabrication of bioelectrodes, the surface property of FCF containing different functional groups play a major role towards the immobilization of biomolecules and is obtained through various modification procedure.

1.2.2 Functionalization of FCF electrode with quinones

The modification of FCF surface is of extreme importance for adhesion, ion adsorption, increase in hydrophilicity and particularly for the enhanced interfacial electron transfer in bioelectrochemical systems (BES). In order to promote the alteration of interfacial region properties, FCF are subjected to surface functionalization. There are several ways to promote the electrode surface functionalization, however two methodologies are highlighted here.[3,34,42–49] The first methodology, known as oxidative treatment, is the recently developed one,[3,34,42] introduced to modify FCF with quinone groups, where the electrode is subjected to one-pot chemical reaction with $KMnO_4$ under different pH conditions. This methodology has been proved to be very successful for producing more efficient and stable electrodes for application in BES, particularly for high electrochemical performance of dehydrogenases-based electrodes.[3,34,42] In this case, one-pot chemical reaction improves the electrode surface properties by subjecting it to oxidation through a fast-chemical reaction, avoiding the complicated separation and purification steps of the intermediates involved, and thus sufficiently reduce the time and use of resources. One possible reaction pathway for one-pot chemical reaction with $KMnO_4$ procedure is shown in Figure 4.

Figure 4 - Possible reaction pathway of FCF oxidation by $KMnO_4$ in H_2SO_4 solution (1.0 mol L^{-1}, pH 0), in sodium phosphate buffer solution (0.1 mol L^{-1}, pH 7.0), and in NaOH solution (1.0 mol L^{-1}, pH 14).

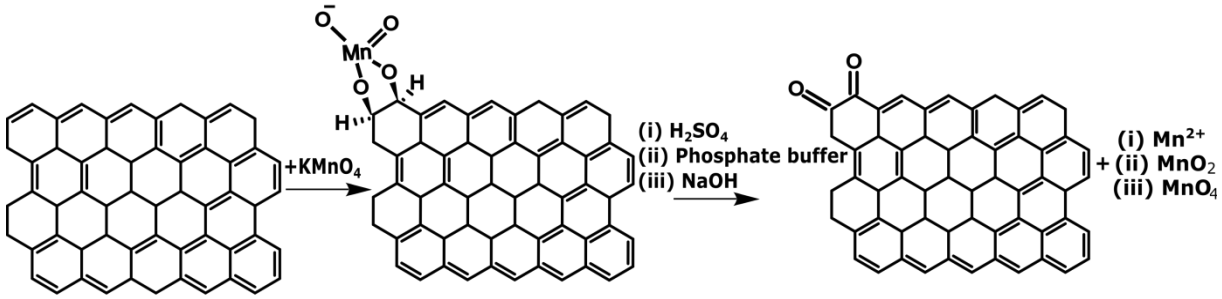

Source: The mechanism for the given reaction is suggested by own authorship.

The second methodology is composed of covalent functionalization through an electrochemical grafting technique to introduce the anthraquinone functionalities to FCF. This methodology has been consolidated from several studies described elsewhere,[47–50] the protocol initially involve the in-situ generation of anthraquinone diazonium cations in aqueous solution containing 1-aminoanthraquinone, $NaNO_2$ and HCl and then the electrochemical grafting of anthraquinonyl (AQN) groups to the surface of the electrode by the application of the potential. The reaction pathway to obtain the electrochemically modified electrodes is shown in Figure 5 and can be found elsewhere.[47–50]

Figure 5 - Electrochemical grafting of AQN groups to FCF in HCl solution (0.5 mol L^{-1}) containing 1-aminoanthraquinone (1.0 mmol L^{-1}) and $NaNO_2$ (4.0 mmol L^{-1}) in Ar atmosphere**.**

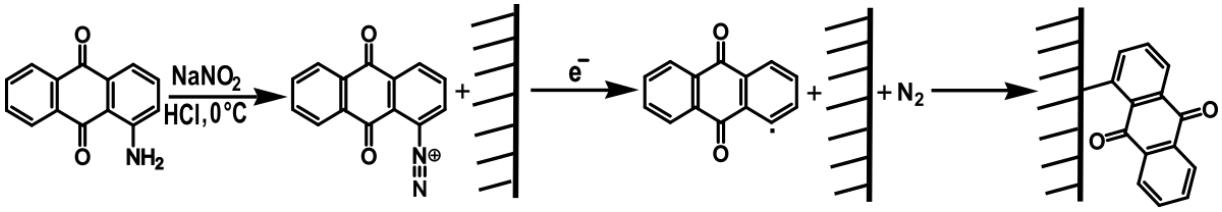

Source: The mechanism for electrochemical grafting was firstly proposed by KULLAPERE, M., SEINBERG, J. M., MÄEORG. U., MAIA. G., SCHIFFRIN. D. J.; TAMMEVESKI. K., 2009, p. 1969.

These surface treatment enables the formation of a material interphase, and may cause amendments to the interfacial electron transfer and may also increase surface stability of the FCF electrodes.[45,46,51,52] In particular, the formation of quinones, such as *ortho*- and anthraquinones on the surface of electrodes after these modification procedures, play an essential role in the bioelectrochemical process, which sufficiently enhance their

electrochemical properties in different redox probes[53–55] as well as in other electrolytes under different pH conditions.[47] The main purpose of FCF surface functionalization with quinones is to enhance their activity towards the electro-oxidation of NADH to NAD^+ [25,56–59], mainly because of its importance in the field of analytical electrochemistry,[60,61] bioelectrocatalysis,[62–64] and biofuel cells.[65]

1.3 X-ray photoelectron spectroscopy and *Operando* techniques

X-ray photoelectron spectroscopy (XPS) is a classical method for the semiquantitative analysis of surface composition. It is also referred to as electron spectroscopy for chemical analysis (ESCA). It is based on the photoelectric effect i-e emission of electron following excitation of core level electrons by photons. XPS is a surface-sensitive spectroscopic technique because of the low inelastic mean free path of electrons and is able to obtain the elemental composition of the elements that exist within material surfaces up to 10 nm depth. The most interesting thing with this technique is its ability to measure binding energy variations resulting from their chemical environment. XPS can be used to investigate the surface chemistry of a material in its as-received state or after some chemical treatment. An XPS setup consists of an X-ray source, a sample chamber and an electron analyzer. It requires a monochromatic source of X-rays i-e either from a lab based anode or from synchrotron radiation, with an X-ray monochromator in both cases. Traditionally, XPS works only in ultrahigh vacuum (UHV) because of scattering of electrons in gases.

In-*situ* spectroscopy of heterogeneous catalysts has been practiced for over 60 years and is an invaluable approach for characterizing catalytic materials over a wide range of environmental conditions. In-*situ* characterization studies allowed scientists to observe catalysts under controlled conditions; however they fall short of providing a direct relationship between catalyst structure (bulk/surface) and performance (activity/selectivity) because of the absence of the corresponding reaction product analysis. This limitation of in-*situ* spectroscopy characterization can be overcome by simultaneously collecting catalyst characterization and online product analysis data and has been referred to as *operando* spectroscopy. The term *operando* first appeared in the catalytic literature by Miguel A. Bañares in 2002,[66] who sought to name the methodology in a way that captured the idea of observing a functional materials, such as catalyst under actual working device operation conditions. The *operando* spectroscopy is actually advancement in the *in-situ* studies, which was made possible because of the continuous efforts of the researchers, such as

electrochemists to have deeper insight of their system and hence to gather the time resolved information from the reactions occurring on the active sites of the electrocatalysts.[67] This technique is not only restricted to electrocatalysis, several other systems, such as batteries and fuel cells have been subject to *operando* studies with respect to their electrochemical function. The ultimate goal of *operando* spectroscopy is to determine the structure-activity relationship of the substrate-catalyst species of the same reaction. By combining two experiments, the performance of a reaction plus the real time spectral acquisition of the reaction mixture on a single reaction facilitates a direct link between the structure of the catalyst and intermediates, and of the catalytic activity/selectivity. There are several studies employing *operando* approaches, such as *operando* electron paramagnetic resonance (EPR), *operand*o X-ray photoelectron spectroscopy and *operando* Raman spectroscopy found elsewhere.[68–72] The purpose of *operando* spectroscopy technique is to measure the catalytic changes that occur on the surface of the catalyst within the reactor during operations. Since, the advent of the term, using *operando* spectroscopy has allowed great strides to be made in catalysis, regardless of the catalytic application. Pioneers of the method recognized the importance of simultaneously tracking the catalyst structure and reaction products to allow for correlations, with some studies even dating back to the 1960s. Because of the significance of these methods, *operando* spectroscopy continues to be adopted, increasing each year and currently approaching about 100 publications annually.

2 OBJECTIVES

The focus of this thesis is to show a comprehensive study of the ethanol bioelectro-oxidation on FCF electrode modified with the enzyme alcohol dehydrogenase (ADH). The main objectives are:

1 – To investigate the surface modification of FCF electrode with quinone by using an oxidative method and electrochemical grafting, in order to alter their interfacial properties.

2 – Ethanol bioelectrocatalysis using NAD-dependent ADH on quinone-functionalized carbon-based electrode surface by using molecular electrochemistry.

3 – To investigate the effect of quinone on the NADH electro-oxidation by using an *operando* electron paramagnetic resonance (*operando* EPR) spectroscopy.

3 EXPERIMENTAL PROCEDURES

The experimental section has been divided into six parts as shown in the flowchart in Figure 6.

Figure 6 - Flow chart representing the surface functionalization of FCF under different conditions along with their electrochemical and structural characterizations.

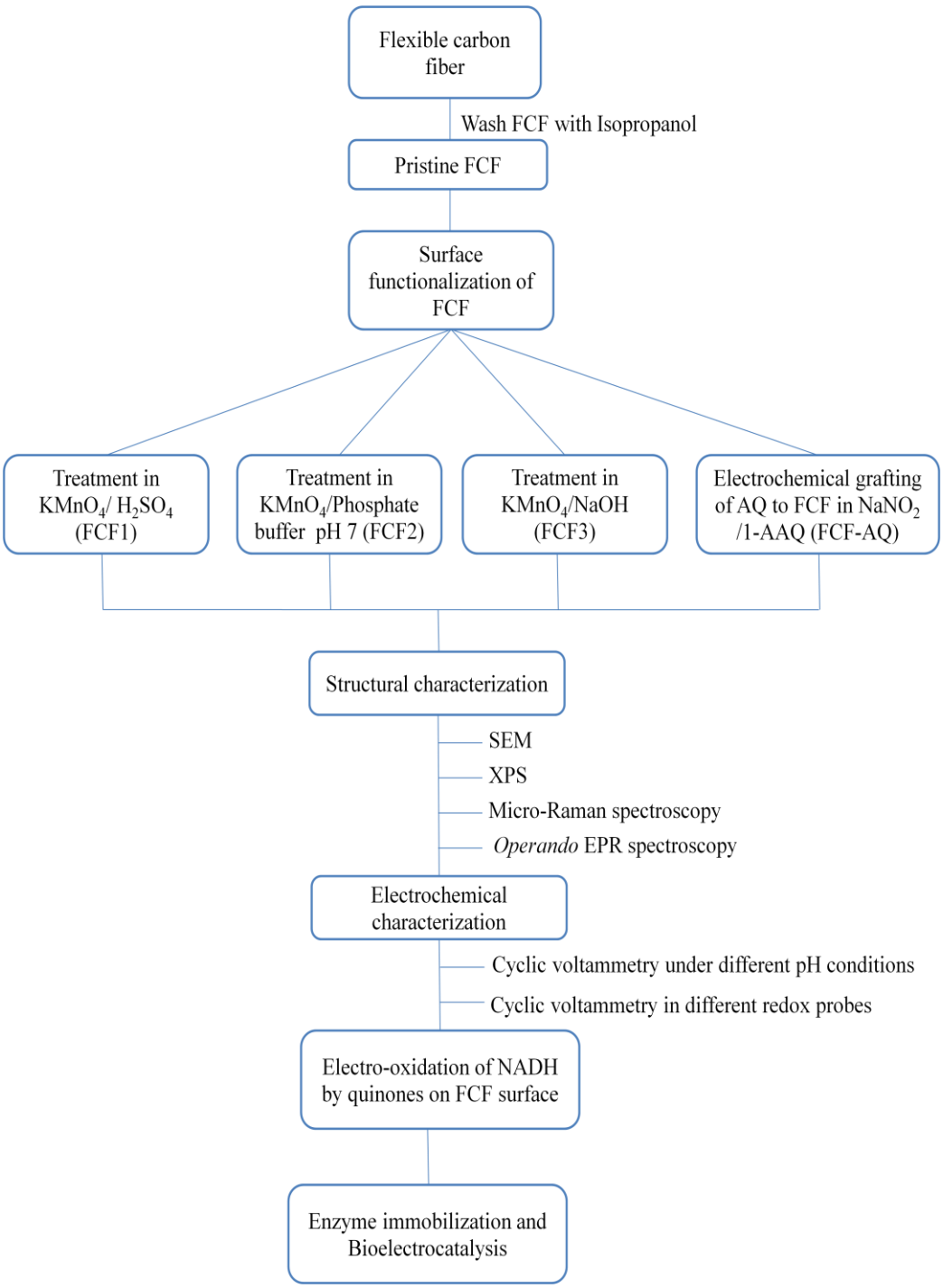

Source: Own authorship

The materials and reagents used throughout this work are described first (section 3.1). The second part described the surface functionalization of FCF under different conditions (section 3.2.). Third part describes the structural characterization of FCF using various characterization techniques, such as SEM, XPS, Micro-Raman and *operando* EPR spectroscopy (section 3.3). Section 3.4 describes the electrochemical characterizations using cyclic voltammetry under different pH conditions as well as in different redox probes. The fifth part represents the electro-oxidation of NADH by different quinone groups on FCF surface (section 3.5). The final part describes the immobilization of ADH and bioelectrocatalysis of ethanol oxidation to acetaldehyde by the enzyme ADH in the presence of co-enzyme NAD^+.

3.1 Materials and reagents

The FCF used as working electrodes were extracted from flexible carbon cloth (CCS200) and are obtained commercially from PAN precursor. The enzyme ADH from *Saccharomyces cerevisae* (EC 1.1.1.1) and absolute ethanol (extra pure) were purchased from Sigma-Aldrich. Nicotinamide adenine dinucleotide both reduced and oxidized form (≥97%); nafion® solution (5 wt %), sodium hydroxide (microbeads 99.99 %), 1-aminoathraquinone (97%), sodium nitrite (≥97%), potassium hexacyanoferrate (II) and potassium hexacyanoferrate (III) (99%) were purchased from Sigma-Aldrich. The monobasic and dibasic sodium phosphate salts (98-102%) used in the preparation of phosphate buffer solutions, sulfuric acid (97%), hydrochloric acid (37%), potassium chloride (99-100.5%) and potassium permanganate (99%) were purchased from Synth. All the solutions were prepared with deionized water and all the glassware were previously cleaned and dried. The temperature of all the electrolytes was controlled using a thermostatic bath (*GE-MultiTemp Thermostatic Circulator*).

3.2 Surface functionalization of FCF

To establish the experimental conditions two methodologies were used for the modification of FCF electrodes i.e the chemical functionalization through oxidative treatment and electrochemical functionalization through the electrochemical grafting of anthraquinone groups. The chemical functionalization involves the oxidative treatment of FCF by $KMnO_4$[3,34,42] under different pH conditions, i-e in H_2SO_4 solution (1.0 mol L^{-1}, pH 0), in sodium phosphate buffer solution (0.1 mol L^{-1}, pH 7) and in NaOH solution (1.0 mol L^{-1}, pH

14) containing 464 mg of $KMnO_4$ by the insertion of 0.5 g FCF. The system was kept on ultrasound for 3 hours. After that, the fibers were washed with HCl (37%) in order to remove the formed MnO_2 and then washed at least 10 times with distilled water to remove all the acid until the pH reached the neutral value. Finally, FCF were dried at room temperature, resulting in the formation of chemically modified FCF electrodes which were assigned as FCF1, FCF2 and FCF3, respectively.

The surface modification of FCF electrodes through electrochemical functionalization was carried out with in situ generated anthraquinone diazonium cation at low temperature in HCl solution (0.5 mol L^{-1}) containing 1-aminoanthraquinone (1.0 mmol L^{-1}). The $NaNO_2$ (4.0 mmol L^{-1}) was added to the reaction mixture 20 minutes before the electrochemical grafting.[47–49] The electrochemical grafting of AQ groups to FCF was performed by cycling the electrodes between -0.4 and 0.7 V versus $Ag/AgCl_{sat}$ in Ar saturated atmosphere at a scan rate of 100 mV s^{-1}.

3.3 Structural characterizations of FCF

The surface functionalization of FCF was confirmed by using different spectroscopic techniques such as scanning electron microscopy (SEM), x-rays photoelectron spectroscopy (XPS) and Micro-Raman spectroscopy, which allowed the determination of the structural alterations that occurred after each chemical treatment. Furthermore, *operando* EPR spectroscopy technique was used to investigate the presence of quinone radicals on the surface of modified FCF electrodes that can participate in the electro-oxidation of NADH to NAD^+.

3.3.1 Scanning electron microscopy (SEM)

The topographic morphology of the FCF surfaces were characterized by using scanning electron microscope (ZEISS LEO 440, Cambridge, England) equipped with a detector (model 7060, Oxford, Cambridge, England) and using an electron beam at 15KW to obtained the SEM images. This equipment has an accessory known as EDX (Energy-dispersive X-ray) spectroscopy, which allows the identification of the elemental chemical composition present in the molecule such as the presence of oxide groups (i-e *ortho* and anthraquinones) on FCF surface after treatment through area, punctual and in-line analyses.

3.3.2 X-rays photoelectron spectroscopy (XPS)

The chemical composition of FCF surface was further studied by X-ray photoelectron spectroscopy (XPS) using a conventional XPS spectrometer (ScientaOmicron ESCA+) with a high-performance hemispheric analyzer (EAC2000) with monochromatic Al Kα (h ν = 1486.6 eV) radiation as the excitation source. The operating pressure in the ultra-high vacuum chamber (UHV) during the analysis was 10^{-9} Pa. The XPS high resolution spectra were recorded at constant pass energy of 20 eV with a 0.05 eV per step. The inelastic noise of the high resolution spectra C 1s, N 1s and O 1s was subtracted using the Shirley method. The atomic percentage composition of the surface layer (<5 nm) was determined by the relative proportions of the areas of the spectra corrected by the Scofield atomic sensitivity factors, with an accuracy of ± 5%. The scale of the spectrum binding energy was corrected using the fixed hydrocarbon component at 285.0 eV. The spectra were deconvoluted using Voigtian type function, with combinations of Gaussian (70%) and Lorentzian (30%). The width at half height varied between 1.2 and 2.1 eV, and the position of the peaks was determined with an accuracy of ± 0.1 eV.

3.3.3 Micro-Raman spectroscopy

Micro-Raman experiments for FCF electrodes were conducted with Horiba Multiline Raman Spectrometer, model LabRam Evolution, with laser excitation at 532 nm. 50× (NA 0.55) objective lens was used, which allows collecting spectra with ca. 590 nm spatial resolution. First order Raman spectra were conducted in the range 800-1900 cm^{-1}. After data acquisition, the baselines of Raman spectra were corrected, and Lorentzian function was used to fit the peaks, then each spectrum was normalized by *G*-band intensity.

3.3.4 *Operando* electron paramagnetic resonance (OEPR) spectroscopy

The presence of quinone radicals on FCF surface was investigated by using an *operando* EPR spectroscopy which was carried out by using an EPR spectrometer Bruker EMXplus (Bruker, Biospin, Rheinstten, Germany) as shown by a photograph in Figure 7a, while Figure 7b represented a photograph of the electrochemical cell designed for use in aqueous electrolyte and was based on three electrodes system, the working electrode (FCF), counter electrode (Pt) and the reference electrode ($Ag/AgCl_{sat}$). The *operando* EPR electrochemistry of FCF electrode was carried out at ambient temperature (273 K). The other spectrum recording conditions were as follows; microwave power 2 mV, microwave

frequency 9.79 GHz, time constant 20.480 ms, conversion time 20.000, center field 3485 G, sweep time 40.960 s, modulation frequency 100 kHz, and modulation amplitude 1 G (Gauss).

Figure 7 - (a) *Operando* EPR set up. (b) *Operando* EPR electrochemical cell design; WE denoted FCF working electrode, RE represent the saturated Ag/AgCl reference electrode and CE denotes the Pt counter electrode.

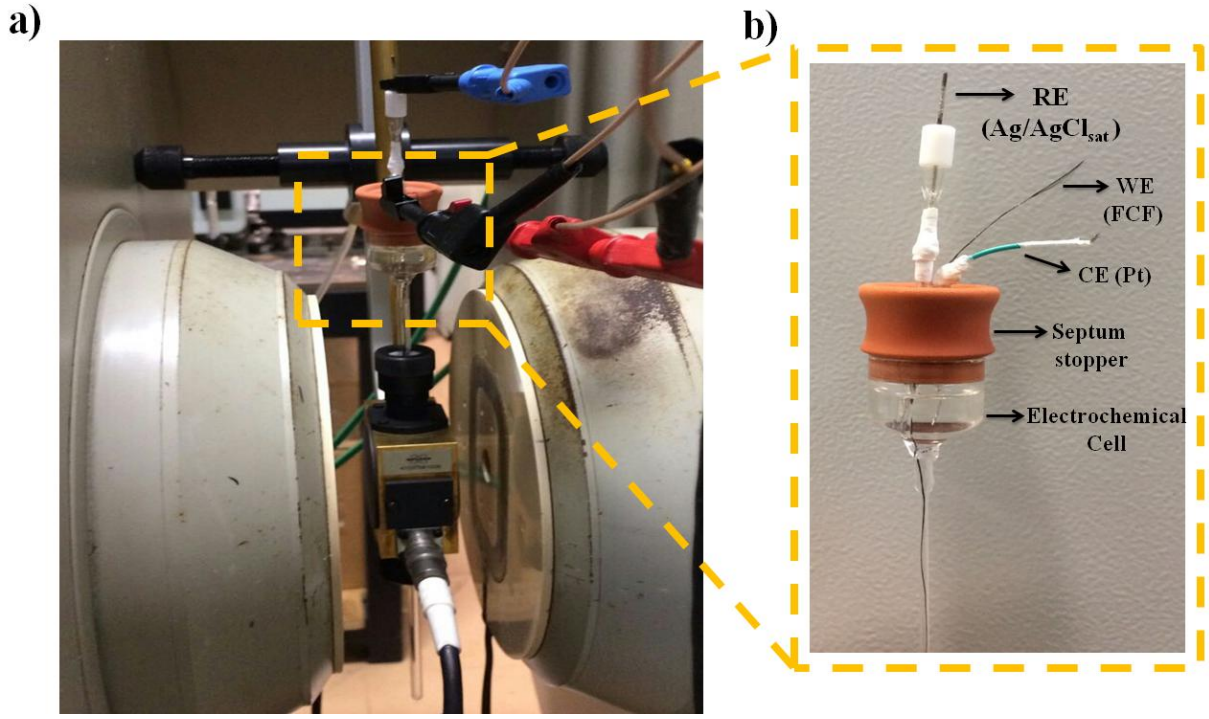

Source: Own authorship. The image represents *operando* EPR electrochemical setup.

3.4 Electrochemical characterization

The electrochemical properties of the modified and pristine FCF electrodes were evaluated by using different electrochemical techniques, including cyclic voltammetry, chronoamperometry, and measurements of the polarization curves. All the electrochemical measurements were performed by using a three electrodes system comprising the pristine FCF and FCF electrodes after chemical treatments as the working electrode, platinum as the counter electrode and a saturated Ag/AgCl as the reference electrode. Before the acquisition of data, the electrolyte solutions were purged with Ar gas for at least 20 minutes. The temperature of the electrolyte was controlled using a thermostatic bath (*GE-MultiTemp Thermostatic Circulator*) and the experiments were performed by using an Autolab PGSTAT128N Potentiostat-Galvanostat. During all the electrochemical measurements, the unmodified region of the working electrode that was in contact with the solution was

delimited with epoxy resin, with a final geometric area of approximately 0.2 cm^2. Figure 8 shows FCF electrode with an area delimited with epoxy resin in order to perform electrochemical analysis.

Figure 8 - (a) Flexible carbon fiber (FCF1) electrode with area delimited with epoxy resin. (b) Zoom region of FCF electrode with epoxy resin. The area of the given electrode is 0.8 cm^2 while the diameter of the electrode is 0.05 cm.

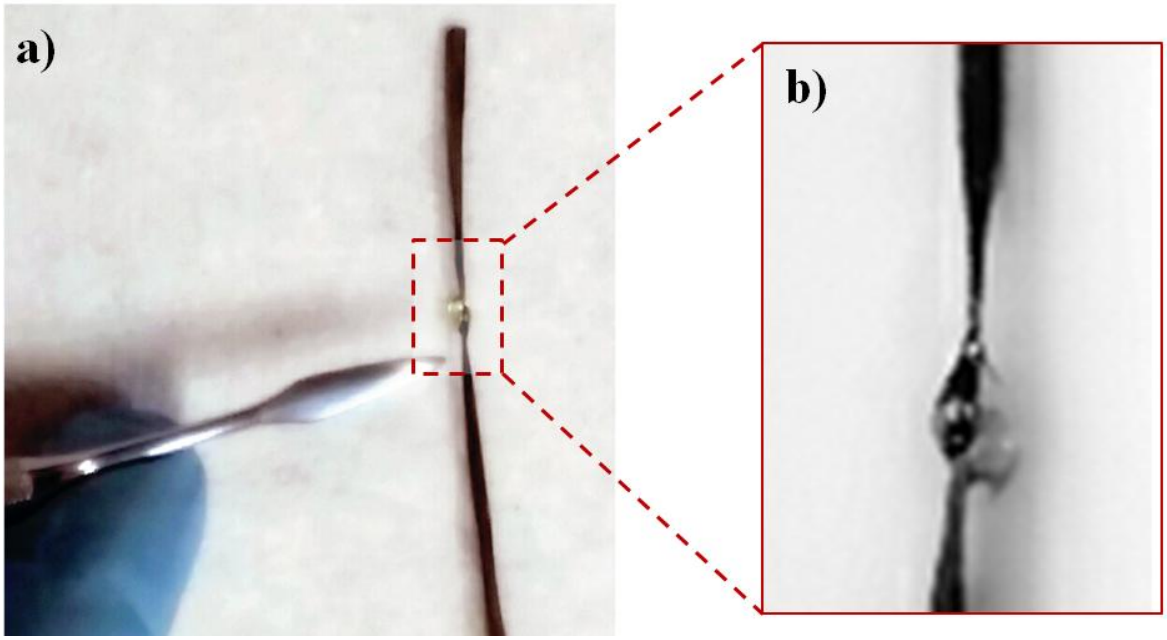

Source: Own authorship

3.4.1 Cyclic voltammetry

To evaluate the electrochemical properties of modified FCF electrodes standard cyclic voltammetry technique was applied. Cyclic voltammetry was performed at three different pH conditions; (i) H_2SO_4 solution (0.5 mol L^{-1}, pH 2.9), (ii) KOH solution (0.1 mol L^{-1}, pH 14) and (iii) sodium phosphate buffer solution (0.1 mol L^{-1}, pH 7.5).

Furthermore, the cyclic voltammetry of modified FCF electrodes was performed in the two different redox probes; $K_4[Fe(CN)_6]/K_3[Fe(CN)_6]$ (5.0 mmol L^{-1}) and $[Ru(NH_3)_6]Cl_2/[Ru(NH_3)_6]Cl_3$ (5.0 mmol L^{-1}) in the presence of a supporting electrolyte KCl (0.5 mol L^{-1}). Figure 9a-9b shows a photograph of carbon cloth and a single carbon fiber electrode extracted from carbon cloth (CCS200); 9c represents FEG-SEM image of a single carbon fiber array and Figure 9d shows FEG-SEM image of single carbon fiber in comparison with a single human hair, where we can clearly see that carbon fiber has a diameter (6.7 µm) much smaller than that of a single human hair (74.9 µm).

Figure 9 - Photographs of (a) Carbon cloth (CCS200); (b) carbon fiber; (c) FEG-SEM image of FCF electrode and (d) comparison of the diameter of a single strand of hair (74.89 μm) and a single carbon fiber (6.696 μm).

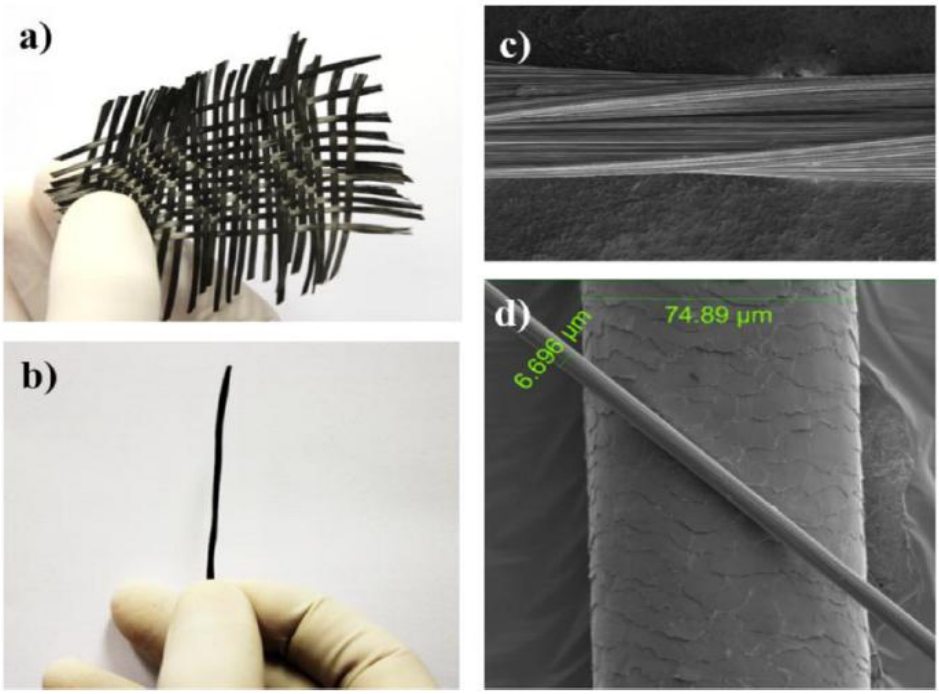

Source: Adapted from Pereira, A. R., Souza, J. C. P., Iost, R. M., Sales, F. C. P. F., Crespilho, F.N., 2016, p. 397.

3.4.2 Chronoamperometry

Chronoamperometry is a very powerful method for the quantitative analysis of a faradaic process occurring at the electrode (caused by the potential step). In chronoamperometry, the current is measured as a function of time as a response to the potential step perturbation of the working electrode. The resultant current is monitored, and its nature can be identified from variations with time. The chronoamperometry experiment was applied here to study the effect of modified FCF bioelectrodes on ethanol oxidation to acetaldehyde by the enzyme ADH in the presence of NADH. These experiments were carried out in sodium phosphate buffer solution (0.1 mol L^{-1}, pH 7.5) containing NAD^+ (0.6 mmol L^{-1}) and different concentrations of ethanol, each addition corresponds to an addition of 200 μL at 25 ° C.

3.4.3 Polarization curves

In order to investigate the electro-oxidation of NADH to NAD^+, the polarization curves were obtained during *operando* EPR spectroscopy at steady state (SS) current which was obtained from chronoamperometric plateau and was carried out in phosphate buffer (0.1 mol L^{-1}, pH 7.5) in the absence and in the presence of NADH (1.0 mmol L^{-1}) at different positive applied potentials, ranging from 0 V up to 0.8 V.

3.5 Electro-oxidation of NADH on quinone modified FCF surface

The electro-oxidation of NADH, on the surfaces of the modified FCF electrodes was investigated through cyclic voltammetry performed in the phosphate buffer solution (0.1 mol L^{-1}, pH 7.5) containing a definite concentration of NADH (1.0 mmol L^{-1}). The potential window (0.8 V to -0.2 V) used in these experiments for the chemically modified electrode was different from the potential window (0.9 V to -0.3 V) of electrochemically modified electrode. All the experiments were carried out in Ar saturated environment for at least 15-20 minutes prior to the recording of a cyclic voltammograms at a scan rate; 5 mVs^{-1} and T = 25 °C.

3.6 Enzyme immobilization on modified FCF electrodes

The modified FCF bioelectrodes were prepared through the physical adsorption of ADH enzyme according to the previously published protocol.[3–5] Enzyme immobilizations through physical adsorption is one of the simplest and easiest methods, and there is little loss of enzymatic activity. Briefly, an area of the modified FCF (0.2 cm^2) was treated with epoxy resin and dried, thereafter all of the electrodes were placed separately in an ADH enzyme solution (8.0 mg mL^{-1}) in sodium phosphate buffer (0.1 mol L^{-1}, pH 7.5) for 24 hours at 4 °C. Before doing the electrochemical evaluation of FCF electrodes, 20 µL of 2.5% nafion solution, which was prepared simply by mixing 1:1 of sodium phosphate buffer (0.1 mol L^{-1}, pH 7.5) and 5 % nafion solution, was dropped onto each FCF electrode modified with ADH and was finally dried under vacuum for about 10 minutes.

4 RESULTS AND DISCUSSION

4.1 FCF functionalized with quinones: pH effect and redox properties

Two methodologies were used for FCF surface functionalization; the first one is a one-point reaction with $KMnO_4$ under different pH conditions (pH 0, pH 7 and pH 14) to produce more robust and stable electrodes modified with quinones for application in bioelectrocatalysis such as ethanol bioelectrocatalysis and NADH bioelectrocatalysis. The electrodes prepared by this method were assigned FCF1, FCF2 and FCF3 notations, respectively. The second methodology involves covalent functionalization through electrochemical grafting of anthraquinone groups to FCF, the electrode names as FCF-AQ. The electrochemical functionalization to obtain FCF-AQ electrode was carried out in aqueous solution containing 1-aminoanthraquinone (1.0 mmol L^{-1}), $NaNO_2$ (4.0 mmol L^{-1}) and HCl (0.5 mol L^{-1}), thereafter the electrochemical grafting of anthraquinonyl (AQN) groups occurred to the surface of FCF electrode as can be seen by the cyclic voltammograms obtained shown in Figure 10a, whereby the formation of a reduction wave at 0.1 V vs. $Ag/AgCl_{sat}$ is indicative of AQN group's attachment to the surface of FCF. The decreasing in the reduction current and the formation of a well-defined redox peaks in the subsequent cycles are consistent with the surface functionalization.

Further characterization of this electrode was performed through cyclic voltammetry in potassium hydroxide (0.1 mol L^{-1}, pH 14) and sulfuric acid (0.5 mol L^{-1}, pH 2.9); and the result was compared with pristine FCF, FCF1, FCF2 and FCF3 electrodes as shown in Figure 10b and 10c, where we show a detailed study of the pH effects on the redox properties. Figure 10b shows cyclic voltammograms of all the modified electrodes in alkaline solution (KOH, pH 14), where the voltammograms for FCF-AQ (in green) presented well-defined redox process of the surface bound AQ groups, thus indicating the surface modification of the electrode while in all other cases (FCF1, FCF2 and FCF3) the presence of weakly resolved redox processes, suggests the surface modification as compared to pristine FCF, which are the consequences of oxidative treatment under different pH conditions. The difference between the two peak potentials ΔE_p (E_{pa} - E_{pc}) and midpoint potential ($E_{1/2} = E_{pa} + E_{pc}$)/2) for FCF1, FCF2, FCF3 and FCF-AQ electrodes are shown in Table 1. Furthermore, the surface concentration (Γ) of anthraquinone groups for FCF-AQ and *ortho*-quinone groups for FCF1, FCF2 and FCF3 electrodes was calculated from integration of the anodic peak by using equation 1.

$$\Gamma = \frac{Q}{nFA} \quad (1)$$

where Q is the amount of charge consumed, n is the number of electrons involved, *F* is the faraday constant and *A* is the geometric surface area. The value of anthraquinone (FCF-AQ) surface concentration was found to be 2.8 × 10^{-9} mol cm^{-2}, while these values were found to be 1.3 × 10^{-9} mol cm^{-2} for FCF1, 1.2 × 10^{-9} mol cm^{-2} for FCF2 and 1.7 × 10^{-9} mol cm^{-2} for FCF3 electrode, respectively.

Table 1 - ΔE_p and $E_{1/2}$ values of FCF1, FCF2, FCF3 and FCF-AQ electrodes.

Electrodes	ΔE_p	$E_{1/2}$
FCF1	0.12 V	-0.56 V
FCF2	0.10 V	-0.52 V
FCF3	0.20 V	-0.55 V
FCF-AQ	0.14 V	-0.78 V

Source: Own authorship

Figure 10 - (a) Cyclic voltammograms obtained during the electrochemical grafting of anthraquinone groups to an FCF electrode in a solution containing 1-aminoanthraquinone (1.0 mmol L^{-1}), $NaNO_2$ (4.0 mmol L^{-1}), and HCl (0.5 mol L^{-1}) in the potential range of -0.4 V to 0.7 V at a scan rate of 100 mV s^{-1}. (b) Cyclic voltammograms obtained in a KOH solution (0.1 mol L^{-1}) for pristine FCF (●), FCF1 (●), FCF2 (●), FCF3 (●) and FCF-AQ (●) at a scan rate of 50 mV s^{-1}. (c) Cyclic voltammograms obtained in a H_2SO_4 solution (0.5 mol L^{-1}) for pristine FCF (●), FCF1 (●), FCF2 (●), FCF3 (●) and FCF-AQ (●) at a scan rate of 50 mV s^{-1}. All experiments were performed in an Ar-saturated atmosphere.

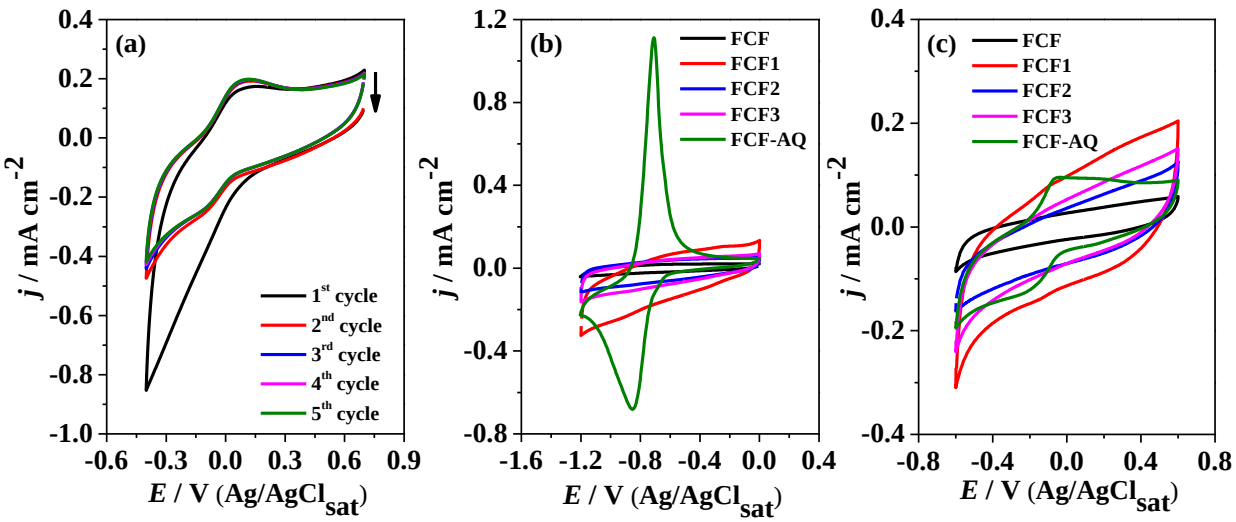

Figure 10c shows the cyclic voltammograms of all the modified electrodes in sulfuric acid solution (0.5 mol L^{-1}, pH 2.9), where a broad and ill-defined cathodic and anodic waves were seen for FCF-AQ, FCF1, FCF2 and FCF3 electrode, where the difference in the cyclic voltammograms profiles is due to decreased in the pH of the electrolyte and different position of the bond between quinone molecules and the electrode. That's why the shape and position of the redox peaks are greatly affected by the pH of the electrolyte, while a good reversibility of the redox couple was observed at alkaline pH for FCF-AQ electrode[47–49] as compared to FCF1, FCF2 and FCF3 electrodes as can be seen very clearly by the cyclic voltammograms in Figure 11d. Figure11 shows the cyclic voltammograms for FCF1, FCF2, FCF3 and FCF-AQ electrodes performed in KOH solution (0.1 mol L^{-1}, pH 14) at different scan rates ranging from 50 mV s^{-1} up to 500 mV s^{-1}, where FCF-AQ electrode (Figure 11d) has shown high reversibility and higher current densities of the anodic (j_{pa}) and cathodic (j_{pc}) peak potentials as compared to the other modified electrodes, the difference between the two peak potentials ΔE_p is given in Table 1.

Figure 11 - Cyclic voltammograms obtained in KOH solution (0.1 mol L^{-1}, pH 14) for (a) FCF1; (b) FCF2; (c) FCF3 and (d) FCF-AQ in Ar-saturated environment at different scan rates; 50 mV s^{-1} up to 500 mV s^{-1}.

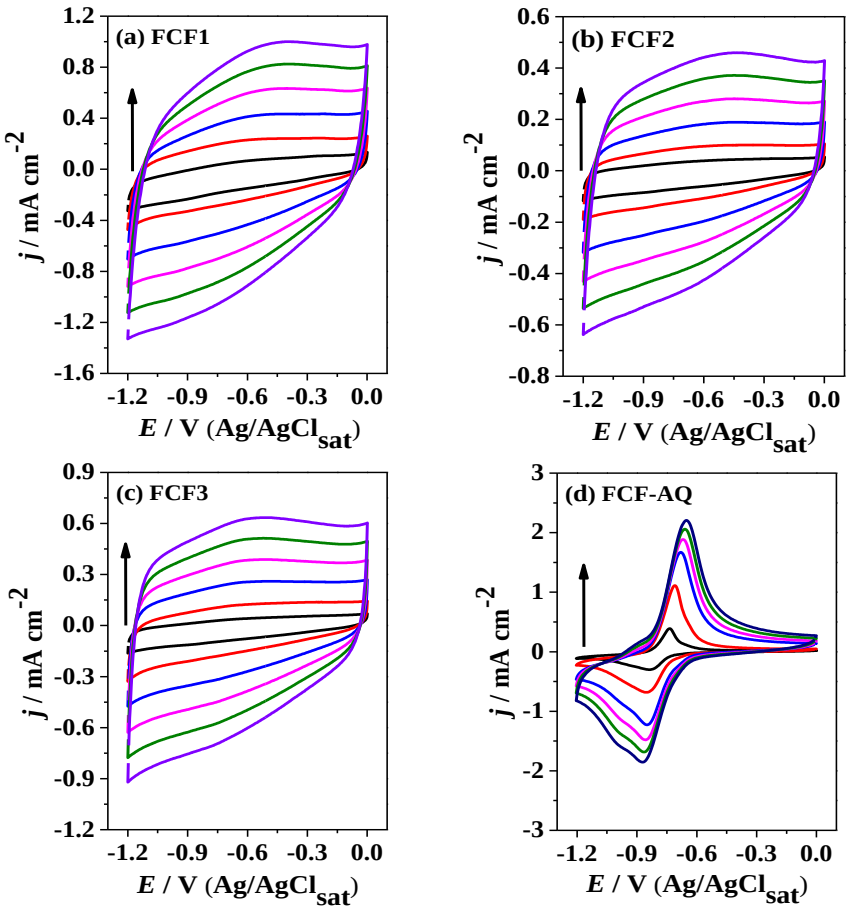

The electrodes are the same in Figure 10b and Figure 11 but the ionic conductivity of the electrolyte are different for FCF1, FCF2 and FCF3 electrodes that's why the cathodic and anodic peak current are different. Moreover, Figure 11a-c are showing the capacitive behavior, visually Figure 11a showing more capacitive current and this could be because of the high ionic conductivity of H_2SO_4 as compared to the neutral (phosphate buffer pH 7) and alkaline electrolyte (NaOH pH 14). The asymptotic behavior is may be because of the resistivity of the electrode and the interface between electrode and electrolyte. The rate capability of these electrodes are high because with increasing the scan rate the current density increases in a symmetric way even at high scan rate of 500 mV s^{-1}. Figure 11d is showing purely redox behavior due to the redox activity of the diazonium ion coupled with capacitive current. For better understanding of Figure 10b, we have plotted the cyclic voltammograms of FCF1, FCF2, FCF3 and FCF-AQ electrodes shown in Figure 11 at different scan rates ranging from 50 up to 500 mV s^{-1} which shows exactly the same behavior given in Figure 10b.

4.2 Scanning electron microscopy (SEM) and energy dispersive X-ray spectroscopy (EDX)

The surface morphology of both the pristine and functionalized FCF electrodes were characterized through scanning electron microscopy (SEM) and the SEM images obtained are shown in Figure 12. Figure 12a shows the SEM image of pristine FCF which exhibits the uniform surface with parallel lines along the surface, with shallow grooves. This morphology is the characteristic of carbon fibers obtained by the carbonization process of PAN filaments through wet spinning procedure. Figure 12b-12d are the SEM images of FCF1, FCF2 and FCF3 electrode at different magnifications, which shows an increase in the depth of the grooves and the formation of defects on the surface that are related to the presence of oxygenated functional groups such as *ortho*-quinones, where the basal planes on the surface are cracked allowing the separation of the 2D graphite layers in the exposed edge planes and these results are consistent with the literature.[3,34,42,73] On the other hand Figure 12e shows the SEM images of FCF-AQ electrode at different magnifications; where the surface is more rough, the stretches are wider and deeper and some defects are generated on the surface suggesting the formation of anthraquinones on FCF surface. Based on the SEM images it can be inferred that the surfaces of all the FCF electrodes are modified with the oxygenated functional groups such as quinones that actively participate in the electro-oxidation of NADH.

EDX was used to obtain information about elemental composition of FCF. Among the important aspects in the measurement of EDX, it is worth mentioning that the acceleration of the electrons in the equipment influences the size of the interaction volume and in the depth of penetration of the electron beam, in the signals generated are of micrometric order, therefore it is an elementary analysis of the bulk of the material. The region analyzed by EDX is approximately 1 μm. According to the microanalysis, pristine FCF is composed of 98.93% of carbon and 1.07% of oxygen, which when subjected to the oxidative treatments increases the percentage of oxygen to 18.34%, 11.89%, 11.18% and 16.56% for the FCF1, FCF2, FCF3 and FCF-AQ treatments, respectively. This shows that oxidation of FCF2 and FCF3 treatment was more mild and superficial, while treatment FCF1 treatment was more aggressive. Table 2 presents the percentage values of the composition of FCF electrodes analyzed by EDX.

Figure 12 - Scanning electron microscopy images at different magnifications of (a) pristine FCF; (b) FCF1; (c) FCF2; (d) FCF3; and (e) FCF-AQ electrodes**.**

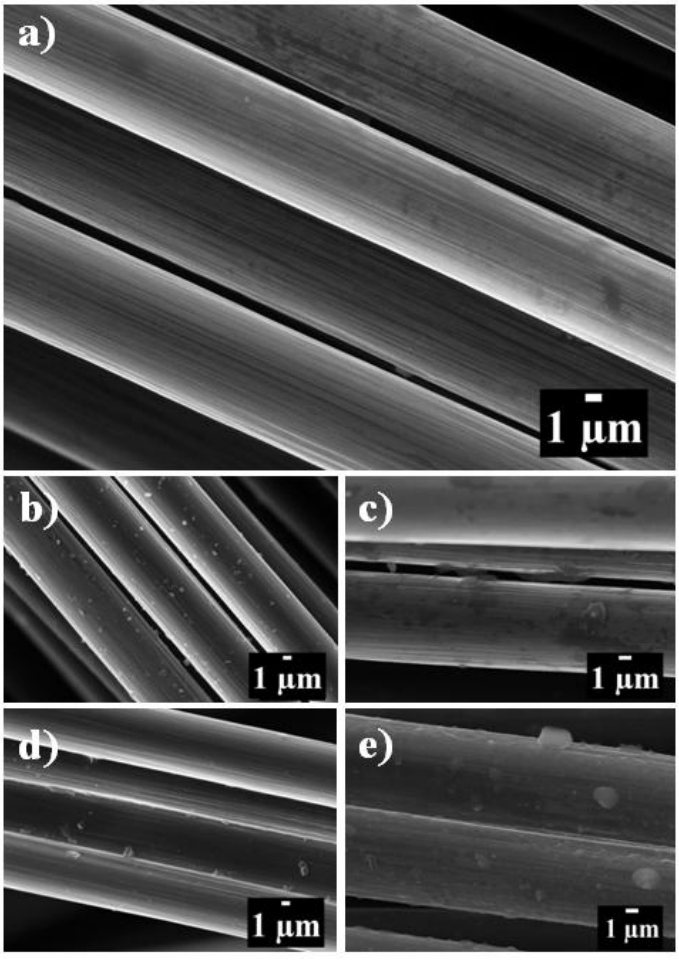

Table 2 - Elemental chemical composition of pristine FCF, FCF1, FCF2 and FCF3 electrodes obtained by EDX.

Electrode	% Carbon	% Oxygen
FCF	98.9 %	1.1 %
FCF1	81.7 %	18.3 %
FCF2	88.1 %	11.9 %
FCF3	88.8 %	11.2 %
FCF-AQ	83.4 %	16.6 %

Source: Own authorship

4.3 X-rays photoelectron spectroscopy (XPS)

The chemical composition of the modified FCF surfaces was further confirmed by using XPS, in which the sampling depth is 3-10 nm. The elemental analysis of the surface (5 nm layer) of FCF was performed by using XPS. Figure 13 shows the total XPS survey spectrums of (a) pristine FCF, (b) FCF1, (c) FCF2, (d) FCF3 and (e) FCF-AQ suggesting that mainly they are composed of carbon and oxygen but, there are also nitrogen and silicon contaminations. The presence of nitrogen is due to the fact of using PAN precursor in the manufacture of FCF, since the presence of silicon occurs, because silicone is used so that the FCF do not agglutinate in the carbonization process.[36] The silicon peaks persist even after the FCF are subjected to the chemical treatments, but with attenuated intensity. The percentage composition of carbon and oxygen for all the modified FCF electrodes were given in Table 3 and the values were compared with pristine FCF electrode.

Table 3 - Elemental chemical composition of pristine FCF, FCF1, FCF2, FCF3 and FCF-AQ electrodes obtained by XPS.

Electrode	% Carbon	% Oxygen
FCF	78.7 %	21.3 %
FCF1	87.5 %	12.5 %
FCF2	89.3 %	10.7 %
FCF3	84.6 %	10.4 %
FCF-AQ	87.5 %	12.5 %

Source: Own authorship

The results of the XPS elemental analysis corroborate with the results of EDS, since both the techniques show that the FCF consist essentially of carbon and oxygen. A peculiarity of the technique of XPS versus EDS is that from it, it is possible to detect nitrogen, which is possibly present in the whole structure because the fiber is obtained from the PAN. Since the other elements are only adsorbed to the surface due to the processes of treatment and manufacture, these elements are: chlorine, sulfur and silicon. Comparing the two techniques, we can also verify that the pristine FCF and modified FCF electrodes presented a high percentage of oxygen on the surface in the XPS spectrum, whereas for the EDS technique the percentage of carbon is much higher for these fibers.

Figure 13 - Total XPS spectra of (a) pristine FCF; (b) FCF1; (c) FCF2; (d) FCF3 and (e) FCF-AQ electrodes in the C 1s and O 1s region.

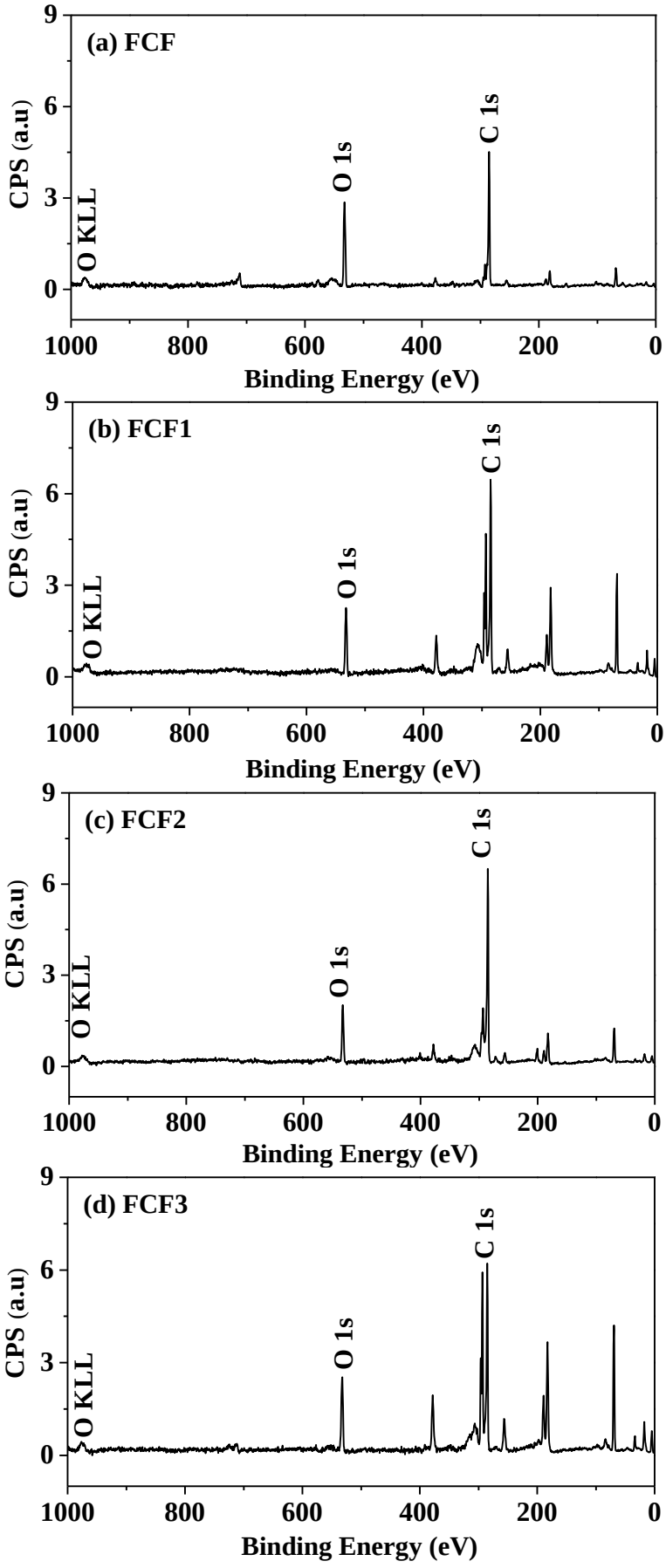

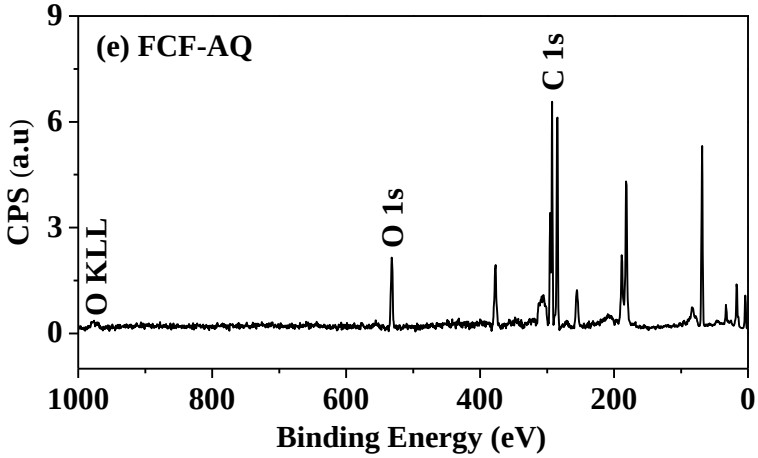

In order to obtain chemical information on the surface of pristine FCF, FCF1, FCF2, FCF3 and FCF-AQ electrodes, XPS spectra were recorded. Figure 145a-14e shows the deconvoluted C 1s core-level XPS spectra for FCF1, FCF2, FCF3 and FCF-AQ electrodes and the results were compared with pristine FCF. Compared to the XPS spectra of pristine FCF electrode; The C 1s spectra for FCF1 electrode was fitted with five peaks using pseudo-Voigt function, while a total of four peaks were observed for FCF2, FCF3 and FCF-AQ electrodes. For all electrodes, peak I is attributed to sp^2 carbon (C-C aromatic) observed at 284.7 eV for pristine FCF, 283.9 eV for FCF1, 284.7 eV for FCF2, 284.5 eV for FCF3 and 284.4 eV for FCF-AQ electrode. The presence of sp^3-bonded carbon atoms (C-H, C-N) is indicated by peak II located at 284.5 eV for FCF1, 285.3 eV for FCF2, 285.0 eV for FCF3 and 285.1 eV for FCF-AQ electrode. Peak III belongs to phenolic, alcohol, or ether groups and is obtained at 286.1 eV for pristine FCF, 285.1 eV for FCF1, 285.7 eV for FCF2, 285.3 eV for FCF3 and 286.1 eV for FCF-AQ electrodes. Carbonyl or quinone groups are associated with peak IV and are observed at 286.0 eV for FCF1 ,288.4 eV for FCF2, 288.4 eV for FCF3 and 288.2 eV for FCF-AQ.[3,73]

The surface concentration of different functional groups, as calculated on the basis of the peaks observed in the XPS spectra, are shown in Figure 14f, where a decrease in the concentration of sp^2 carbon and increase in the concentration of sp^3 carbon (C-H, C-N) were observed for FCF1, FCF2, FCF3 and FCF-AQ electrodes, respectively, which clearly confirms the surface functionalization of these electrodes. However, most of the studies report that sp^3 C peaks to be higher than sp^2 C peaks, although few literature data reported this information in the opposite way.[74] On the other hand, the increase in the carbonyl peak at 286.0 eV for FCF1, 288.4 eV for FCF2, 288.4 eV for FCF3 and 288.2 eV for FCF-AQ clearly confirm the formation of quinone molecules on their surfaces.

Figure 14 - Deconvoluted XPS spectra of the FCF electrodes. (a) FCF pristine, (b) FCF1, (c) FCF2, (d) FCF3 and (e) FCF-AQ shows the C 1s spectrum and figures; (■) carbon sp^2, (●) carbon sp^3, (▶) C–O, (◀) C=O, (▼) O–C=O, (♦) plasmon π-π*, black line is the total C 1s spectra and green line the background. (f) Plot of concentration vs. functional groups of all the electrodes.

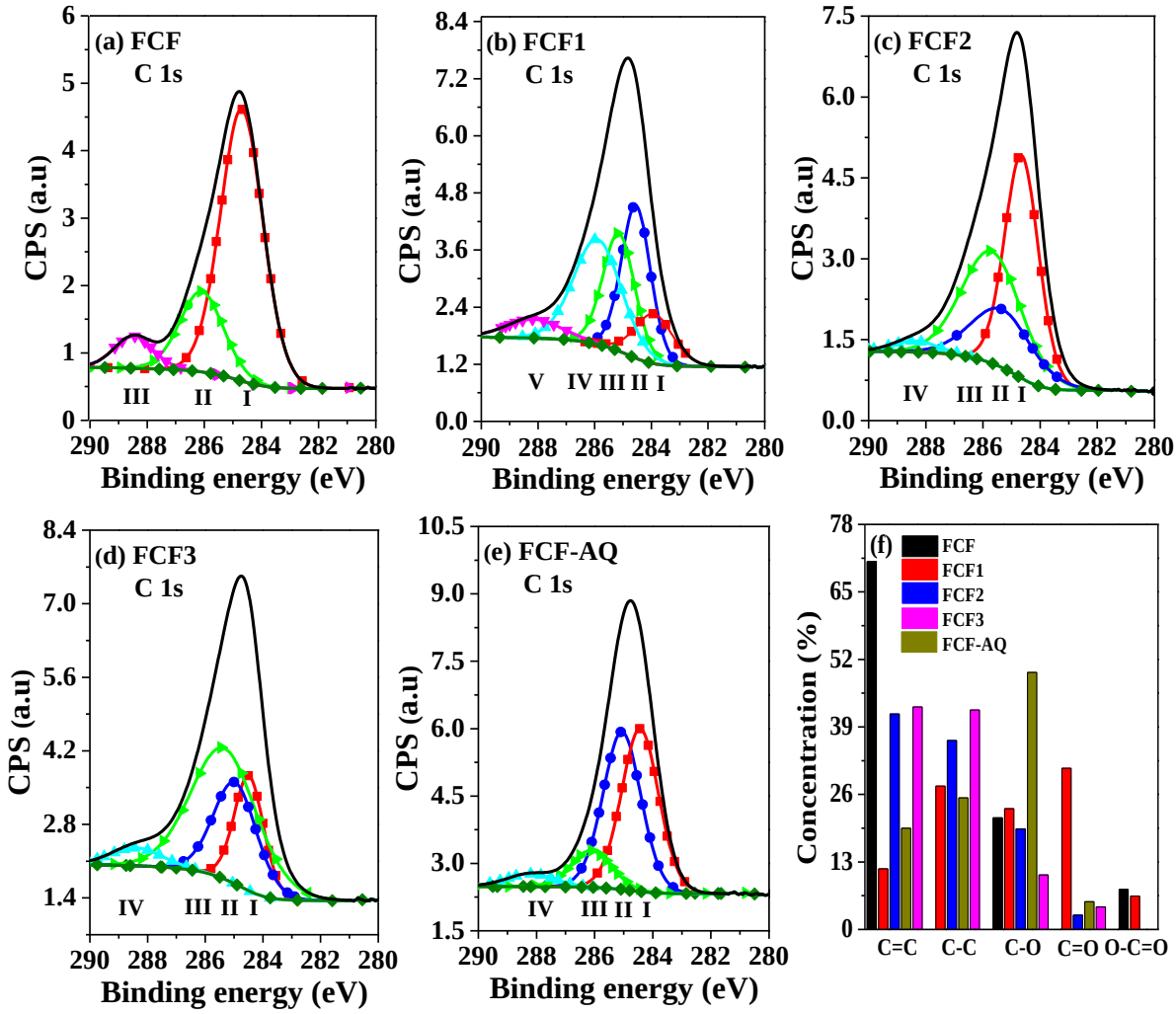

Figure 15a-15e shows the deconvoluted XPS spectra in the O 1s region for pristine FCF, FCF1, FCF2, FCF3 and FCF-AQ electrodes, where three peaks were observed for all the electrodes; here peak I is related to carbonyl or quinone and is observed at 531.0 eV for pristine FCF, 531.62 eV for FCF1, 531.49 eV for FCF2, 531.45 eV for FCF3 and 531.45 eV for FCF-AQ electrodes. Peak II corresponds to carbon in phenolic, alcoholic or ether groups, which is observed at 532.05 eV, 532.62 eV, 532.83 eV, 532.51 eV and 532.74 eV for pristine FCF, FCF1, FCF2, FCF3 and FCF-AQ electrodes, respectively. Additional peaks were observed at 533.05 eV for pristine FCF, 533.57 eV for FCF1, 533.83 eV for FCF2, 533.51 for FCF3 and 533.74 eV for FCF-AQ electrodes, respectively, which correspond to carboxylic acids. The deconvoluted XPS spectra in the O 1s region corroborate the spectra in the C 1s

region, exhibiting an increase in the surface oxidation for both electrodes. The increase in the surface oxidation can be observed by the decrease in the intensity as well as concentration of C-O groups after treatments. Figure 15f shows a decrease in the concentration of C-O groups and an increase in the concentration of C=O groups on the FCF1, FCF2, FCF3 and FCF-AQ electrodes compared to pristine FCF.

Figure 15 - Deconvoluted XPS spectra of the FCF electrodes. (a) pristine FCF; (b) FCF1; (c) FCF2; (d) FCF3 and (e) FCF-AQ shows the O 1s spectrum and figures; (■) C=O, (●) C–O, (▼) O–C=O, (♦) plasmon π-π*, black line is the total C 1s spectra and green line the background. (f) Plot of concentration vs. functional groups of all the electrodes.

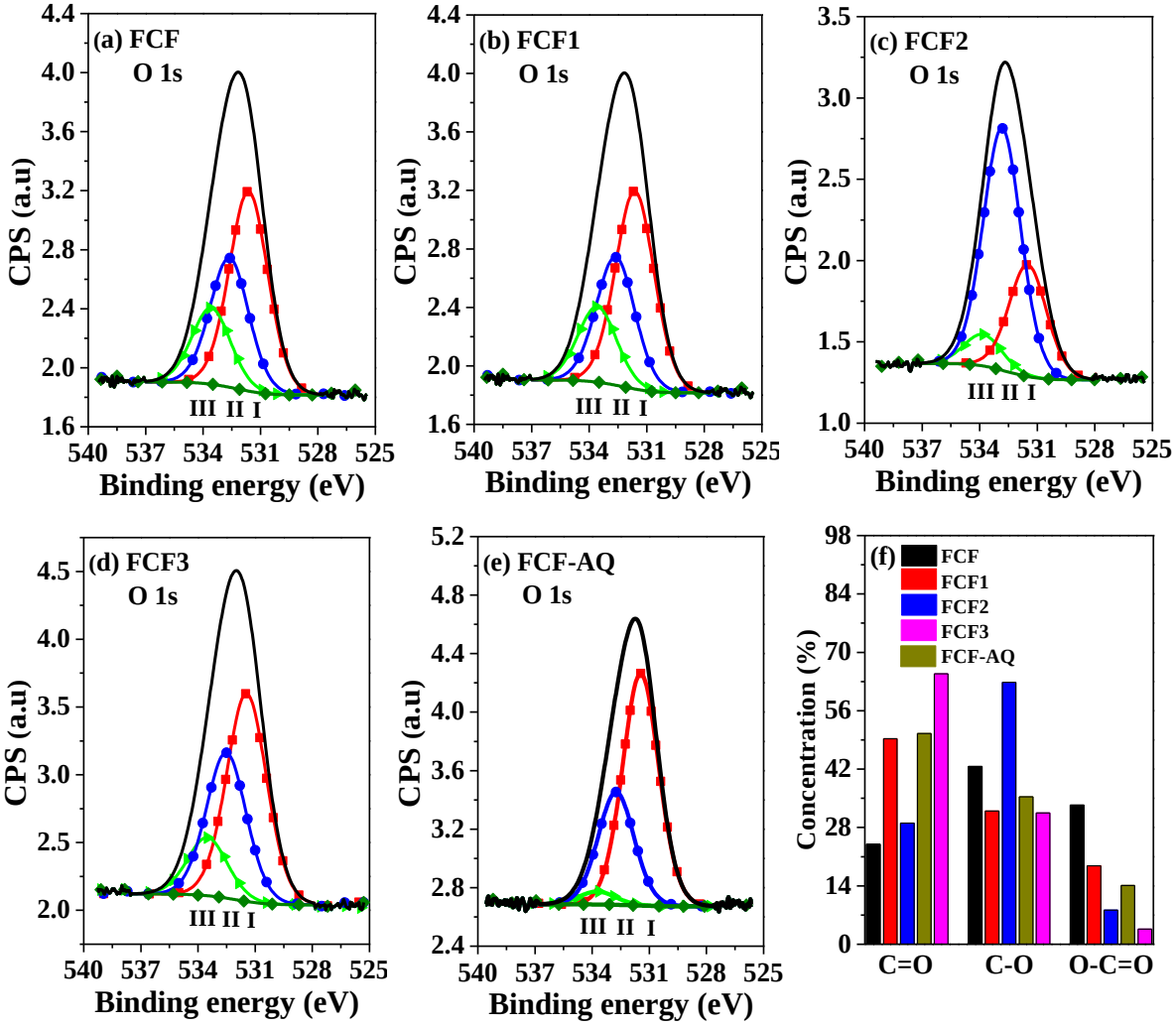

The carbon atoms in the C-O groups have a lower oxidation number when compared with C=O and O-C=O in the O 1s region of XPS spectra.[3,73] The increase of these peaks also revealed that FCF was oxidized successfully. It is confirmed from several studies describes elsewhere,[75,76] that XPS is one of the better technique to investigate the formation of oxygen

containing functional groups on these kind of surfaces. Based on XPS results, the increase of C=O species on FCF1 and FCF-AQ surface in the C 1s regions affect drastically the NADH oxidation, thus enhancing the electro-oxidation of NADH to NAD^+ with a possible reduction of quinone to dihydroquinone, respectively.

4.4 Micro-Raman spectroscopy of FCF

Micro-Raman spectroscopic measurements were conducted in order to investigate the introduction of defects on FCF structure by the functionalization methodologies. Micro-Raman spectra were collected for FCF1 and FCF-AQ electrodes in comparison with pristine FCF electrode, mainly because of their better electrochemical properties as discussed earlier. Figure 16a-16c shows the Raman spectra and curve fitting for pristine FCF, FCF1 and FCF-AQ electrodes. Figure 16d shows the first-order region of the Raman spectra of pristine FCF, FCF1 and FCF-AQ electrodes. Each spectrum consists of two main characteristics bands, namely *D*- and *G*-bands centered at about 1365 cm^{-1} and 1603 cm^{-1}, respectively. *G*-band is associated with the presence of sp^2 carbon networks in the sample, while *D*-band is a defect induced Raman feature, which is related to the presence of amorphous or disordered carbon forms.[77] The line decomposition of the raw spectra shows the presence of weak shoulder, the *A*-band at 1555 cm^{-1}. This band is assigned to amorphous forms of carbon[78] and is commonly observed in carbon fibers.[79,80]

Table 4 - Peak positions of *D, G and A* bands and the calculated I_D/I_G ratios for pristine FCF, FCF1 and FCF-AQ electrodes.

Electrode	*D*-band position (cm^{-1})	*G*-band position (cm^{-1})	*A*-band position (cm^{-1})	I_D/I_G
FCF	1369	1603	1551	0.98
FCF1	1364	1603	1550	1.27
FCF-AQ	1368	1602	1557	1.03

Source: Own authorship

The ratio of intensities between the *D*- and *G*-bands (I_D/I_G)[77] was used for characterizing the defect quantity present in the carbon fibers promoted by the surface modification methodologies. The calculated values of I_D/I_G were 0.98, 1.27 and 1.03 for pristine FCF, FCF1 and FCF-AQ, respectively, as shown in Table 4. According to the literature, the greater the values of the ratio of *D*- and *G*-bands, the greater the number of defects in the hexagonal carbon structure.[81–88] Since the values of I_D/I_G increase with increasing disorder,[77] the results indicate that the introduction of quinone functionalities by both methodologies increases the quantity of defects on the carbon fiber structure. In addition, it can be concluded that the chemical treatment with $KMnO_4$ under acidic condition promotes larger number of defects on FCF surface than the functionalization through electrochemical grafting.

Figure 16 - Raman spectra and curve fitting of (a) pristine FCF; (b) FCF1 and (c) FCF-AQ. (d) Raman spectra of pristine FCF (●), FCF1 (●), and FCF-AQ (●) electrodes along with their relative intensity ratio (I_D/I_G).

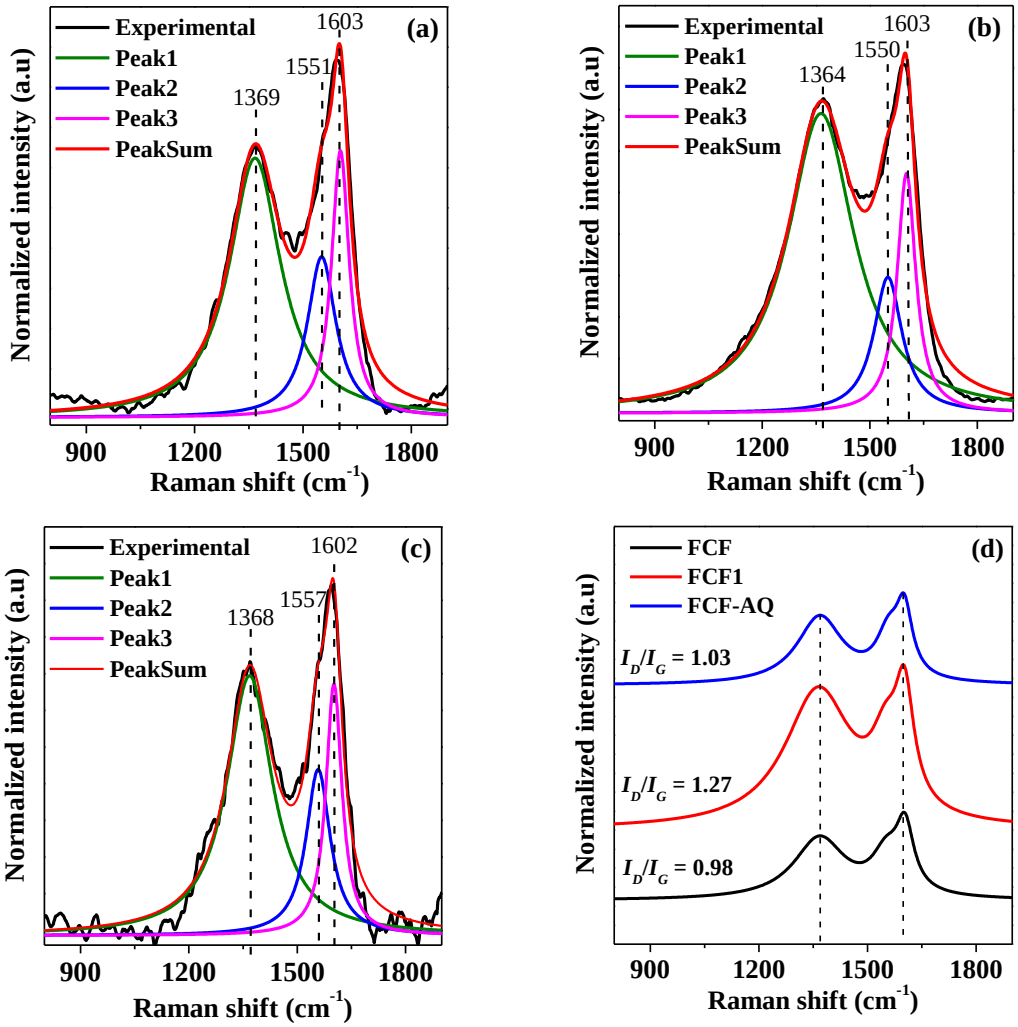

4.5 Heterogeneous electrons transfer rate

The effect of scan rate on the electrochemical redox properties of quinone molecules were investigated in sodium phosphate buffer (0.1 mol L^{-1}, pH 7.5) at different scan rates ranging from 50 mV s^{-1} to 1000 mV s^{-1} for the chemically modified FCF electrodes (viz. FCF1, FCF2 and FCF3), while from 50 mV s^{-1} to 500 mV s^{-1} for electrochemically modified FCF-AQ electrodes as shown in Figure 17a-17d, where a linear increase in the oxidation of current is observed concomitantly with the increase in the scan rates, revealing the presence of *ortho*-quinone molecules on FCF1, FCF2, FCF3 and anthraquinone molecule on FCF-AQ surface. On the basis of these results, it can be concluded that the shape of the redox peaks are greatly affected in acidic electrolyte (pH 2.9) as compared to the alkaline electrolyte (pH 14 and pH 7.5). Figure 17e-17h shows dependence of current densities of the anodic (j_{pa}) and cathodic (j_{pc}) peaks as a function of scan rate for both the modified electrodes; where an increase in the scan rate promoted an increase in the current densities of oxidation (j_{pa}) and reduction (j_{pc}) peaks. A linear relationship was observed in the range from 50 mV s^{-1} to 1000 mV s^{-1} for chemically modified FCF electrodes and from 50 mV s^{-1} to 500 mV s^{-1} for electrochemically modified FCF-AQ electrodes. These results indicate that the electrochemical processes are governed by the transfer of electron at the solution-electrode interface.

The cyclic voltammetry results of modified FCF electrodes have been shown in Figure 17. As shown in Figure 17a, the electrode (FCF1) has shown high reversibility as well as higher current densities of the anodic and cathodic peak potentials as compared to Figure 17b and 17c. Figure 17d (FCF-AQ) shows entirely different behavior in terms of peak current densities and peak potentials. The values of E_{pa} and E_{pc} determined from cyclic voltammograms are -0.05 V and -0.13 V for FCF1 and -0.33 V and -0.84 V for FCF-AQ, respectively. Figure 18 shows the cyclic voltammograms of both the modified FCF electrodes obtained after the subtraction of the capacitive currents, where both the chemically and electrochemically modified FCF1 and FCF-AQ electrodes have shown the higher faradaic response revealing that charge-transfer reactions occur at electrode-solution interface.

Figure 17 - Cyclic voltammograms obtained in sodium phosphate buffer solution (0.1 mol L^{-1}, pH 7.5) for (a) FCF1; (b) FCF2; (c) FCF3 and (d) FCF-AQ. (e-h) Dependence of current densities of the anodic (j_{pa}) and cathodic (j_{pc}) peaks as a function of scan rate ranging from 5 mV s^{-1} up to 100 mV s^{-1} in Ar-saturated environment at T = 25 °C.

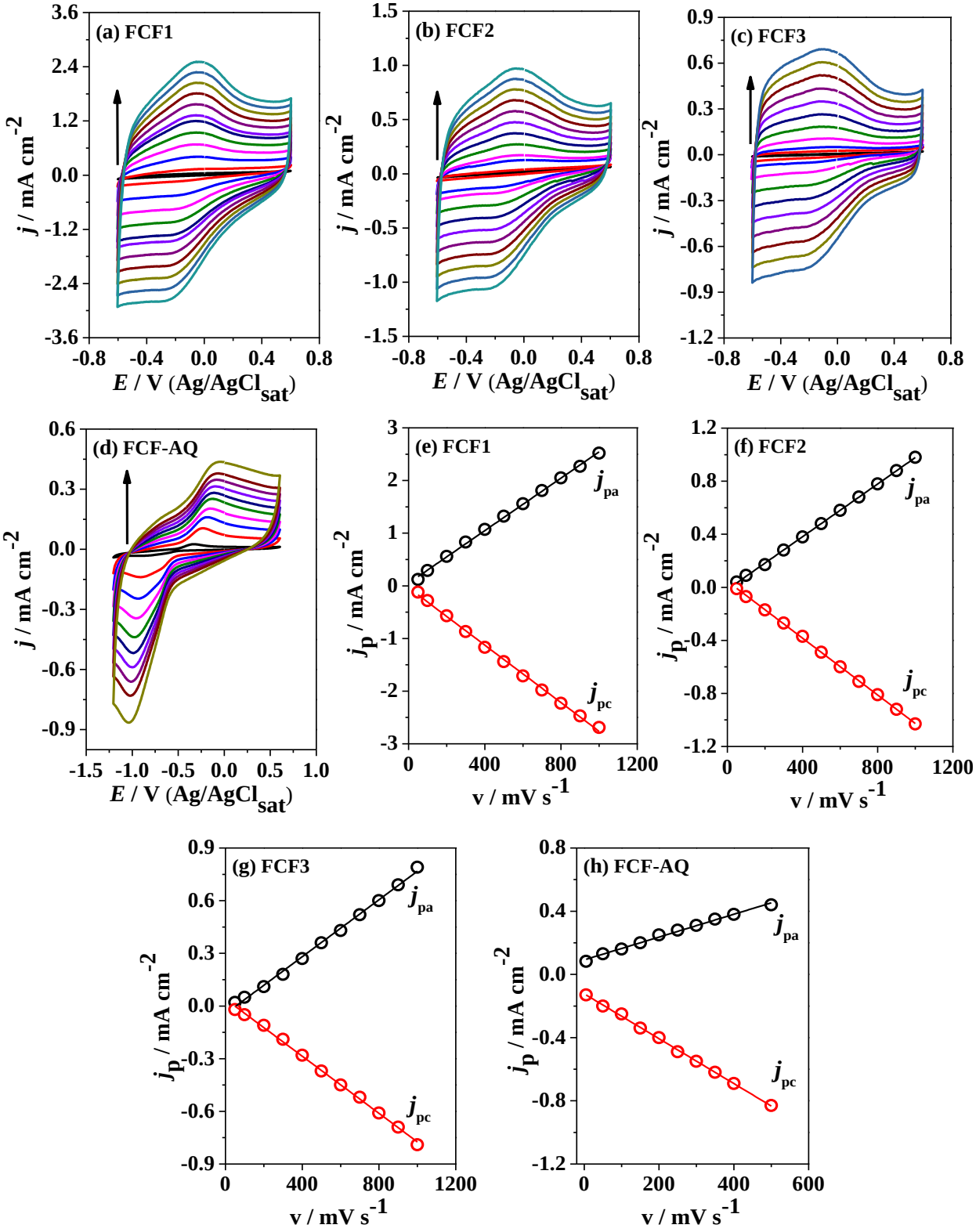

Figure 18 - Cyclic voltammograms after subtraction of the capacitive currents obtained in sodium phosphate buffer solution (0.1 mol L^{-1}, pH 7.5) for (a) FCF1; (b) FCF2; (c) FCF3 and (d) FCF-AQ in Ar-saturated environment at different scan rates; 5 mV s^{-1} up to 1000 mV s^{-1} and T = 25 °C.

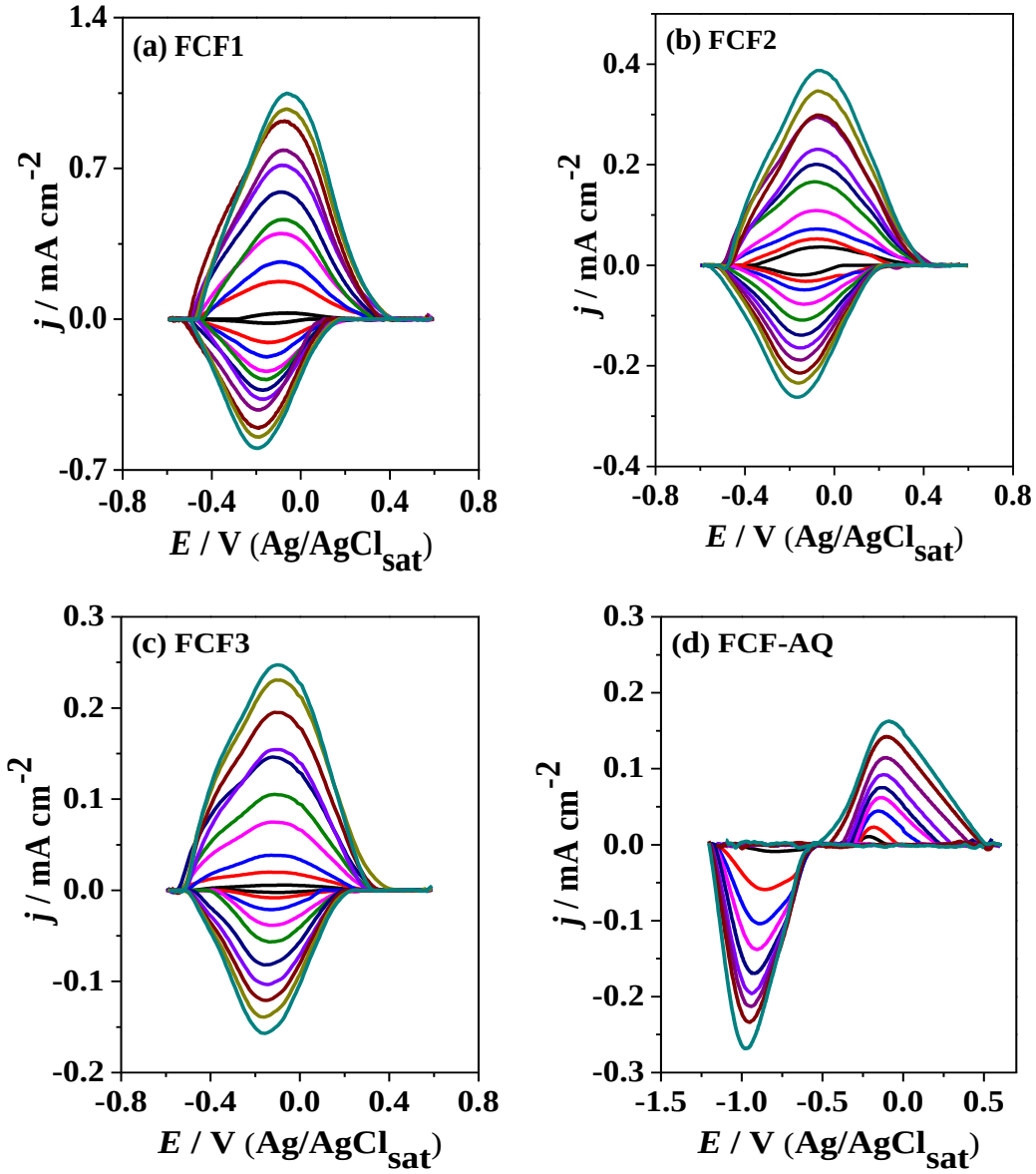

Figure19a-19d shows variation of anodic and cathodic peak overpotential ($E - E^0$) as a function of log (ν) for FCF1, FCF2, FCF3 and FCF-AQ electrodes. By using Butler–Volmer (BV) approach, which describes a semi-empirical exponential dependence of the rate constants with the overpotential ($E - E^0$), $k_{oxi/red}$ were obtained according to equation 2 and 3:

$$k_{\mathrm{red}} = k^0 \ exp(-\alpha nF(E - E^{0'})/RT) \quad (2)$$

$$k_{\mathrm{oxi}} = k^0 \ exp(1 - \alpha)nF(E - E^{0'})/RT) \quad (3)$$

Where, k^0 is the standard rate constant at zero overpotential (s^{-1}), R is the universal gas constant (J K^{-1} mol^{-1}), F is the faraday constant (C mol^{-1}), T is the temperature (K), n is the number of electrons transferred (C), and α is the transfer coefficient representing the degree of symmetry of the energy barrier of the redox reaction. In an ideal solution, the symmetrical case is represented by α = 0.5. However, α has been observed to deviate from 0.5 in several cases;[29,30] thus, the determination of α is crucial for estimating $k_{oxi/red}$ value. Generally, α may be experimentally estimated from the slope of the straight lines of E_{pa} and E_{pc} versus log (ν) by using the mathematical treatment proposed by Laviron,[29,30] according to equation 4 and 5, Once the value of α is known, k^0 can be calculated by using equation 6, where ν_a and ν_c are the x-intercepts of the anodic and cathodic lines, respectively.

$$Slope\ (E_{pa}\ vs.\ log\ \nu) = \frac{-2.3\ RT}{\alpha nF} \quad (4)$$

$$Slope\ (E_{pc}\ vs.\ \ log\ \nu) = \frac{2.3\ RT}{(1-\alpha)nF} \quad (5)$$

$$k^0 = \frac{\alpha nF\nu_c}{RT} = \frac{(1-\alpha)nF\nu_a}{RT} \quad (6)$$

The values of α and k^0 for FCF1, FCF2, FCF3 and FCF-AQ electrodes were calculated from the above equations as shown in Table 5. Results based on the variation in the anodic and cathodic peak overpotential ($E - E^0$) as a function of log (ν) for FCF1, FCF2, FCF3 and FCF-AQ revealed that FCF-AQ has very high values of the standard rate constant at zero potential (k^0) compared to the other modified electrodes.

Table 5 - Parameters α and k^0 for FCF1, FCF2, FCF3 and FCF-AQ electrodes were obtained by Laviron.

Electrode	α	k^0
FCF1	0.33	6.4 s^{-1}
FCF2	0.47	4.8 s^{-1}
FCF3	0.44	5.5 s^{-1}
FCF-AQ	0.57	11.9 s^{-1}

Source: Own authorship

Figure 19 - Variation of the anodic and cathodic peak overpotential (E - E^0) as a function of log (ν) obtained in sodium phosphate buffer solution (0.1 mol L^{-1}, pH 7.5) for (a) FCF1; (b) FCF2; (c) FCF3 and (d) FCF-AQ electrodes in Ar-saturated environment and T= 25 °C.

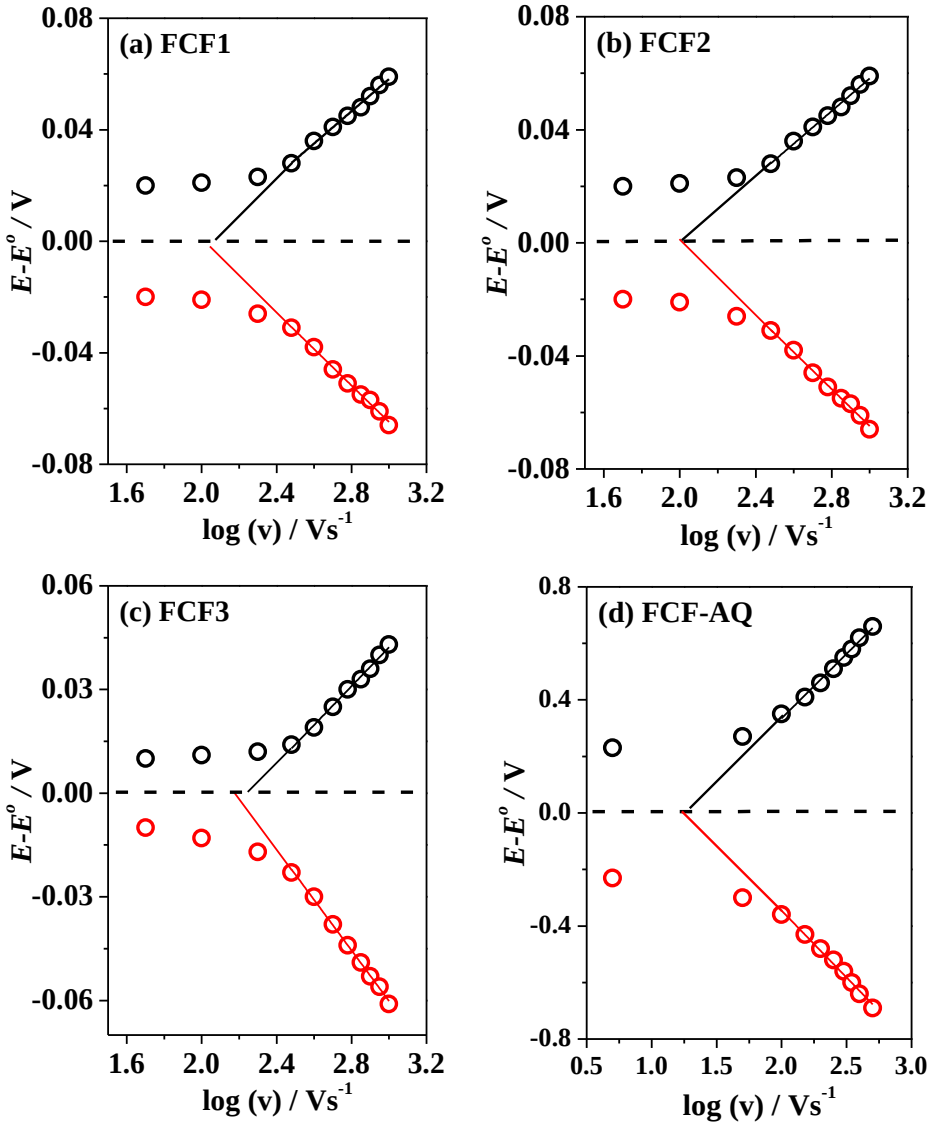

4.6 Electrochemistry of modified FCF electrodes by using different redox probes

The surface of carbon based materials are significantly more complex than that of metals,[89] because of their different allotropic structures and the presence various functional groups on their surfaces.[90] Since the electrochemistry is fundamentally based on interfacial phenomena occurring on the surface of electrodes, in this part of the work it will be discussed how the presence of various functional groups on the surface of the FCE electrode will influence the electrochemical interfacial processes.

To evaluate the electrochemical properties of the modified FCF electrodes; two different redox probes $K_4[Fe(CN)_6]/K_3[Fe(CN)_6]$ and $[Ru(NH_3)_6]Cl_2/[Ru(NH_3)_6]Cl_3$ were used. The oxidation/reduction of $Fe(CN)_6^{4-/3-}$ couple and of $Ru(NH_3)_6^{2+/3+}$ couple in aqueous solution has served as benchmark reactions in fundamental electrochemistry since these redox processes involves the transfer of a single electron and exhibit close to the ideal quasi-reversible outer sphere kinetic behavior, especially at carbon electrode where there is minimum bonding (or adsorption) interaction between the electrode material and the reactant ions in solution. From the results shown in Figure 20a for FCF1, FCF2, FCF3 and FCF-AQ electrodes performed in $K_4[Fe(CN)_6]/K_3[Fe(CN)_6]$ redox probe, it can be suggested that FCF1 and FCF-AQ electrodes presented a very high reversibility as well as higher current densities for cathodic and anodic peak potentials as compared to pristine FCF, FCF2 and FCF3 electrodes, which are consistent with the faster reaction kinetics previously observed for these kinds of electrodes.[34,73] On the other hand, the results obtained in the presence of the redox probe $[Ru(NH_3)_6]Cl_2/[Ru(NH_3)_6]Cl_3$ are quite different, where a quasi-reversible behavior was shown by both the chemically and electrochemically modified FCF electrodes as shown in Figure 20b, though both FCF1 and FCF-AQ electrodes have shown higher current densities and reversibility for cathodic and anodic peak potential as compared to the other electrodes similar to that in the case of $K_4[Fe(CN)_6]/K_3[Fe(CN)_6]$ redox probe. The reason for the different reversibility of all these electrodes in different type of redox probes may be due to the different nature of these probes. The redox probe hexamine ruthenium chloride has a positive charge and the process of oxidation and reduction occurs in the negative potentials as compared to the redox probe hexacyanoferrate which has a negative charge, but the process of oxidation-reduction occurs in the more positive potentials. The difference of charges of the complexes can exert different interactions in the electrode-solution interface. The reactivity of the basal planes are different in relation to the edge planes, thus presenting different electron transfer kinetics.[53–55] The edge planes are more sensitive when the redox probe is $Fe(CN)_6^{4-}/Fe(CN)_6^{3-}$ as compared to the basal planes. On the other hand the redox probe $Ru(NH_3)_6^{2+}/[Ru(NH_3)_6^{3+}$ transfers electrons with the same rate for both the basal and edge planes.

Figure 20 - Cyclic voltammograms obtained for pristine FCF (●), FCF1 (●), FCF2 (●), FCF3 (●) and FCF-AQ (●) obtained in the redox probes a) $K_4[Fe(CN)_6]/K_3[Fe(CN)_6]$ and (b) $[Ru(NH_3)_6]Cl_2/[Ru(NH_3)_6]Cl_3$ solution (5.0 mmol L^{-1}) along with KCl (0.5 mol L^{-1}) as a supporting electrolyte in an inert N_2-atmosphere at a scan rates; 5 mV s^{-1}.

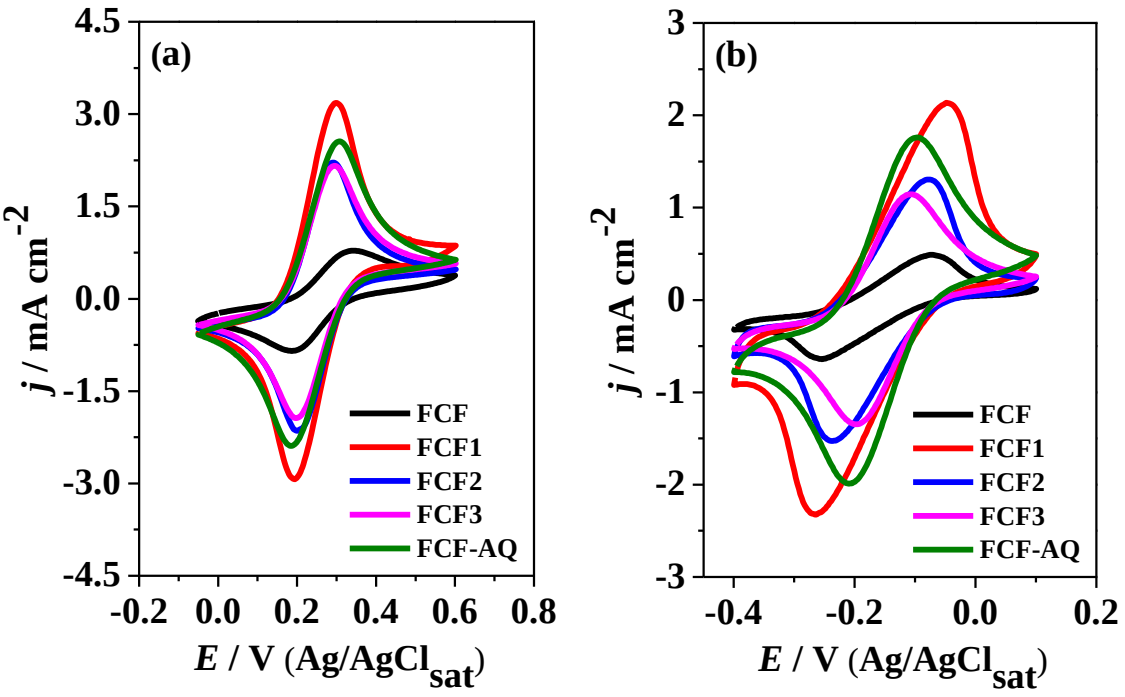

The reversibility of electrochemical reactions is associated with the rate through which the electrons are exchanged, faster the exchange, more reversible is the reaction. The parameter used to measure the reversibility is the separation between the oxidation and reduction peaks and is represented by ΔE and can be calculated by the equation, ($\Delta E = E_{pa} - E_{pc)}$, where E_{pa} represent the anodic and E_{pc} represent the cathodic peak potentials. The ΔE values calculated for all the modified FCF electrodes in these two different redox probes from the cyclic voltammograms are given in Table 6. Further, we have conducted stability test of one of the electrode for 100 cycles at 5 mV s^{-1}. The reversibility of the modified FCF electrodes was reduced after 100 cycles at 5 mV s^{-1} while the current remains intact in the cyclic voltammetric curve. As a result these electrodes are stable.

Table 6 - Δ*E* Values of pristine FCF, FCF1, FCF2, FCF3 and FCF-AQ electrodes in the redox probe hexacyanoferrate $K_4[Fe(CN)_6]/K_3[Fe(CN)_6]$ and hexamine ruthenium chloride $[Ru(NH_3)_6]Cl_2/[Ru(NH_3)_6]Cl_3$.

Electrode	Δ*E* values in $K_4[Fe(CN)_6]/K_3[Fe(CN)_6]$	Δ*E* values in $[Ru(NH_3)_6]Cl_2/[Ru(NH_3)_6]Cl_3$
FCF	0.15 V	0.19 V
FCF1	0.11 V	0.09 V
FCF2	0.09 V	0.16 V
FCF3	0.10 V	0.09 V
FCF-AQ	0.12 V	0.11 V

Source: Own authorship

4.7 Electro-oxidation of NADH catalyzed by quinones on FCF surface

It is worth mentioning that the oxidation of NADH during the bioelectrocatalysis of ethanol by ADH is very similar to the electro-oxidation of NADH on modified electrodes with quinones. It has been shown previously that quinone molecules participate in the electro-oxidation of NADH to NAD^+ with concomitant reduction of quinone to dihydroquinones.[56,57,91] Therefore, the FCF electrodes modified with different quinone functionalities can significantly improve the electro-oxidation of NADH and hence the efficiency of bioelectrocatalytic process of NAD-dependent enzymes.[56,57,91] Currently, cyclic voltammetry technique has been used to measure the kinetics and the dynamic of the NAD^+/NADH inter-conversion, where usually carbon electrodes functionalized with quinone groups are used to study this reaction. The term “electrocatalysis” has been frequently used to explain the NADH oxidation[25,56–59] mechanism on quinone-modified electrode, mainly due to the shape find in the cyclic voltammograms. Cyclic voltammetry was firstly performed in phosphate buffer solution (0.1 mol L^{-1}, pH 7) in the absence of NADH, as shown in Figure

21a for FCF1, FCF2, FCF3 electrodes and in Figure 21c for FCF-AQ electrode, where oxidation peaks were observed for the modified electrodes which are related to the presence of *ortho*-quinone and anthraquinone moieties as compared to the pristine FCF electrode where no redox process was observed. The electrochemical activity of the modified electrodes towards the NADH electro-oxidation was then evaluated in the presence of a definite concentration of NADH (1.0 mmol L^{-1}) and the results obtained was compared with pristine FCF, as shown in Figure 21b for FCF1, FCF2, FCF3 electrodes and in Figure 21d for FCF-AQ electrode.

Figure 21 - Cyclic voltammograms obtained in sodium phosphate buffer solution (0.1 mol L^{-1}, pH 7.5) for (a-b) pristine FCF (●), FCF1 (●), FCF2 (●) and FCF3 (●). (c-d) Cyclic voltammograms obtained in sodium phosphate buffer solution (0.1 mol L^{-1}, pH 7.5) for pristine FCF (●) and FCF-AQ (●); (a) and (c) in the absence of NADH; (b) and (d) in the presence of NADH (1.0 mmol L^{-1}) in Ar-saturated environment at a scan rate; 5 mV s^{-1} and T = 25 °C.

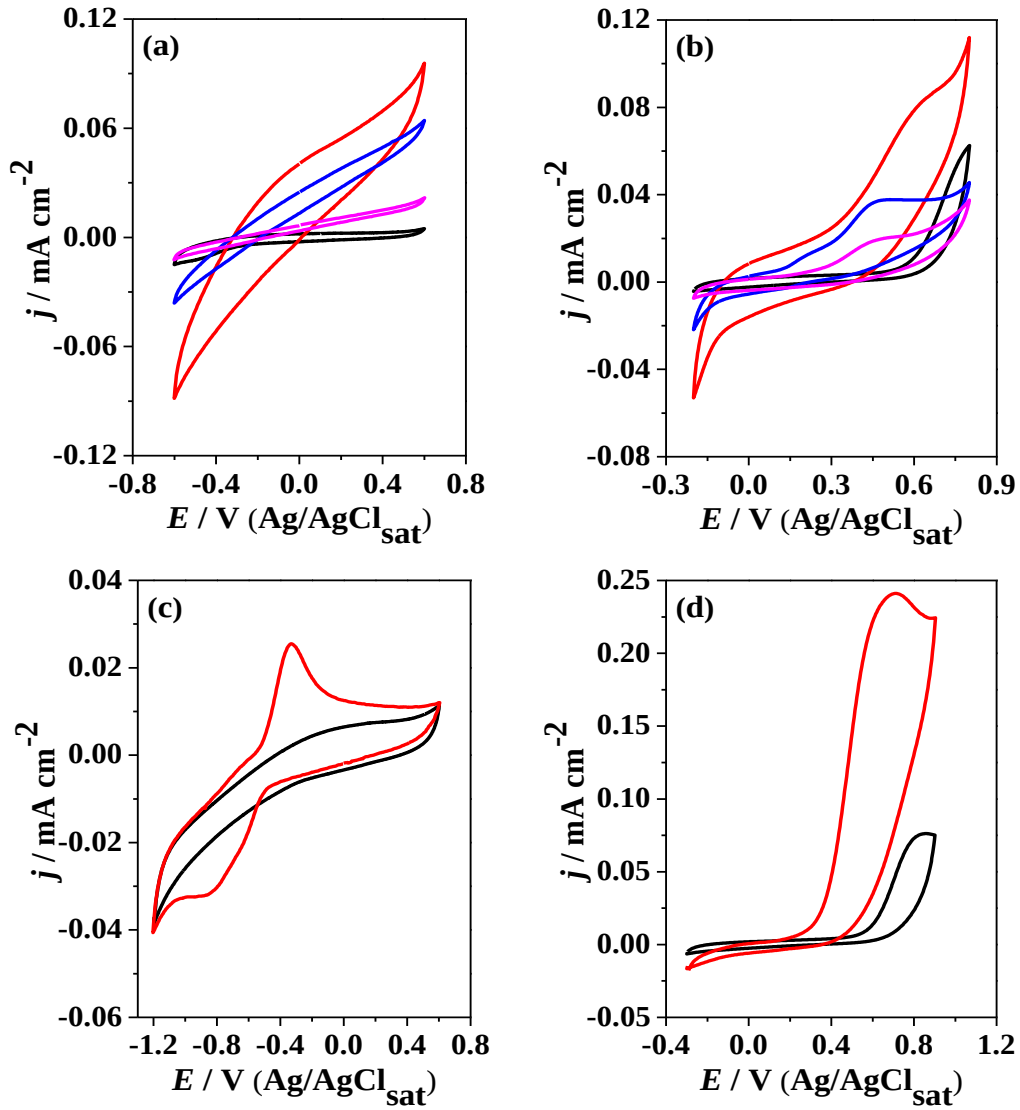

Compared to the pristine FCF electrode, the addition of NADH brings drastic changes in the cyclic voltammograms of all the modified electrodes, where an increase of the oxidative peak currents indicates the occurrence of electro-oxidation of NADH on the surfaces of these modified electrodes. Nevertheless, the extent to which the electro-oxidation of NADH occurs on the surfaces of these electrodes is different and was observed in the descendant order: FCF-AQ> FCF1>FCF2>FCF3 based on the oxidative peak current density of 0.24, 0.08, 0.04 and 0.02 mA cm^{-2} respectively. The results obtained for the electro-oxidation of NADH to NAD^+ are consistent with the literature.[3] These results suggest that the electrochemically modified electrode and the FCF electrode treated chemically in phosphate buffer solution (0.1 mol L^{-1}, pH 7.5) showed the best electrochemical activity towards the NADH electro-oxidation. Different mechanisms have been proposed in the literature for the electro-oxidation of NADH in the presence of redox mediator,[18–24] where the redox mediators have been coupled with NAD-dependent enzymes. In our case, the electro-oxidation of NADH catalyzed by *ortho*- and anthraquinone modified FCF electrodes is followed by a reaction pathway shown in Figure 22.

Figure 22 – Electro-oxidation of NADH by (a) *ortho*-quinone and (b) anthraquinone on the surface of modified FCF electrodes.

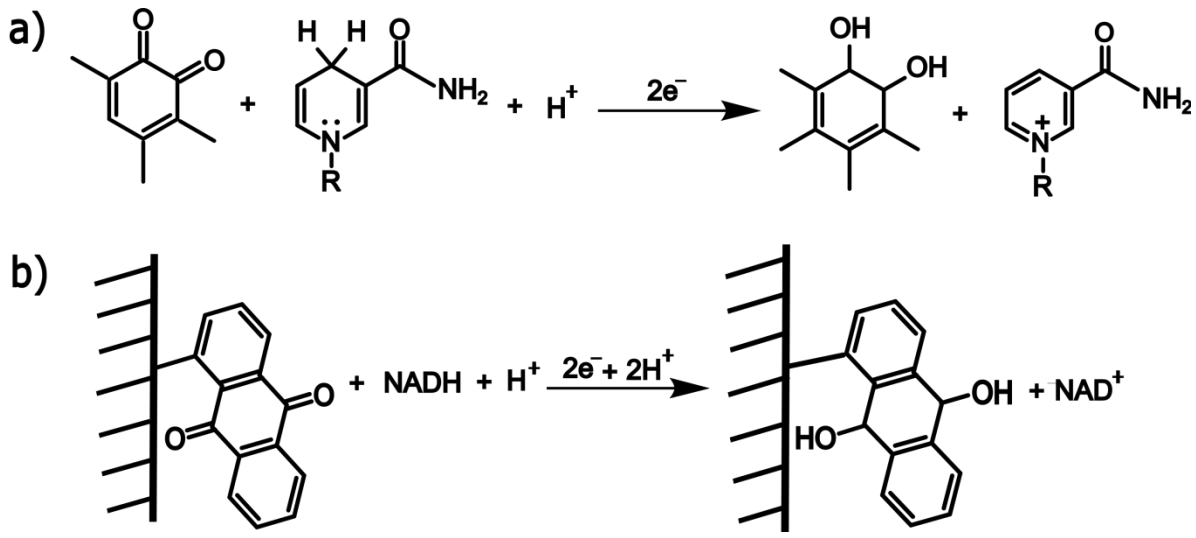

Source: Adopted from CARLSON, B. W., MILLER, L. L., 1985, p. 479.

4.8 *Operando* EPR of modified FCF

Operando EPR experiments were carried out by using an X-band EPR spectrometer coupled with a potentiostat/galvanostat µAutolab. An *operando* EPR electrochemical cell (EC) was designed for use with aqueous electrolyte.[68-70,92,93] This cell consists of a capillary system with three electrodes comprising the pristine FCF, FCF1, FCF2, FCF3 and FCF-AQ electrodes as the working electrode (WE), platinum as the counter electrode, and saturated Ag/AgCl as the reference electrode, as schematically shown in Figure 23a. Using this experimental setup, the EPR spectra are recorded simultaneously with chronoamperometric measurements after 50 s, when the steady-state current (SS) current is obtained. The X-band EPR spectra of FCF electrodes were obtained at ambient temperature (273 K) with a microwave frequency of 9.8 GHz and microwave power of 2 mV after applying potential for six (6) minutes.[94–99] The EPR spectra are the average of eight (8) scans and represented by a single line of Lorentzian shape with no signs of hyperfine structure; simultaneously a chronoamperometric curves was obtained during the experiment.

Figure 23 – (a) *Operando* EPR set up. (b) Plot of relative spin concentration vs. potential representing an increasing and decreasing order of unpaired electron spin concentrations of EPR signals. (c) Electro-oxidation of NADH to NAD^+ by quinones on modified FCF surfaces.

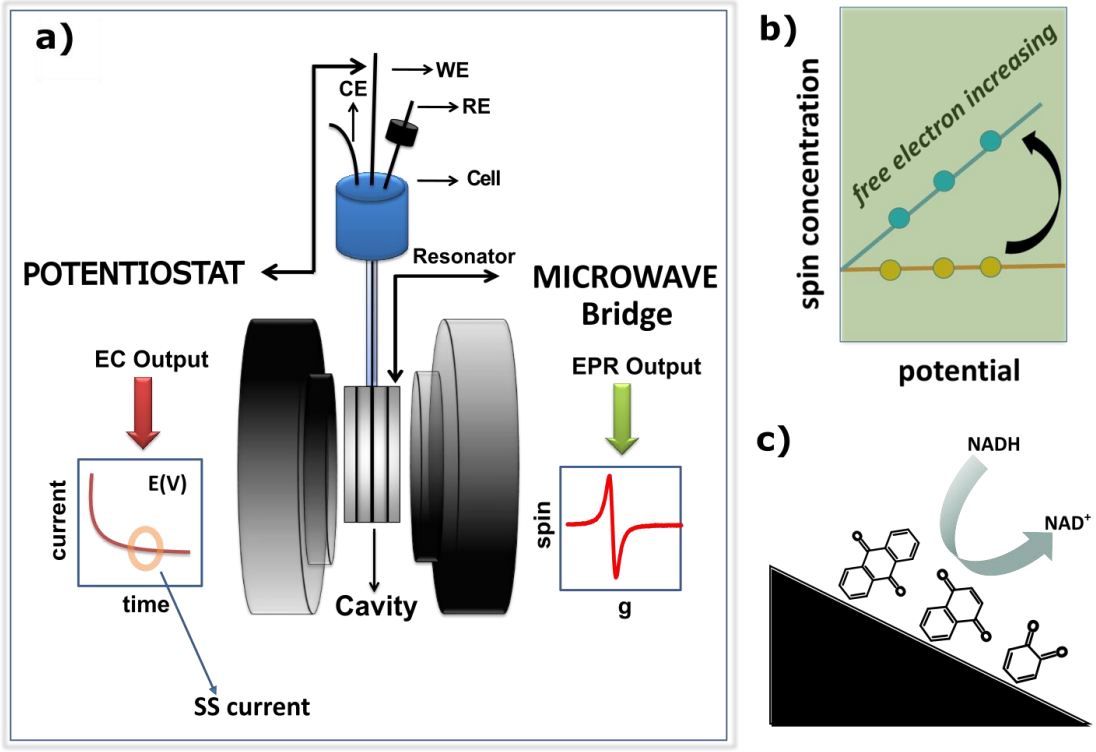

Source: Own authorship

Figure 23b shows plot of relative spin concentration versus potential of an EPR signals, showing the typical decreasing free electrons spin concentrations (shown by yellow line) in phosphate buffer solution (0.1 mol L^{-1}, pH 7.5) in the absence of NADH and an increasing free electrons spin concentrations (shown by blue line) in phosphate buffer in the presence of a of NADH (1.0 mmol L^{-1}) at applying positive potentials. Figure 23c shows the scheme of NADH electro-oxidation catalyzed by *ortho*-quinones and anthraquinones on modified FCF surfaces.

4.8.1 *Operando* EPR of modified FCF in KOH to investigate the formation of quinone radicals

Furthermore, the formation of quinone radicals on the modified FCF electrodes were investigated in KOH solution (0.1 mol L^{-1}, pH 14) and the results obtained was compared with pristine FCF electrode as shown in Figure 24. Figure 24a shows the X-band EPR spectra of pristine FCF, FCF1, FCF2, FCF3 and FCF-AQ electrode at -0.6 V applying potential at ambient temperature. An increase in the EPR signal intensities were observed for FCF-AQ and FCF1 electrodes as compared to pristine FCF and the other modified electrodes suggesting the formation of unpaired electrons. Figure 24b shows the chronoamperometric response of pristine FCF, FCF1, FCF2, FCF3 and FCF-AQ electrode in KOH solution (0.1 mol L^{-1}, pH 14) at -0.6 V applying potential, where the modified FCF electrodes have shown the high current densities with respect to time as compared to pristine FCF electrodes. However, the current density for FCF1 electrodes is significantly greater than pristine FCF and the other modified FCF electrodes. EPR results (Figure 24a) cannot be compared with chronoamperometry (Figure 24b). For better clarity we can compare chronoamperometry results (Figure 24b) with cyclic voltammetry (see Figure 11), where upon applying -0.6 V the electrochemical behavior of FCF2 and FCF-AQ electrode are showing almost the same current densities. The reason for selecting a specific potential (-0.6 V) is due a fact that the faradaic process begins at this potential. Figure 24c represents the bars graph of all the modified electrodes in KOH solution (0.1 mol L^{-1}, pH 14), where higher unpaired electron relative spin concentrations were observed for FCF1 electrode as compared to pristine and the other modified FCF electrodes. Figure 24d are the plot relative spin concentration of unpaired electrons for pristine FCF and the modified FCF electrode (FCF1) at different applying potentials ranging from -1.2 V up to 0 V, where higher relative unpaired electrons spin concentration was observed for all the modified FCF electrodes as compared to the un-modified pristine FCF electrode indicating the formation of quinone radicals. The results

obtained for both the chemically and electrochemically modified FCF electrodes in alkaline solution (KOH) by using the *operando* EPR experiments, indicates the formation of quinone radicals on the surface of the electrodes that can actively participate in the electro-oxidation of NADH to NAD^+.

Figure 24 - (a) X-band EPR spectra obtained in KOH solution (0.1 mol L^{-1}, pH 14) for pristine FCF (●), FCF1 (●), FCF2 (●), FCF3 (●) and FCF-AQ (●) at -0.6 V applying potential; (b) Chronoamperometry response for all the electrodes at -0.6 V for 300 second. (c) Bars graph obtained in KOH solution (0.1 mol L^{-1}, pH 14) for pristine FCF (●), FCF1 (●), FCF2 (●), FCF3 (●) and FCF-AQ (●) at -0.6 V applying potential. (d) Plot of relative spin concentration versus the applied potential obtained in KOH solution (0.1 mol L^{-1}, pH 14) for pristine FCF (●) and functionalized FCF1 (●) at different applying potential ranging from 0 V up to -1.2 V. All the experiments were carried out at T = 273 K.

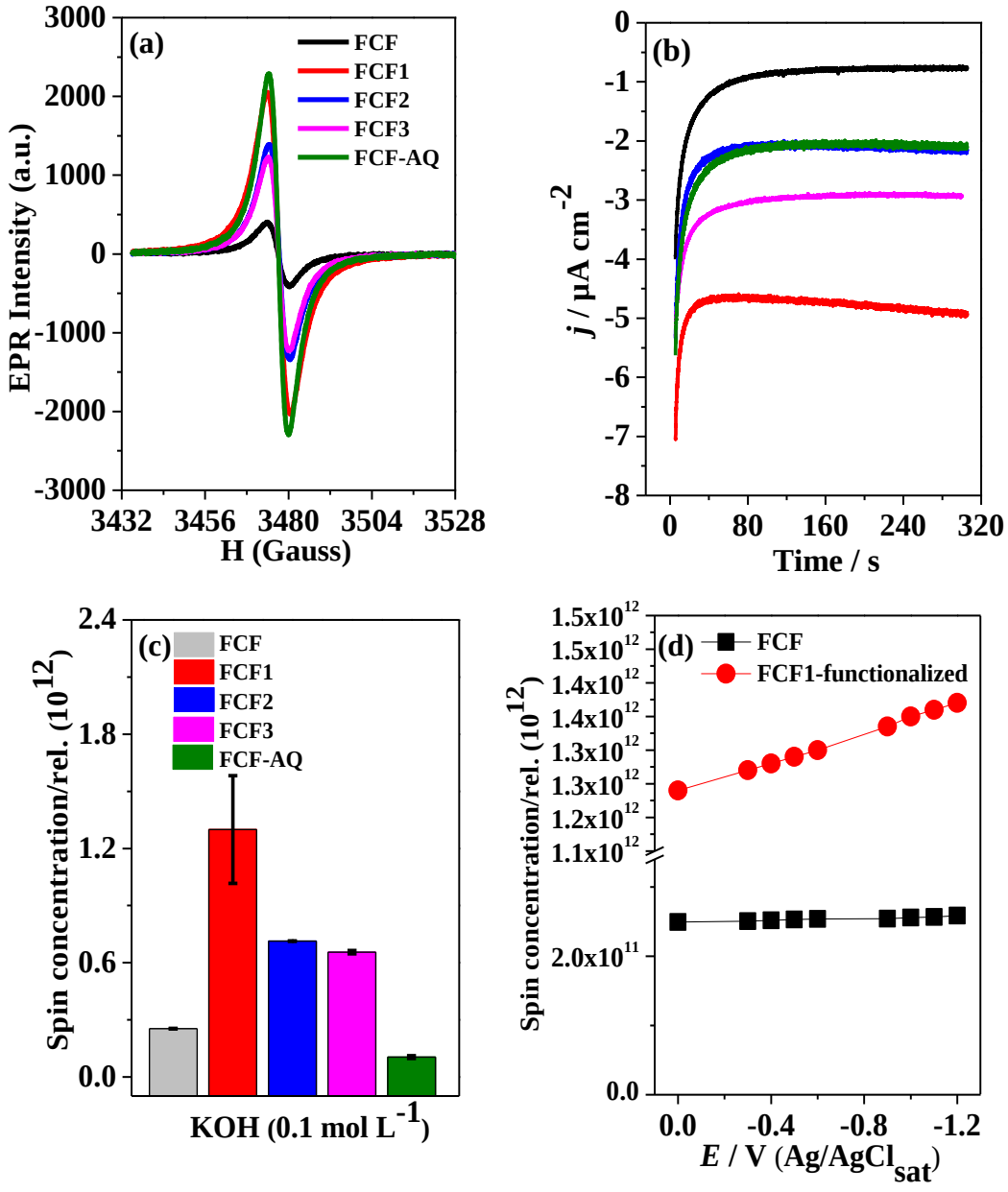

4.8.2 *Operando* EPR of modified FCF for NADH electro-oxidation

Operando EPR is the only direct method to detect the presence of free radicals as well as quantifies the amount of unpaired electrons produced after applying potential in the context of electron transfer reaction[100–103] and it has the unique power to indentify the paramagnetic species. In this part of the work it will be discussed *operando* EPR of modified FCF electrodes to investigate the NADH/NAD^+ redox reaction. Figure 25a shows the X-band EPR spectra of pristine FCF (black line), FCF1 (red line), FCF2 (blue line), FCF3 (pink line) and FCF-AQ (green line) electrodes recorded in phosphate buffer (0.1 mol L^{-1}, pH 7.5) in the absence of NADH at 0.6 V. As can be seen, an increase in the EPR signal intensities are observed for FCF1, FCF2, FCF3 and FCF-AQ electrodes as compared to pristine FCF, suggesting that the presence of quinone functionalities causes an increase in the number of unpaired electrons on the electrode surface. Interestingly, in the presence of a definite concentration of NADH (1.0 mmol L^{-1}) as shown in Figure 25b, a higher EPR signal intensities with better bioelectrocatalytic activity of NADH electro-oxidation was observed for FCF1 and FCF-AQ electrodes. The density of unpaired electrons increases for all the electrodes, however, for FCF1 and FCF-AQ the EPR signal is significantly higher in comparison to pristine FCF. For FCF1, the density of unpaired electron (spin density, *SD*) increased 44% (Δ*SD*) in presence of NADH, while for FCF-AQ the Δ*SD* was 80%. This value indicates that FCF-AQ presents a superior activity for the oxidation of NADH. The spin ratio between FCF1 and FCF-AQ ($SR_{\mathrm{FCF1/FCF-AQ}}$) provides useful quantitative information about the electro-oxidation process and can be determined by equation 7.

$$SR_{\mathrm{FCF1/FCF-AQ}} = \frac{\Delta SD_{\mathrm{FCF1}}}{\Delta SD_{\mathrm{FCF-AQ}}} \qquad (7)$$

The $SR_{\mathrm{FCF1/FCF-AQ}}$ was 0.75, which indicates higher unpaired electron density for FCF-AQ in *operando* condition (in presence of NADH under 0.60 V). This value agrees with the ratio of surface density of quinone groups between FCF1 (1.3×10^{-9} mol cm^{-2}) and FCF-AQ (2.8×10^{-9} mol cm^{-2}), which is 0.46. This concordance corroborates with the hypothesis that quinones interacts with NADH molecules during the electro-oxidation reaction. Figure 25c shows the bars graph for pristine FCF and all the modified FCF electrodes in phosphate buffer (0.1 mol L^{-1}, pH 7.5) in the absence of NADH as well as in the presence of a definite concentration of NADH (1.0 mmol L^{-1}), where high relative unpaired electrons spin densities were observed for FCF1 (red line) and FCF-AQ (green line) electrodes as compared to

pristine FCF (black line) and the other modified electrodes, respectively in the presence of NADH as compared to the results obtained in the absence of NADH.

Figure 25 - X-band EPR spectra obtained in sodium phosphate buffer solution (0.1 mol L^{-1}, pH 7.5) for pristine FCF (●), FCF1 (●), FCF2 (●), FCF3 (●) and FCF-AQ (●); (a) in the absence of NADH; (b) in the presence of NADH (1.0 mmol L^{-1}) at 0.6 V. (c) Bars graph obtained in sodium phosphate buffer solution (0.1 mol L-1, pH 7.5) for pristine FCF (●), FCF1 (●), FCF2 (●), FCF3 (●) and FCF-AQ (●) in the absence of NADH and in the presence of NADH (1.0 mmol L^{-1}). (d) Plot of relative spin concentration versus the applied potential for modified FCF electrode (FCF1) obtained in sodium phosphate buffer solution (0.1 mol L^{-1}, pH 7.5) at different applying potential ranging from 0 V up to 0.6 V; (●) in the absence of NADH; (●) in the presence of NADH (1.0 mol L^{-1}) . All the experiments were carried out at T = 273 K.

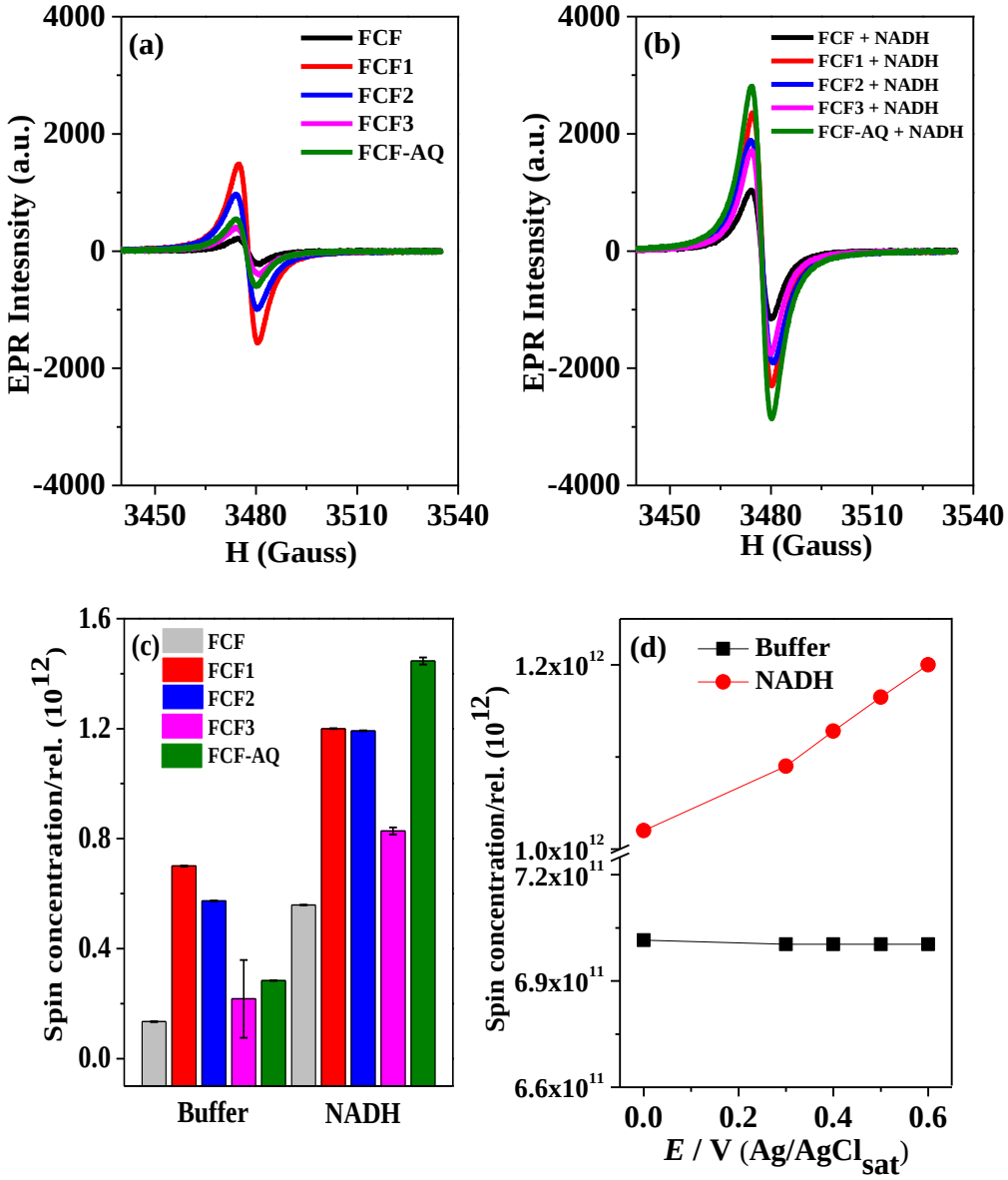

The increasing of spin density with the applied potential suggests the kinetics of NADH electro-oxidation has a B-V behavior, like the polarization curve. This result also corroborate with the limiting step reaction is the NADH oxidation, since k^0 observed were 6.4 $s^{-1}$and 11.94 s^{-1} for FCF-O and FCF-AQ, respectively. Since, the unpaired electron is associated to semiquinone radical, the EPR results suggest a new mechanism for electron transfer, as shown in Figure 26. Figure 25d shows the plot of relative spin concentration versus applied potential for modified FCF electrode in phosphate buffer (0.1 mol L^{-1}, pH 7.5) in the absence of NADH (shown by the black line) and in the presence of a definite concentration of NADH (shown by the red line) at different applying positive potentials ranging from 0 V to 0.6 V, where an increasing unpaired electrons relative spin density was observed for modified FCF electrodes (preferably FCF1 and FCF-AQ) in the presence of NADH as compared to the plot in black in the absence of NADH.

Figure 26 – Possible reaction mechanism of the formation of unpaired electrons formation on the surface of quinone-modified carbon electrode. Semiquinone is a free radical. This scheme shows an anion radical as an intermediate (highlighted in red) between the fully reduced and the fully oxidized states catalyzed by the NADH. The NADH intramolecular reactions are omitted in this model.

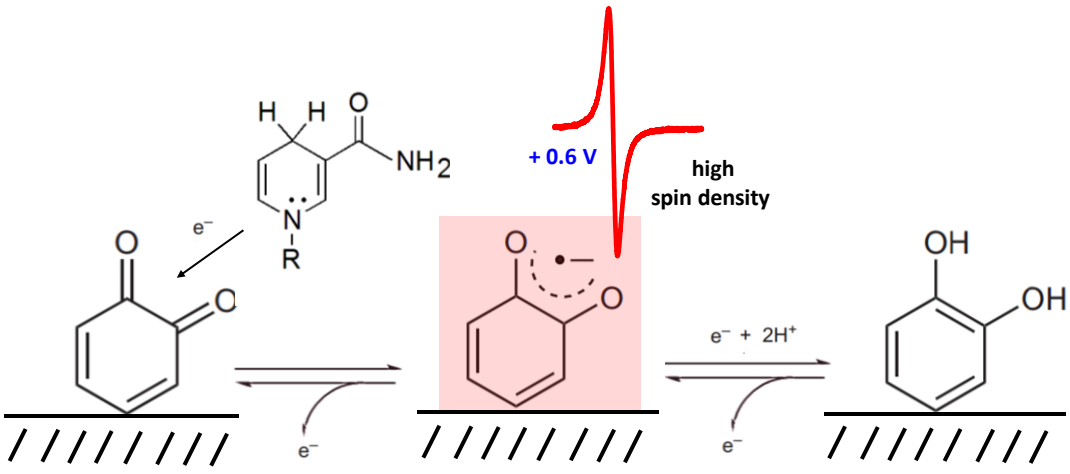

The proposed mechanism is based on clear evidence that C=O group from quinones is responsible for enhancing the electro-oxidation of NADH. Accordingly, for an increase in the content of spins to occur, intimate contact between NADH and the surface of the electrode is expected; during the steady-state (chronoamperometry plateau), electro-oxidation is influenced by the electronic properties of the quinones on the surface. This is a typical characteristic of electrocatalyic behavior. Two steps can be considered for electron transfer during the NADH oxidation:1) the proton-coupled electron transfer from NADH to quinone and 2) the reduction of hydroquinone. For the first time, we show a new correlation for the

spin content that clearly reveals an increasing number of free unpaired electrons with increasing applied overpotential and NADH oxidation, which corroborates the fact that the quinone groups on carbon surfaces acts as electrocatalyst towards the oxidation of NADH to NAD^+.

Figure 27a-27e shows the chronoamperometry response of FCF1 (red line), FCF2 (blue line), FCF3 (pink line) and FCF-AQ (green line) electrodes in phosphate buffer (0.1 mol L^{-1}, pH 7.5) in the absence of NADH at different applying positive potential ranging from 0 V up to 0.6 V for 300 seconds at ambient temperature (T = 273 K) and the result was compared with pristine FCF (black line) electrode, where an increase in current density for FCF1 electrode is observed as compared to pristine FCF and the other modified electrodes as can be in Figure 27f, suggesting that the presence of quinone molecule causes an increase of unpaired electrons on electrode surface as earlier discussed.

Figure 27 - Chronoamperometry response of (a) pristine FCF; (b) FCF1: (c) FCF2; (d) FCF3 and (e) FCF-AQ obtained in sodium phosphate buffer solution (0.1 mol L^{-1}, pH 7.5) at different applying positive potential ranging from 0 V up to 0.6 V for 300 seconds at T = 273 K. (f) Chronoamperometry of pristine FCF (●), FCF1 (●), FCF2 (●), FCF3 (●) and FCF-AQ (●) at 0.6 V and at T = 273 K.

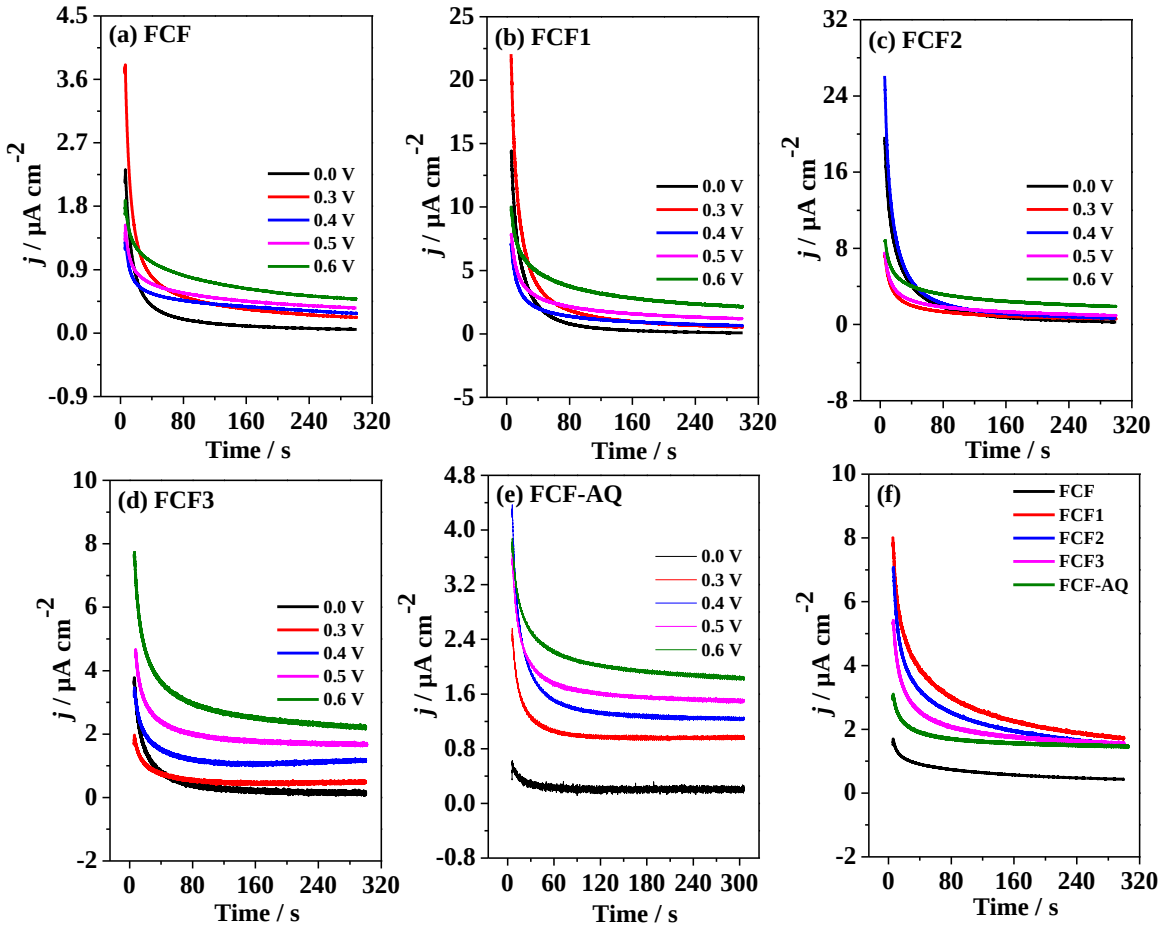

Figure 28a-28e shows the chronoamperometry response of pristine FCF, FCF1, FCF2, FCF3 and FCF-AQ electrodes in phosphate buffer (0.1 mol L^{-1}, pH 7.5) in the presence of NADH (1.0 mmol L^{-1}) at different applying positive potential ranging from 0 V up to 0.8 V for 300 seconds at ambient temperature (T = 273 K) and the results were compared with pristine FCF electrode, where higher current densities as well as high electrocatalytic activity of NADH oxidation was observed for FCF-AQ and FCF1 electrode as compared to the results obtained in the absence of NADH for all the composites as can be seen by the chronoamperometry curves in Figure 28f , the current density is higher for all the modified electrodes. However, for FCF-AQ and FCF1 the current density is significantly higher than pristine FCF and the other modified FCF electrodes.

Figure 28. Chronoamperometry response of (a) pristine FCF; (b) FCF1: (c) FCF2; (d) FCF3 and (f) FCF-AQ obtained in phosphate buffer (0.1 mol L^{-1}, pH 7.5) containing NADH (1.0 mmol L^{-1}) at different applying positive potential ranging from 0 V up to 0.8 V for 300 seconds at T = 273 K. (f) Chronoamperometry of pristine FCF (●), FCF1 (●), FCF2 (●), FCF3 (●) and FCF-AQ (●) at 0.6 V and at T = 273 K.

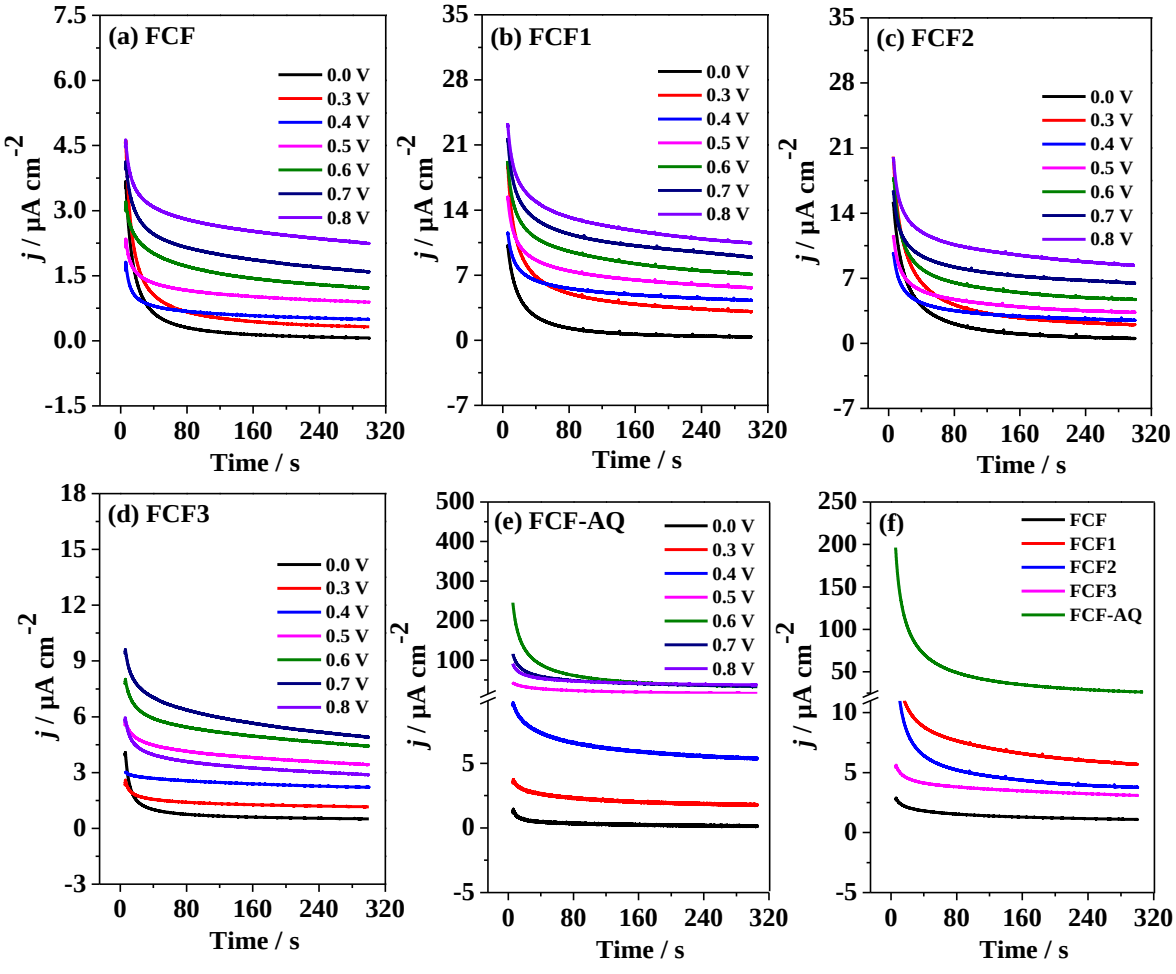

Figure 29a are the plot of current density versus applied potential representing the polarization curves obtained from chronoamperometry plateau at steady state (SS) current in phosphate buffer solution (0.1 mol L^{-1}, pH 7.5) in the absence of NADH for pristine FCF (in black), FCF1 (in red), FCF2 (in blue), FCF3 (in pink) and FCF-AQ (in green) electrodes, where high current densities values were obtained at steady state current (SS) for all the modified electrodes as compared to the pristine FCF electrode at different applying positive potentials ranging from 0 V up to 0.6 V. However, for FCF1 electrode significantly higher current values were observed at a steady state (SS) as compared to pristine FCF and the other modified electrodes. On the other hands in the presence of NADH (1.0 mmol L^{-1}) high values of current densities were observed with better electrocatalytic activity of NADH oxidation at different applying positive potential (0 V up to 0.8 V) for FCF1 and FCF-AQ electrodes as compared to the pristine FCF and the other modified FCF electrodes as can be seen by the polarization curves obtained at steady state (SS) current in Figure 29b. All the experiments were performed at ambient temperature (T = 273 K).

Figure 29 - Polarization curves obtained at steady state current in sodium phosphate buffer solution (0.1 mol L^{-1}, pH 7.5) for pristine FCF (●), FCF1 (●), FCF2 (●), FCF3 (●) and FCF-AQ (●); (a) in the absence of NADH at different applying positive potential ranging from 0 V upto 0.6 V; (b) in the presence of NADH (1.0 mmol L^{-1}) at 0 V up to 0.8 V and T = 273 K.

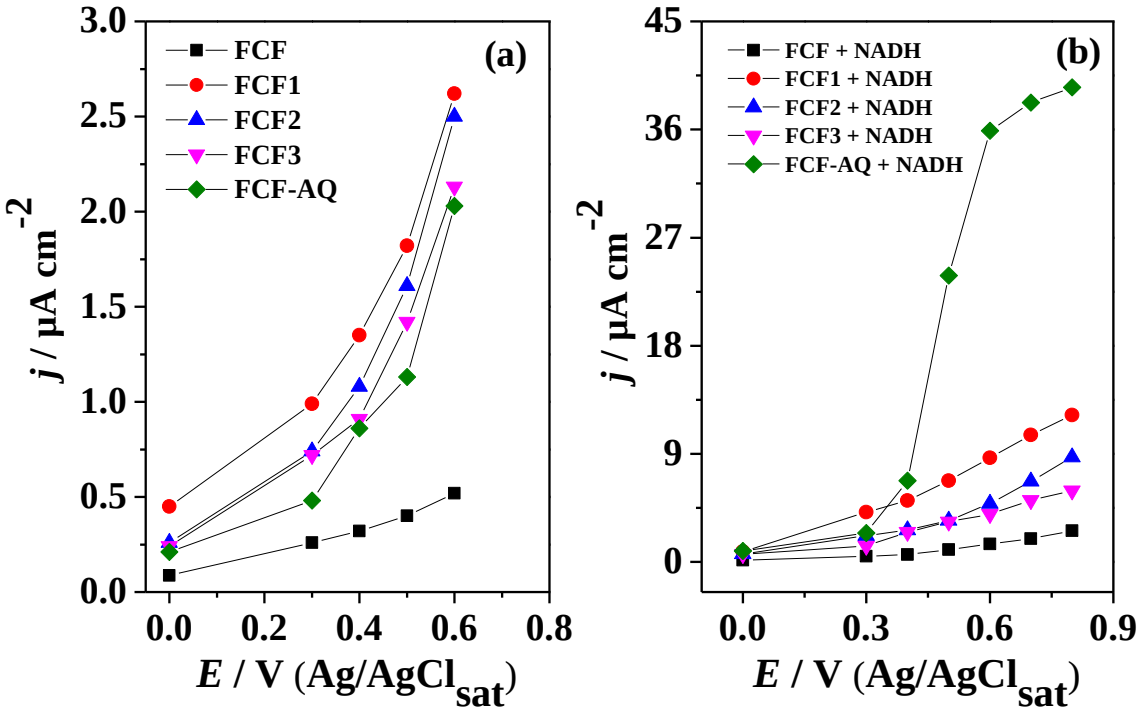

4.9 Bioelectrocatalysis of ADH for ethanol oxidation

Alcohol dehydrogenase is basically an NAD-dependent enzyme that catalyzes the interconversion of alcohol to aldehyde or ketones and can be utilized as anodic biocatalysts in biofuel cells. The electro-oxidation of NADH is necessary to regenerate an NAD-dependent enzyme. Thus, in order to obtain an active FCF array for buildup of NAD-dependent enzyme, the FCF surfaces were functionalized with *ortho*- and anthraquinones which improves the electro-oxidation of NADH as can be seen in Figure 21, thus enhancing the bioelectrocatalysis based on NAD-dependent dehydrogenase. The modified FCF electrodes show excellent conditions to immobilization of ADH.

4.9.1 Influence of ADH and NAD^+ on ethanol bioelectrocatalysis

The activity of ADH enzyme towards the bioelectrocatalysis of ethanol on modified FCF surface was evaluated in the presence and absence of ADH enzyme. For this purpose, the cyclic voltammetry of the modified FCF electrode (FCF1 in this case) was initially performed in the absence of ethanol and then in the presence of ethanol (50 % v/v) in sodium phosphate buffer solution (0.1 mol L^{-1}, pH 7.5) containing NAD^+ (0.6 mmol L^{-1}) in solution which was added to the electrolyte before the electrochemical analysis, the experiment was carried out under N_2 saturated atmosphere for about 10 minutes in order to remove the dissolved oxygen. The experiment was repeated for the modified FCF electrode (FCF1), but this time immobilized with ADH enzyme and the results obtained are shown in Figure 30. As can be seen, the bioelectrocatalysis occurs only for the modified FCF electrode immobilized with ADH (Figure 30b), whereas for the modified FCF electrode in the absence of enzyme (Figure 30a), the cyclic voltammograms does not show any bioelectrocatalytic behavior, since no increase in the current density was observed after the addition of ethanol.

To verify the influence of NAD^+ on ethanol oxidation, cyclic voltammograms of FCF bioelectrode was compared in the absence and in the presence of ethanol as shown by the results in Figure 30c, where no increase in catalytic current was observed after the addition of ethanol in the absence of coenzyme NAD^+ from the electrolyte solution. The on-set potentials were 0.12 V for FCF1 electrode without ADH (Figure 30a); 0.22 V for FCF1-ADH bioelectrode (Figure 30b) in the presence of NAD^+ (0.6 mmol L^{-1}) and 0.2 V for FCF1-ADH bioelectrode (Figure 30c) in the absence of NAD^+. All the experiments were performed in the presence of ethanol with a final concentration of 0.78 mol L^{-1}. An increase in the current

density for FCF1-ADH (Figure 30b) bioelectrode was observed in the presence of NAD^+ as compared to FCF1-ADH (Figure 30c) in the absence of NAD^+ revealing the oxidation of ethanol to acetaldehyde with concomitant reduction of NAD^+ to NADH. Thus, it is concluded that for the bioelectrocatalysis of ethanol by ADH, the use of coenzyme NAD^+ is necessary that work as an electron acceptor.

Figure 30 - (a) Cyclic voltammograms obtained in sodium phosphate buffer solution (0.1 mol L^{-1}, pH 7.5) containing NAD^+ (0.6 mmol L^{-1}) for FCF1 electrode in the absence of ethnaol (●) and in the presence of ethanol (●); (b) Cyclic voltammograms obtained in sodium phosphate buffer solution (0.1 mol L^{-1}, pH 7.5) contaning NAD^+ (0.6 mmol L^{-1}) for FCF1-ADH bioelectrode in the absence of ethanol (●) and in the presence of ethanol (●); (c) Cyclic voltammograms of FCF1-ADH bioelectrode obtained in sodium phosphate buffer solution (0.1 mol L^{-1}, pH 7.5) without NAD^+ in the absence of ethnaol (●) and in the presence of ethanol (●). Final concentration of ethanol in the electrolyte: 0.78 mol L^{-1}. All the experiments were perfromed in N_2-saturated environment at a scan rate; 50 mV s^{-1} and T = 25 °C.

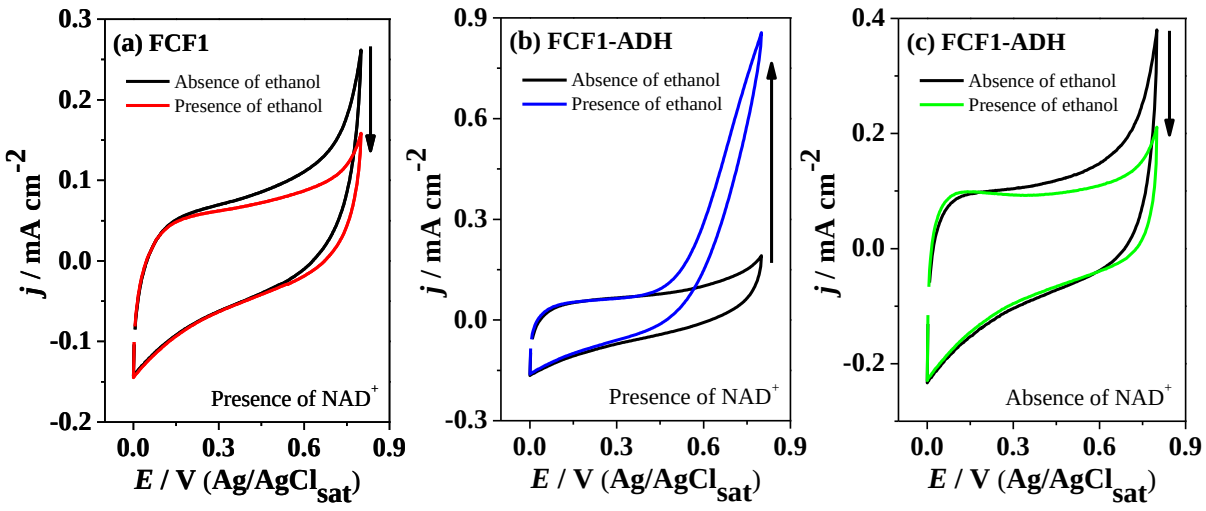

4.9.2 Influence of functionalized FCF on ethanol bioelectrocatalysis

The influence of functionalization on the surface of the FCF electrode performed was demonstrated, and how it interferes in the bioelectrocatalytic response can be seen in Figure 31. Figure 31a-31e shows the cyclic voltammograms obtained in phosphate buffer solution (0.1 mol L^{-1}, pH 7.5) containing NAD^+ (0.6 mmol L^{-1}) with successive addition of ethanol to the electrolyte, with each addition being 200 µL (0.085 mol L^{-1}) for FCF1, FCF2, FCF3 and FCF-AQ electrodes immobilized with ADH enzymes. Since, all these electrodes were immobilized with ADH, they were named as FCF1-ADH, FCF2-ADH, FCF3-ADH and FCF-

AQ-ADH bioelectrodes. For comparative purpose, the pristine FCF was immobilized with ADH and was named as pristine FCF-ADH. An increase in the catalytic current was observed at each addition of ethanol, with subsequent additions being made until there was no increase in the current values, with the maximum values of substrate concentration being 0.43 mol L^{-1} for pristine FCF-ADH, 0.78 mol L^{-1} for FCF1-ADH, 0.51 mol L^{-1} for FCF2-ADH, 0.59 mol L^{-1} for FCF3-ADH and 0.68 mol L^{-1} for FCF-AQ-ADH bioelectrode.

However, for FCF1-ADH (Figure 31b) and FCF-AQ-ADH (Figure 31e) bioelectrodes, the substrate saturation is achieved in the presence of higher concentration of ethanol as compared to the pristine FCF-ADH, FCF2-ADH and FCF3-ADH, shown in Figures 31a, 31c, and 31d, respectively. On the other hand, the on-set potential for ethanol oxidation is 0.63 V for pristine FCF-ADH, 0.22 V for FCF1-ADH, 0.31 V for FCF2-ADH, 0.48 V for FCF3-ADH and 0.15 V for FCF-AQ-ADH. On the basis of lower substrate saturation and higher onset potential values, observed for pristine-FCF-ADH bioelectrode as compared to the modified bioelectrodes, it is inferred that the surface functionalization of the FCF electrodes through chemical and electrochemical treatments procedure is an effective strategy for improving the bioelectroactivity of these electrodes. It is worth mentioning that the increase in the catalytic current profile corresponds to the process of the oxidation of ethanol to acetaldehyde by the enzyme ADH.[104–109]

Regarding the reaction mechanism of ethanol oxidation by ADH, the reaction between the coenzyme NAD^+ and ethanol indicates that some dissociations of coenzyme by active ternary complex ADH-NAD^+-ETOH may occur. The coenzyme initially binds the enzyme (ADH-NAD^+), with subsequent substrate binding (ADH-EtOH) thereby forming a ternary complex (ADH-NAD+-EtOH) that undergoes an intramolecular reaction resulting in the acetaldehyde along with NADH species, the ADH-acetaldehyde-NADH complex is formed. The limiting step of the oxidation rate of ethanol is the dissociation of NADH from the ADH-NADH complex. The coenzyme NAD^+ is released much faster from ADH-NAD^+ complex as compared to NADH dissociates from ADH-NADH, the overall reaction was proposed by Dickension and Dickinson,[110] and the kinetic mechanism of the ADH enzyme has been consolidated from several studies described elsewhere.[111–118]

Figure 31 - Cyclic voltammograms obtained in sodium phosphate buffer (0.1 mol L^{-1}, pH 7.5) containing NAD^+ (0.5 mmol L^{-1}) and different concentration of ethanol for (a) FCF-ADH; (b) FCF1-ADH; (c) FCF2-ADH; (d) FCF3-ADH and (e) FCF-AQ-ADH at a scan rate; 50 mV s^{-1} and T = 25 °C. (f) Cyclic voltammograms of pristine FCF-ADH (●), FCF1-ADH (●), FCF2-ADH (●), FCF3-ADH (●) and FCF-AQ-ADH (●). Initial and final concentration of ethanol in the electrolyte: 0.085 mol L^{-1} and 0.78 mol L^{-1}. All the experiments were performed in N_2-saturated environment at a scan rate: 50 mV s^{-1} at T= 25 °C.

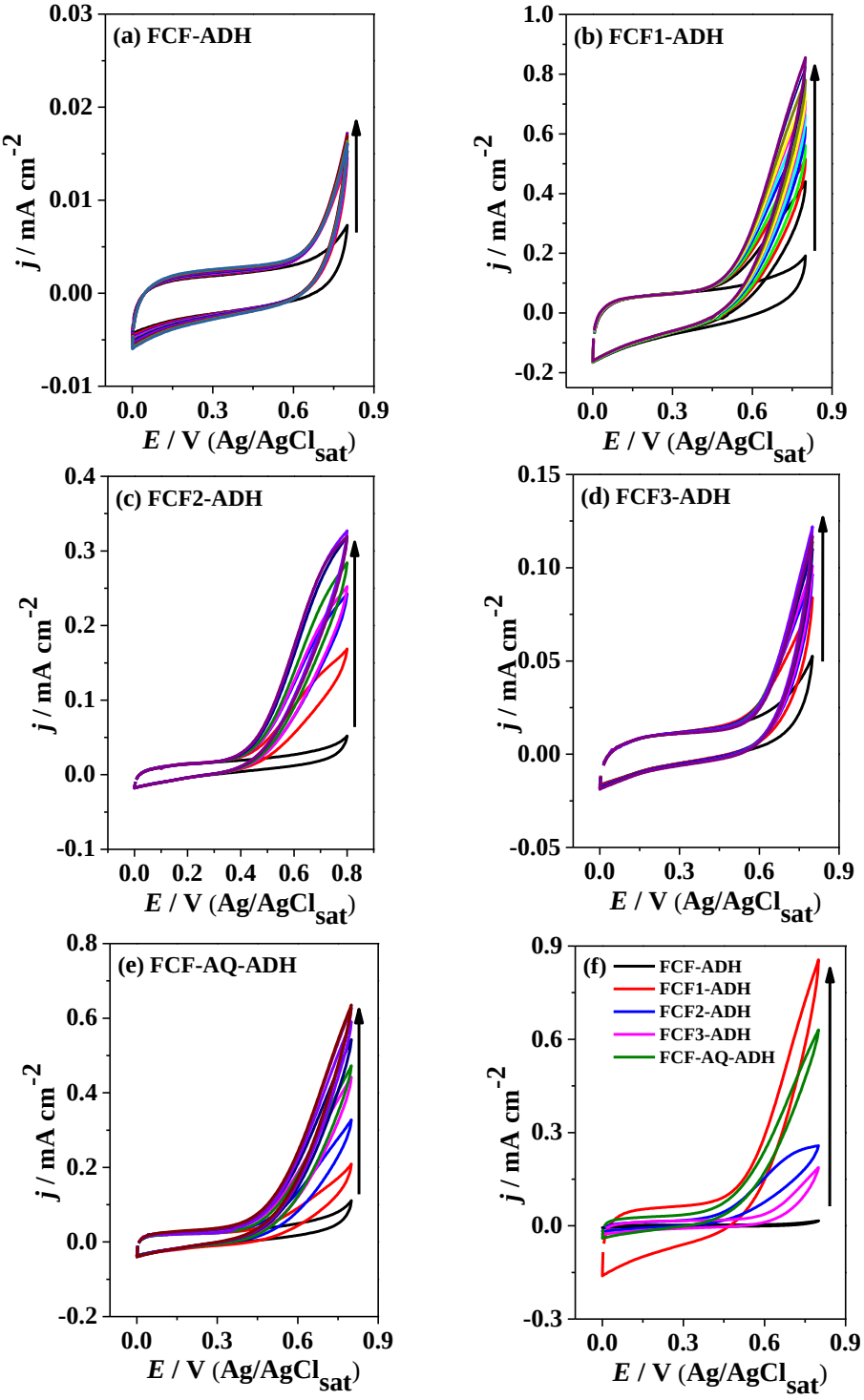

4.9.3 Bioelectrocatalysis of ethanol

The bioelectrocatalytic activity of FCF1-ADH and FCF-AQ-ADH was further tested by using chronoamperometric experiments. Figure 32a shows the current-time transient of increasing ethanol concentration for pristine FCF (in black), FCF1 (in red) and FCF-AQ (in blue) electrodes obtained in phosphate buffer solution (0.1 mol L^{-1}, pH 7.5) containing NAD^+ (0.6 mmol L^{-1}) at 0.6 V applied potential during 2200 seconds in the presence of successive additions of ethanol, each addition corresponds to an addition of (200 µL) of ethanol at a concentration of 8.56 mol L^{-1}. The response time was less than 10 seconds indicating a fast process and well bioelectrocatalytic oxidation of ethanol by modified FCF-ADH bioelectrodes. The current increase linearly with the increase in ethanol concentration until it reached steady state, rapidly promotes oxidation in the cycle as can be seen by the calibration curves in Figure 32b, where the substrate saturation is achieved at a higher concentration of ethanol i-e 0.80 mol L^{-1} for FCF1-ADH as compared to FCF-AQ-ADH (0.60 mol L^{-1}) and pristine FCF-ADH (0.26 mol L^{-1}) bioelectrodes.

Figure 32 – (a) Chronoamperometric response obtained in 0.1 mol L^{-1} sodium phosphate buffer solution (pH 7.5) containing NAD^+ (0.6 mmol L^{-1}) and different concentrations of ethanol (200 µL) at 0.6 V applied potential for pristine FCF-ADH (●), FCF1-ADH (●), and FCF-AQ-ADH (●); (b) Plot of the ethanol concentration versus current for pristine FCF-ADH (●), FCF1-ADH (●), and FCF-AQ-ADH (●) obtained in 0.1 mol L^{-1} sodium phosphate buffer solution (pH 7.5) containing NAD^+ (0.6 mmol L^{-1}) and different concentrations of ethanol (200 µL) at 0.6 V applied potential. All the experiments were carried out in N_2-saturated environment at T= 25 °C.

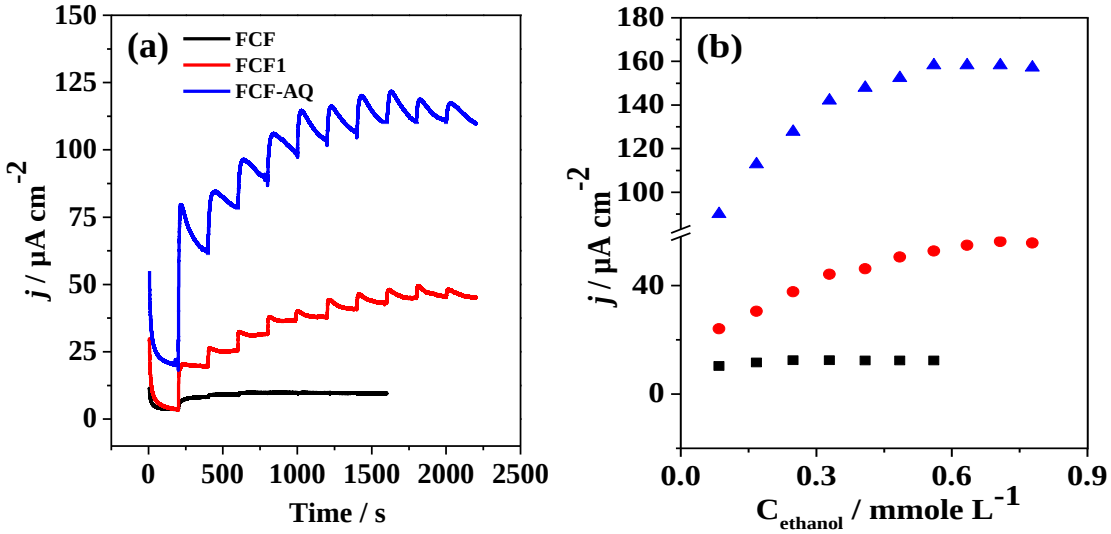

This implies that most of the catalytic centers are occupied at a larger concentration of the substrate such as in case of both the FCF1-ADH and FCF-AQ-ADH, where the substrate saturation is achieved at a higher concentration of ethanol. Therefore, no substantial increase in current was observed with ethanol addition after saturation was achieved.

5 CONCLUSION

This study showed the development of quinone-modified FCF electrodes by using oxidative treatment with permanganate and by using the electrochemical grafting of anthraquinone groups on FCF. We conclude that the presence of quinone functionality in the FCF surfaces improves the electro-oxidation of NADH. As consequence, we propose the use of both of these methodologies for the development of the FCF modified with ADH to be used for ethanol bio-electrocatalysis. As far as fundamental exploration is concerned, it can infers that defects and C=O groups in the FCF-modified electrode play an important role on the electro-oxidation of NADH.

The understanding of NADH electro-oxidation mechanism on quinone-modified carbon electrode is also an important point to be addressed. We implemented an *operando* EPR measurement using modified FCF electrodes under NADH electro-oxidation, where the quantity of unpaired electron spin produced on the electrode surface can be identified. *Operando* EPR spectroscopy proved to be very useful for investigating the NADH/NAD^+ redox reaction. Herein, we proposed how to probe the number of free electrons on a carbon electrode surface and correlate it with the electrocatalytic mechanism. The correlation with the spin concentration reveals an increasing number of free unpaired electrons with increasing applied overpotential and NADH oxidation, which corroborates that quinone groups on modified FCF surfaces can act as electrocatalysts towards the oxidation of NADH to NAD^+.

In the final part of the thesis, the quinone-modified FCF electrodes were immobilized with ADH for the fabrication of bioelectrodes. Subsequently, the developed bioelectrodes were tested towards the bioelectrocatalysis of ethanol and the results were compared with the pristine FCF biolectrodes prepared under identical conditions. The quinone-modified FCF electrodes showed high stability and bioelectrocatalytic activity as compared to the pristine FCF electrode, which enable these bioelectrodes to be used in cyclic voltammetry experiments. Additionally, the as-prepared ADH on FCF could also be very useful in bioelectrocatalysis as well as a perspective bioelectrode to develop enzyme biofuel cells and biosensors.

6 REFERENCES

1 MAY, S. W.; PADGETTE, S. R. Oxidoreductase enzymes in biotechnology: current status and future potential. **Nature Biotechnology**, v. 1, n. 8, p. 677–686, 1983.

2 GODBOLE, S. S.; D'Souza, S. F.; NADKARNI, G. B. Regeneration of NAD(H) by alcohol dehydrogenase in gel-entrapped yeast cells. **Enzyme and Microbial Technology**, v. 5, n. 2, p. 125–128, 1983.

3 PEREIRA, A. R.; SOUZA, J. C. P.; GONÇALVES, A. D.; PAGNONCELLI, A. C CRESPILHO, F. N. Bioelectro-oxidation of ethanol using NAD-dependent alcohol dehydrogenase on oxidized flexible carbon fiber arrays. **Journal of the Brazilian Chemical Society**, 2017.

4 SOUZA, J. C. P.; SILVA, W.O.; LIMA, F. H. B.; CRESPILHO, F. N. Enzyme activity evaluation by differential electrochemical mass spectrometry. **Chemical Communications**, v. 53, n. 60, p. 8400–8402, 2017.

5 PAGNONCELLI, K. C.; PEREIRA, A. R.; SEDENHO, G. C.; BERTAGLIA, T.; CRESPILHO, F. N. Ethanol generation, oxidation and energy production in a cooperative bioelectrochemical system. **Bioelectrochemistry**, v. 122, p. 11–25, 2018.

6 GRUBB, W.T. Catalysis, electrocatalysis, and hydrocarbon fuel cells. **Nature**, v. 198, n. 4883, p. 883–884, 1963.

7 GHINDILIS, A.L.; ATANASOV, P.; WILKINS, B. Enzyme-catalyzed direct electron transfer: fundamentals and analytical applications. **Electroanalysis**, v. 9, n. 9, p. 661–674, 1997.

8 XU, F. Applications of oxidoreductases: recent progress. **Industrial Biotechnology**, v. 1, n. 1, p. 38–50, 2005.

9 BOUJTITA, M.; MURR, N. Biosensors for analysis of ethanol in foods. **Journal of Food Science**, v. 60, n. 1, p. 201–204, 1995.

10 ALPAT, Ş.; TELEFONCU, A. Development of an alcohol dehydrogenase biosensor for ethanol determination with toluidine blue O covalently attached to a cellulose acetate modified electrode. **Sensors**, v. 10, n. 1, p. 748–764, 2010.

11 KOYUNCU, D.; ERDEN, P.E.; PEKYARDIMCI, Ş.; KILIÇ. E. A New amperometric carbon paste enzyme electrode for ethanol determination. **Analytical Letters**, v. 40, n. 10, p. 1904–1922, 2007.

12 KIM, Y. H.; CAMPBELL, E.; YU, J.; MINTEER, S. D.; BANTA, S. Complete oxidation of methanol in biobattery devices using a hydrogel created from three modified dehydrogenases. **Angewandte Chemie International Edition**, v. 52, n. 5, p. 1437–1440, 2013.

13 ADDO, P. K.; ARECHEDERRA, R. L.; MINTERR, S. D. Evaluating enzyme cascades for methanol/air biofuel cells based on NAD+-dependent enzymes. **Electroanalysis**, v. 22, n. 7–8, p. 807–812, 2010.

14 TOPCAGIC, S.; MINTEER, S. D. Development of a membraneless ethanol/oxygen biofuel cell. **Electrochimica Acta**, v. 51, n. 11, p. 2168–2172, 2006.

15 BOUJTITA, M.; CHAPLEAU, M.; MURR, N. E. Biosensors for analysis of ethanol in food: effect of the pasting liquid. **Analytica Chimica Acta**, v. 319, n. 1–2, p. 91–96, 1996.

16 MA, Y.; JIN, Z.; PENG, B.; DING, J. Investigation of direct electro-oxidation behavior of NADH at a chemically modified glassy carbon electrode. **Journal of The Electrochemical Society**, v. 162, n. 6, p. H317–H320, 2015.

17 AIZAWA, M.; COUGHLIN, R.W.; CHARLES, M. Electrochemical regeneration of nicotinamide adenine dinucleotide. **Biochimica et Biophysica Acta (BBA) - General Subjects**, v. 385, n. 2, p. 362–370, 1975.

18 HAAS, J.; SCHÄTZLE, M. A.; HUSAIN, S. M.; SCHULZ-FINKCE, J.; JUNG, M.; HUMMEL, W.; MÜLLER, M.; LÜDEKE, S. A quinone mediator drives oxidations catalysed by alcohol dehydrogenase-containing cell lysates. **Chemical Communications**, v. 52, n. 29, p. 5198–5201, 2016.

19 LIU, T.; FRITH, J. T.; KIM, G.; KERBER, R. N.; DUBOUIS, N.; SHAO, Y.; LIU, Z.; MAGUSIN, P. C. M.; CASFORDM, M. T. L.; GARCIA-ARAEZ, NGREY, C. P. The Effect of water on quinone redox mediators in nonaqueous Li-O2 batteries. **Journal of the American Chemical Society**, v. 140, n. 4, p. 1428–1437, 2018.

20 PREGER, Y.; GERKEN, J. B.; BISWAS, S.; ANSON, C. W.; JOHNSON, M. R.; ROOT, T. W.; STAHL, S. S. Quinone-mediated electrochemical O2 reduction accessing high power density with an off-electrode Co-N/C catalyst. **Joule**, v. 2, n. 12, p. 2722–2731, 2018.

21 ZHU, W.; YU, D.; SHI, M.; ZHANG, Y.; HUANG, T. Quinone-mediated microbial goethite reduction and transformation of redox mediator, anthraquinone-2,6-disulfonate (AQDS). **Geomicrobiology Journal**, v. 34, n. 1, p. 27–36, 2017.

22 ZEE, F. P. BOUWMAN, R. H. M.; STRIK, D. P. B. T. B.; LETTINGA, G.; FILED, J. A. Application of redox mediators to accelerate the transformation of reactive azo dyes in anaerobic bioreactors. **Biotechnology and Bioengineering**, v. 75, n. 6, p. 691–701, 2001.

23 YEH, S. Y.; WANG, C. M. Anthraquinone-modified electrodes, preparations and characterizations. **Journal of Electroanalytical Chemistry**, v. 592, n. 2, p. 131–138, 2006.

24 SARAPUU, A.; HELSTEIN, K.; VAIK, K.; SCHIFFRIN, D. J.; TAMMEVESKI, K. Electrocatalysis of oxygen reduction by quinones adsorbed on highly oriented pyrolytic graphite electrodes. **Electrochimica Acta**, v. 55, n. 22, p. 6376–6382, 2010.

25 GORTON, L.; DOMÍNGUEZ, E. Electrocatalytic oxidation of NAD(P)H at mediator-modified electrodes. **Reviews in Molecular Biotechnology**, v. 82, n. 4, p. 371–392, 2002.

26 SAKAI, H.; NAKAGAWA, T.; TOKITA, Y.; HATAZAWA, T.; IKEDA, T.; TSUJIMURA, S.; KANO, K. A high-power glucose/oxygen biofuel cell operating under quiescent conditions. **Energy and Environmental Science**, v. 2, n. 1, p. 133–138, 2009.

27 MILTON, R.D.; HICKEY, D.P.; ABDELLAOUI, S.; LIM, K.; WU, F.; TAN, B.; MINTEER, S. D. Rational design of quinones for high power density biofuel cells. **Chemical Science**, v. 6, n. 8, p. 4867–4875, 2015.

28 MURATA, K.; NAKAMURA, N.; OHNO, H. Electrocatalytic oxidation of NADH on electrochemically oxidized carbon fiber paper electrodes for a simple biofuel cell anode. **Electrochemistry**, v. 76, n. 8, p. 563–565, 2008.

29 SASSOLAS, A.; BLUM, L.J.; LECA-BOUVIER, B. D. Immobilization strategies to develop enzymatic biosensors. **Biotechnology Advances**, v. 30, n. 3, p. 489–511, 2012.

30 LUZ, R.A.S.; PEREIRA, A.R.; SOUZA, J.C.P.; SALES, F. C. P. F.; CREPILHO, F. N. Enzyme biofuel cells: thermodynamics, kinetics and challenges in applicability. **ChemElectroChem**, v. 1, p. 1751–1777, 2014.

31 FRANK, E.; STEUDLE, L. M.; INGILDEEV, D.; SPÖRL, J. M.; BUCHMEISER, M. R. Carbon fibers: precursor systems, processing, structure, and properties. **Angewandte Chemie International Edition**, v. 53, n. 21, p. 5262–5298, 2014.

32 PENEV, E. S.; ARTYUKHOV, V. I.; YAKOBSON, B. I. Basic structural units in carbon fibers: atomistic models and tensile behavior. **Carbon**, v. 85, p. 72–78, 2015.

33 DEAN, G. D.; TURNER, P. The elastic properties of carbon fibres and their composites. **Composites**, v. 4, n. 4, p. 174–180, 1973.

34 PEREIRA, A. R.; SOUZA, J. C. P.; IOST, R.M.; SALES, F. C. P. F.; CREPILHO, F. N. Application of carbon fibers to flexible enzyme electrodes. **Journal of Electroanalytical Chemistry**, v. 780, p. 396–406, 2016.

35 EDIE, D. D. The effect of processing on the structure and properties of carbon fibers. **Carbon**, v. 36, n. 4, p. 345–362, 1998.

36 FRANK, E.; HERMANUTZ, F.; BUCHMEISER, M. R. Carbon fibers: precursors, manufacturing, and properties. **Macromolecular Materials and Engineering**, v. 297, n. 6, p. 493–501, 2012.

37 HANNA, S. B.; YEHIA, A. A.; ISMAIL, M. N.; KHALAF, A. I. Preparation and characterization of carbon fibers from polyacrylonitrile precursors. **Journal of Applied Polymer Science**, v. 123, n. 4, p. 2074–2083, 2012.

38 PARK, S.-J., HEO, G.-Y. Precursors and manufacturing of carbon fibers. In: PARK, G.Y.; HEO, S. **Carbon fibers**. Dordrecht: Springer, 2015. p. 31–66.

39 LIU, J.; WANG, P. H.; LI, R. Y. Continuous carbonization of polyacrylonitrile-based oxidized fibers: aspects on mechanical properties and morphological structure. **Journal of Applied Polymer Science**, v. 52, n. 7, p. 945–950, 1994.

40 SAHA, B.; SCHATZ, G. C. Carbonization in polyacrylonitrile (PAN) based carbon fibers studied by reaxFF molecular dynamics simulations. **The Journal of Physical Chemistry B**, v. 116, n. 15, p. 4684–4692, 2012.

41 RAHMAN, M. S. A.; ISMAIL, A. F.; MUSTAFA, A. A review of heat treatment on polyacrylonitrile fiber. **Polymer Degradation and Stability**, v. 92, n. 8, p. 1421–1432, 2007.

42 MARTINS, M. V. A.; PEREIRA, A. R.; LUZ, R. A.; IOST, R. M.; CRESPILHO, F. N. Evidence of short-range electron transfer of a redox enzyme on graphene oxide electrodes. **Physical Chemistry Chemical Physics**, v. 16, n. 33, p. 17426–17436, 2014.

43 LADBURY, J. W.; CULLIS, C. F. Kinetics and mechanism of oxidation by permanganate. **Chemical Reviews**, v. 58, n. 2, p. 403–438, 1958.

44 DASH, S.; PATEL, S.; MISHRA, B. K. Oxidation by permanganate: synthetic and mechanistic aspects. **Tetrahedron**, v. 65, n. 4, p. 707–739, 2009.

45 SZÁZDI, L.; GULYÁS, J.; PUKÁNSZKY, B. Surface characterization of electrochemically oxidized carbon fibers: surface properties and interfacial adhesion. **Composite Interfaces**, v. 9, n. 2, p. 219–232, 2002.

46 TIWARI, S.; BIJWE, J. Surface treatment of carbon fibers - a review. **Procedia Technology**, v. 14, p. 505–512, 2014.

47 WEISSMANN, M.; CROSNIER, O.; BROUSSE, T.; BÉLANGER, D. Electrochemical study of anthraquinone groups, grafted by the diazonium chemistry, in different aqueous media-relevance for the development of aqueous hybrid electrochemical capacitor. **Electrochimica Acta**, v. 82, p. 250–256, 2012.

48 KULLAPERE, M.; SEINBERG, J. M.; MÄEORG. U.; MAIA. G.; SCHIFFRIN. D. J.; TAMMEVESKI. K. Electroreduction of oxygen on glassy carbon electrodes modified with in situ generated anthraquinone diazonium cations. **Electrochimica Acta**, v. 54, n. 7, p. 1961–1969, 2009.

49 KULLAPERE, M.; MARANDI.; SAMMELSELG. V.; MENEZES. H. A.; MAIA. G.; TAMMEVESKI. K. Surface modification of gold electrodes with anthraquinone diazonium cations. **Electrochemistry Communications**, v. 11, n. 2, p. 405–408, 2009.

50 KIM, R. S.; CHUNG, T. D. The Electrochemical reaction mechanism and applications of quinones. **Bulletin of the Korean Chemical Society**, v. 35, n. 11, p. 3143–3155, 2014.

51 YUAN, L. Y.; SHYU, S.S.; LAI, J. Y. Plasma surface treatments on carbon fibers. II. Mechanical property and interfacial shear strength. **Journal of Applied Polymer Science**, v. 42, n. 9, p. 2525–2534, 1991.

52 TRAN, M. Q.; HO, K. K. C.; KALINKA, G.; SHAFFER, M. S. P.; BISMARK, A. Carbon fibre reinforced poly(vinylidene fluoride): impact of matrix modification on fibre/polymer adhesion. **Composites Science and Technology**, v. 68, n. 7–8, p. 1766–1776, 2008.

53 KNETEN, K. R.; MCREERY, R. L. Effects of redox system structure on electron-transfer kinetics at ordered graphite and glassy carbon electrodes. **Analytical Chemistry**, v. 64, n. 21, p. 2518–2524, 1992.

54 POON, M.; MCREERY, R. L.; ENGSTROM. R. Laser activation of carbon electrodes. Relationship between laser-induced surface effects and electron transfer activation. **Analytical Chemistry**, v. 60, n. 17, p. 1725–1730, 1988.

55 CHEN, P.; MCREERY, R. L. Control of electron transfer kinetics at glassy carbon electrodes by specific surface modification. **Analytical Chemistry**, v. 68, n. 22, p. 3958–3965, 1996.

56 CARLSON, B. W.; MILLER, L. L. Mechanism of the oxidation of NADH by quinones. Energetics of one-electron and hydride routes. **Journal of the American Chemical Society**, v. 107, n. 2, p. 479–485, 1985.

57 TSE, D. C. -S.; KUWANA, T. Electrocatalysis of dihydronicotinamide adenosine diphosphate with quinones and modified quinone electrodes. **Analytical Chemistry**, v. 50, n. 9, p. 1315–1318, 1978.

58 JAEGFELDT, H.; TORSTENSSON, A. B. C.; GORTON, L. G. O.; JOHANSSON, G. Catalytic oxidation of reduced nicotinamide adenine dinucleotide by graphite electrodes modified with adsorbed aromatics containing catechol functionalities. **Analytical Chemistry**, v. 53, n. 13, p. 1979–1982, 1981.

59 ČÉAS, N. K.; KANAPIENIENÉ, J. J.; KULYS, J. J. NADH oxidation by quinone electron acceptors. **Biochimica et Biophysica Acta (BBA) - Bioenergetics**, v. 767, n. 1, p. 108–112, 1984.

60 RADOI, A.; COMPAGNONE, D. Recent advances in NADH electrochemical sensing design. **Bioelectrochemistry**, v. 76, n. 1–2, p. 126–134, 2009.

61 VALENTINI, F.; SALIS, A.; CURULLI, A.; PALLESCHI, G. Chemical reversibility and stable low-potential NADH detection with nonconventional conducting polymer nanotubule modified glassy carbon electrodes. **Analytical Chemistry**, v. 76, n. 11, p. 3244–3248, 2004.

62 PALMORE, G. T. R.; BERTSCHY, H.; BERGEN, S .H. A methanol/dioxygen biofuel cell that uses NAD^+-dependent dehydrogenases as catalysts: application of an electro-enzymatic method to regenerate nicotinamide adenine dinucleotide at low overpotentials. **Journal of Electroanalytical Chemistry**, v. 443, n. 1, p. 155–161, 1998.

63 LI, H.; WORLEY, K.E.; BARTON, S. C. Quantitative analysis of bioactive NAD^+ regenerated by NADH electro-oxidation. **ACS Catalysis**, v. 2, n. 12, p. 2572–2576, 2012.

64 LIMOGES, B.; MARCHAL, D.; MAVRE, F.; SAVÉANT, J-M.; SCHÖLLHORN, B. Theory and practice of enzyme bioaffinity electrodes. Direct electrochemical product detection. **Journal of the American Chemical Society**, v. 130, n. 23, p. 7259–7275, 2008.

65 ARECHEDERRA, M.N.; ADDO, P.K.; MINTEER, S. D. Poly(neutral red) as a NAD+ reduction catalyst and a NADH oxidation catalyst:tTowards the development of a rechargeable biobattery. **Electrochimica Acta**, v. 56, n. 3, p. 1585–1590, 2011.

66 BAÑARES, M. A.; GUERRERO-PÉREZ, M. O.; FIERRO, J. L. G.; CORTEZ, G. G. Raman spectroscopy during catalytic operations with on-line activity measurement (operando spectroscopy): a method for understanding the active centres of cations supported on porous materials. **Journal of Materials Chemistry**, v. 12, n. 11, p. 3337–3342, 2002.

67 WECKHUYSEN, B. M. Operando spectroscopy: fundamental and technical aspects of spectroscopy of catalysts under working conditions. **Physical Chemistry Chemical Physics**, v. 5, n. 20, p. 1, 2003.

68 WANG, B.; FIELDING, A. J.; DRYFE, R. A. In situ electrochemical electron paramagnetic resonance spectroscopy as a tool to probe electrical double layer capacitance. **Chemical Communications**, v. 54, n. 31, p. 3827–3830, 2018.

69 WANDT, J.; MARINO, C.; GASTEIGER, S. A.; JAKES, P.; Eichel, R-A.; GRANWEHR, J. Operando electron paramagnetic resonance spectroscopy – formation of mossy lithium on lithium anodes during charge–discharge cycling. **Energy & Environmental Science**, v. 8, n. 4, p. 1358–1367, 2015.

70 SATHIYA, M.; LERICHE, J.-B.; SALAGER, E.; GOURIER , DTARASCON, J. -M.; VEZIN, H. Electron paramagnetic resonance imaging for real-time monitoring of Li-ion batteries. **Nature Communications**, v. 6, n. 1, p. 6276, 2015.

71 MASUDA, T.; YOSHIKAWA, H.; NOGUCHI, H.; KAWASAKI, T.; KOBATA, M.; KOBAYASHI, K.; UOSAKI, K. In situ x-ray photoelectron spectroscopy for electrochemical reactions in ordinary solvents. **Applied Physics Letters**, v. 103, n. 11, p. 111605, 2013.

72 CHAKRABARTI, A.; FORD, M.E.; GREGORY, D.; HU, R.; KETURAKIS, C. J.; LWIN, S.; TANG, Y.; YANG, Z.; ZHU, M.; BAÑARES, M. A.; WACHS, I. E. A decade+ of operando spectroscopy studies. **Catalysis Today**, v. 283, p. 27–53, 2017.

73 SOUZA, J. C. P.; Iost, R.M.; CRESPILHO, F. N. Nitrated carbon nanoblisters for high-performance glucose dehydrogenase bioanodes. **Biosensors and Bioelectronics**, v. 77, p. 860–865, 2016.

74 FUJIMOTO, A.; YAMADA, Y.; KOINUMA, M.; SATO, S. Origins of sp 3 C peaks in C 1s X-ray photoelectron spectra of carbon materials. **Analytical Chemistry**, v. 88, n. 12, p. 6110–6114, 2016.

75 BANERJEE, J.; BOJAN, V.; PANTANO, C. G.; KIM, S. H. Effect of heat treatment on the surface chemical structure of glass: oxygen speciation from in situ XPS analysis. **Journal of the American Ceramic Society**, v. 101, n. 2, p. 644–656, 2018.

76 KUNDU, S.; WANG, Y.; XIA, W.; MUHLER, M. Thermal stability and reducibility of oxygen-containing functional groups on multiwalled carbon nanotube surfaces: a quantitative high-resolution XPS and TPD/TPR study. **The Journal of Physical Chemistry C**, v. 112, n. 43, p. 16869–16878, 2008.

77 PIMENTA, M. A.; DRESSELHAUS, G.; DRESSELHAUS, M. S.; CANÇADO, L. G. Studying disorder in graphite-based systems by Raman spectroscopy. **Physical Chemistry Chemical Physics**, v. 9, n. 11, p. 1276–1290, 2007.

78 JAWHARI, T.; ROID, A.; CASADO, J. Raman spectroscopic characterization of some commercially available carbon black materials. **Carbon**, v. 33, n. 11, p. 1561–1565, 1995.

79 LIU, J.; TIAN, Y.; CHEN, Y.; LIANG, J.; ZHANG, L.; FONG, H. A surface treatment technique of electrochemical oxidation to simultaneously improve the interfacial bonding strength and the tensile strength of PAN-based carbon fibers. **Materials Chemistry and Physics**, v. 122, n. 2–3, p. 548–555, 2010.

80 TAO, L.; WANG, Q.; DOU, S.; MA, Z.; HUO, J.; WANG, S.; DAI, L. Edge-rich and dopant-free graphene as a highly efficient metal-free electrocatalyst for the oxygen reduction reaction. **Chemical Communications**, v. 52, n. 13, p. 2764–2767, 2016.

81 SCHWAN, J.; ULRICH, S.; EHRHARDT, H. Raman spectroscopy on amorphous carbon films. **Journal of Applied Physics**, v. 80, n. 1, p. 440–447, 1996.

82 FERRARI, A. C. Raman spectroscopy of graphene and graphite: disorder, electron–phonon coupling, doping and nonadiabatic effects. **Solid State Communications**, v. 143, n. 1–2, p. 47–57, 2007.

83 KANIYOOR, A.; RAMAPRABHU, S. A Raman spectroscopic investigation of graphite oxide derived graphene. **AIP Advances**, v. 2, n. 3, p. 032183, 2012.

84 FERRARI, A. C.; ROBERTSON, J. Interpretation of Raman spectra of disordered and amorphous carbon. **Physical Review B**, v. 61, n. 20, p. 14095–14107, 2000.

85 WANG, Y.; ALSMEYER, D. C.; MCREERY, R. L. Raman spectroscopy of carbon materials: structural basis of observed spectra. **Chemistry of Materials**, v. 2, n. 5, p. 557–563, 1990.

86 TAMOR, M. A.; VASSSELL, W.C. Raman '"fingerprinting"' of amorphous carbon films. **Journal of Applied Physics**, v. 76, n. 6, p. 3823–3830, 1994.

87 FERRARI, A. C.; ROBERTSON, J. Raman spectroscopy of amorphous, nanostructured, diamond-like carbon, and nanodiamond. **Philosophical Transactions of the Royal Society A: Mathematical, Physical and Engineering Sciences**, v. 362, n. 1824, p. 2477–2512, 2004.

88 REICH, S.; THOMSEN, C. Raman spectroscopy of graphite. **Philosophical Transactions of the Royal Society A: Mathematical, Physical and Engineering Sciences**, v. 362, n. 1824, p. 2271–2288, 2004.

89 PUJADÓ, M.P. **Carbon nanotubes as platforms for biosensors with electrochemical and electronic transduction.** Berlin: Springer, 2012.p. 208.

90 STANKOVICH, S.; DIKIN, D. A.; PINER, R. D.; KOHLHAAS, K. A.; KLEINHAMMES, A.; JIA, Y.; WU, Y.; NGUYEN, S. B. T.; RUOFF, R. S. Synthesis of graphene-based nanosheets via chemical reduction of exfoliated graphite oxide. **Carbon**, v. 45, n. 7, p. 1558–1565, 2007.

91 GUIN, P. S.; DAS, S.; MANDAL, P. C. Electrochemical reduction of quinones in different media: a review. **International Journal of Electrochemistry**, v. 2011, p. 1–22, 2011.

92 GOLDBERG, I. B.; BARD, A. J. Simultaneous electrochemical-electron spin resonance measurements. I. Cell design and preliminary results. **The Journal of Physical Chemistry**, v. 75, n. 21, p. 3281–3290, 1971.

93 GOLDBERG, I. B.; BOYD, D.; HIRASAWA, R.; BARD, A. J. Simultaneous electrochemical-electron spin resonance measurements. III. Determination of rate constants for second-order radical anion dimerization. **The Journal of Physical Chemistry**, v. 78, n. 3, p. 295–299, 1974.

94 KOVARSKII, A. L.; KASPAROV, V. V.; SHATALOVA, O. V.; KRIVANDIN, A. V.; KOROKHIN, R. A.; KUPERMAN, A. M. EPR spectroscopic and X-Ray diffraction studies of carbon fibers with different mechanical properties. **Russian Journal of Physical Chemistry B**, v. 11, n. 2, p. 233–241, 2017.

95 KEMPIŃSKI, W.; ŁOŚ, S.; KEMPIŃSKI, M.; MARKOWSKI, D. Experimental techniques for the characterization of carbon nanoparticles – a brief overview. **Beilstein Journal of Nanotechnology**, v. 5, p. 1760–1766, 2014.

96 TAMPIERI, F.; SILVESTRINI, S.; RICCO, R.; MAGGINI, M.; BARBON, A. A comparative electron paramagnetic resonance study of expanded graphites and graphene. **Journal of Materials Chemistry C**, v. 2, n. 38, p. 8105–8112, 2014.

97 CHIPARA, M.; ZALESKI, J. M.; HUI, D.; DU, C.; PAN, N. Electron spin resonance on carbon nanotubes-polymer composites. **Journal of Polymer Science Part B: Polymer Physics**, v. 43, n. 23, p. 3406–3412, 2005.

98 WIĘCKOWSKI, A. B.; NAJDER-KOZDROWSKA, L.; RECHNIA, P.; MALAIKA, A.; KRZYŹYŃSKA, B.; KOZŁOWSKI, M. EPR Characteristics of activated carbon for hydrogen production by the thermo-catalytic decomposition of methane. **Acta Physica Polonica A**, v. 130, n. 3, p. 701–704, 2016.

99 BARKLIE, R. C. Characterisation of defects in amorphous carbon by electron paramagnetic resonance. **Diamond and Related Materials**, v. 12, n. 8, p. 1427–1434, 2003.

100 HAGEN, W. **Biomolecular EPR Spectroscopy**. New York: CRC Press, 2009. p. 248.

101 WEBESTER, R. D.; DRYFE, R. A. W.; COLES, B. A.; COMPTON, R. G. In situ electrochemical ePR studies of charge transfer across the liquid/liquid interface. **Analytical Chemistry**, v. 70, n. 4, p. 792–800, 1998.

102 WALLER, A. M.; COMPTON, R. G. In-situ electrochemical ESR. In: COMPTO, R. G. **Comprehensive chemical kinetics**. Amsterdam: Elsevier, 1989. Cap. 7, p. 297–352.

103 COLES, B. A.; COMPTON, R. G. Photoelectrochemical ESR. **Journal of Electroanalytical Chemistry and Interfacial Electrochemistry**, v. 144, n. 1–2, p. 87–98, 1983.

104 KONTANI, A.; MASUDA, M.; MATSUMURA, H.; NAKAMURA, N.; YOHA, M.; OHNO, H. A bioanode using thermostable alcohol dehydrogenase for an ethanol biofuel cell operating at high tempratures. **Electroanalysis**, v. 26, n. 4, p. 682-686, 2014.

105 CAI, C.-X.; XUE, K.-H.; ZHOU, Y.-M.; YANG, H. Amperometric biosensor for ethanol based on immobilzation of alcohol dehydrogenase on a nickel hexacyanoferrate modified microband gold electrode. **Talanta**, v. 44, n. 3, p. 339-347,1997.

106 CHOI, H. N.; LYU, Y.-K.; HAN, J.-H, LEE, W.-Y. Amperometric ethanol biosensor based on carbon nanotube dispersed in sol-gel-derived titania-nafion composite film. **Electroanalysis**, v. 19, n. 14, p. 1524-1530, 2007.

107 NASRI, Z.; SHAMS, E.; AHMADI, M. Direct modification of a glassy carbon electrode with toluidine blue diazoinium salt: application to NADH determination and biosensing of ethanol. **Electroanalysis**,v. 25, n. 8, p. 1917-1925, 2013.

108 SHAN, C.; YANG, H.; HAN, D.; ZHANG, Q.; IVASKA, A.; NIU, L. Electrochemical determination of NADH and ethanol basedon ionic liquid-functionalized graphene. **Biosensors and Bioelectronics**, v. 25, n. 6, p. 1504-1508, 2010.

109 LEE, C.-A.; TSAI, Y.-C. Preparation of multiwalled carbon nanotube-chitosan-alcohol dehydrogenase nanobiocomposite for amperometric detection of ethanol. **Sensors and Actuators B: Chemical**, v. 138, n. 2, p. 518-523, 2009.

110 DICKENSON, C. J.; DICKINSON, F. M. A study of the pH- and temperature-dependence of the reactions of yeast alcohol dehydrogenase with ethanol, acetaldehyde and butyraldehyde as substrates. **Biochemical Journal**, v. 147, n. 2, p. 303–311, 1975.

111 DICKINSON, F. M.; MONGER, G. P. A study of the kinetics and mechanism of yeat alcohol dehydrogenase with a variety of substrates. **Biochemical Journal**, v. 131, n. 2, p. 261-270, 1971.

112 LESKOVAC, V.; TRIVIĆ, S.; PERIČIN, D. The three zinc-containing alcohol dehydrogenases from baker's yeast, *Saccharomyces cerevisiae*. **FEMS Yeats Research**, v. 2, n. 4, p. 481-494, 2002.

113 TRIVIĆ, S.; LESKOVAC, V.; Structure and function of yeat alcohol dehydrogenase. **Journal of the Serbian Chemical Society**, v. 65, n. 4, p. 207-227, 2000.

114 GANZHORN, A. J.; GREEN, D. W.; HERSHEY, A. D.; GOULD, R. M.; PLAPP, B. V. Kinetic characterization of yeast alcohol dehydrogenses. Amino acid residue 294 and substrate specificity. **Jounal of Biological Chemistry**, v. 262, n. 8, p. 3754-3761, 1987.

115 KLINMAN, J. P.; Probes of mechanism and transition-state structure in the alcohol dehydrogenase reaction. **Critical Reviews in Biochemistry**, v. 10, n. 1, p. 39-78, 1981.

116 YAMADA, T.; YAMATO, M. Interaction of yeast alcohol dehydrogenase with variuos substrates. I. Binding of coenzymes. **The Journal of Biochemistry**, v. 74, n. 5, p. 971-984, 1973.

117 FORTI, J. C.; AQUINO NETO, S.; ZUCULOTO, V.; CIANCAGLINI, P.; DE ANDRADE, A. R. Development of noval bioanodes for ethanol biofuel cell using PAMAM dendrimers as matrix for enzyme immobilization. **Biosensors and Bioelectronics**, v. 26, n. 5, p. 2675-2679, 2011.

118 ABUIN, E.; LISSI, E.; LEÓN, L. Kinetics of ethanol oxidation catalyzed by yeat al cohol dehydrogenase in aqueous solutions of sodium dodecylsulfate. **Protein Journal**, v. 27, n. 4, p. 247-252, 2008.